DISCLAIMER:

This document does not meet the
current format guidelines of
the Graduate School at
The University of Texas at Austin.

It has been published for
informational use only.

Copyright

by

Nkemakonam Uzodimma Egboga

2016

The Thesis Committee for Nkemakonam Uzodimma Egboga
Certifies that this is the approved version of the following thesis:

Investigative Study and Sensitivity Analysis of Thermal Stimulation in Unconventional Shale Reservoirs

APPROVED BY
SUPERVISING COMMITTEE:

Supervisor: _____
Matthew T. Balhoff

Co-supervisor: _____
Kishore K. Mohanty

Investigative Study and Sensitivity Analysis of Thermal Stimulation in Unconventional Shale Reservoirs

by

Nkemakonam Uzodimma Egboga, BSPE

Thesis

Presented to the Faculty of the Graduate School of

The University of Texas at Austin

in Partial Fulfillment

of the Requirements

for the Degree of

Master of Science in Engineering

The University of Texas at Austin

December 2016

Dedication

This work is dedicated to my loving parents, whose sacrifices have made it possible for me to pursue my goals, whose guidance has helped me grow into the man I am today, and who have continued to unconditionally believe in me and support all my endeavors. Thank you mom and dad for all your prayers and words of encouragement; without you, I would not be here today; I am eternally grateful. And to Somto, Orby and Chukelu, thank you for inspiring me.

And most importantly to God, who has made all things possible.

Acknowledgements

I would like to wholeheartedly thank Dr. Matthew Balhoff for believing in me and for the countless opportunities he has provided over the past three years. Working with him has been a truly wonderful experience and under his stewardship I have developed into a better student and researcher. He sparked my interest in reservoir engineering, particularly reservoir simulation, and has been a mentor ever since. He has inspired and pushed me to limits I didn't realize I could reach and for that, my deepest gratitude goes to him.

I would also like to thank Dr. Kishore Mohanty for his support during my two years as a graduate student. He has provided exceptional guidance, exposed me to numerous opportunities and provided me with challenging projects. I am very grateful for his wisdom and faith in me.

Finally, I would like to thank the faculty, staff and students of the Department of Petroleum and Geosystems Engineering for making my time at the University of Texas at Austin an exciting experience. Particularly, I would like to thank Mercedes Bamgbose, Dr. John Foster, Frankie Hart, Barbara Messmore and Amy Douglas Stewart for being such wonderful people. And to the rest of the students in Dr. Balhoff's research group, thank you and remain awesome!

Abstract

Investigative Study and Sensitivity Analysis of Thermal Stimulation in Unconventional Shale Reservoirs

Nkemakonam Uzodimma Egboga, MSE

The University of Texas at Austin, 2016

Supervisors: Matthew T. Balhoff & Kishore K. Mohanty

Shale oil production from plays such as the Bakken and Eagle Ford, driven by advances in horizontal well drilling and hydraulic fracturing technology, has helped improve US domestic oil production. However, due to the low permeability of shale oil reservoirs, primary depletion only produces 5 – 10% of the original oil in place and there is an enormous potential for improved recovery. Chemical and gas huff-and-puff methods have been piloted with varying degrees of success, but no breakthrough recovery method has been discovered.

In this study, we examined improved oil recovery from shale reservoirs by thermal stimulation, consisting of primary depletion (early in a well's life), followed by conversion of the well to a heat injector to elevate reservoir temperature, and finally a secondary depletion. A 2D black oil, thermal, reactive transport simulator was developed to test the viability of the proposed method and then CMG STARS, a more advanced compositional/thermal simulator, was used to investigate the mechanisms involved, as well as key parameters affecting recovery during thermal stimulation.

We found that 1000 days of thermal stimulation with a 700 °F heater has the potential to increase economical oil recovery from about 7% to more than 11.5%, with potential for even greater recovery if heat injection time and temperature are optimized, as well as if heat is injected while producing oil from an adjacent well. Thermal pressurization of oil is the primary mechanism for the improved recovery. Kerogen decomposition into oil and gas results in a significant increase of hydrocarbons in place but is only a minor contribution to the additional recovery because production is limited by a lack of flow capacity. Furthermore, a two-fold increase in permeability is observed as a result of kerogen decomposition, but its contribution to recovery is also minor because the heated region is not well connected with the fractured region. The heating scheme may be improved in the future to better connect the heated region with the fractured region.

Table of Contents

List of Tables

List of Figures

Chapter 1: Introduction

Over the past decade, US production of oil and natural gas has increased rapidly. As shown in Fig. 1-1, oil production in 2015 was the highest in the US since the 1970s and natural gas production reached an all-time high. Recent growth in oil and gas production can be attributed to increased development of unconventional resources, particularly from shale oil and gas reservoirs; advances in drilling and hydraulic fracturing technology have provided access to oil and gas in these extremely low permeability reservoirs, previously considered uneconomic. Fig. 1-1 shows an increase in shale oil production from less than 1 MMBPD between 2002 and 2011 to 4.5 MMBPD (almost half of total US oil production) in 2015.

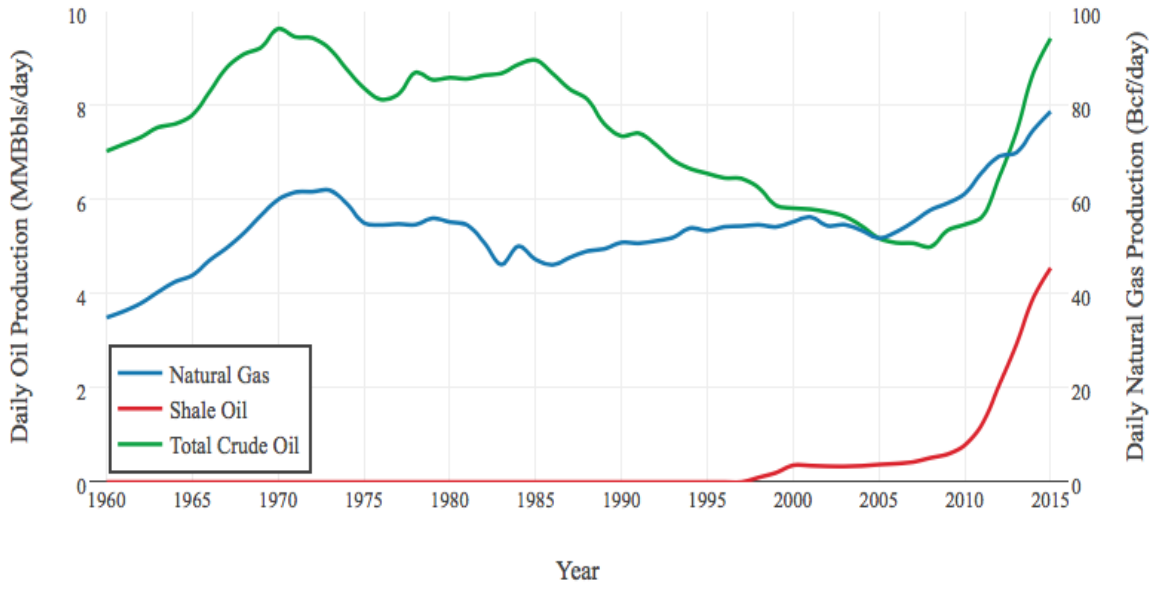

Figure 1-1: United States daily oil and gas production (US EIA, 2015)

Economic production from shale oil reservoirs such as the Bakken, which extends across Montana and North Dakota, the Eagle Ford in Texas, and the Spraberry, Bonespring and Wolfcamp plays in the Permian Basin which stretches across West Texas and Southeastern New Mexico, is accomplished by drilling long lateral horizontal wells with several stages of hydraulic fractures. However, because of the steep production decline behavior of hydraulically fractured wells (75% 2-year well decline rate) (Adekunle and Hoffman, 2014), primary depletion produces only 5 – 10% of the total oil in place, necessitating enhanced oil recovery methods to increase production (Shoaib and Hoffman, 2009). Chemical and gas (produced gas or CO_2) huff-and-puff have been used to increase shale oil production with varying degrees of success (Shuler et al., 2011, Yu et al., 2014).

Here, we propose a novel approach to increase oil recovery from shale oil reservoirs by thermal stimulation. Four potential mechanisms for thermal improved recovery from shale reservoirs are proposed and investigated using numerical reservoir simulation. First, solid kerogen in the rock matrix can be converted through a series of chemical reactions into oil and gas at elevated reservoir temperatures, which increases oil in place. Second, matrix porosity and permeability can increase as some of the rock grain volume (i.e. kerogen) is converted to fluid pore volume. Third, reduction in oil viscosity at elevated temperatures may aid recovery. Finally, heating of the oil may result in increased reservoir pore pressure, which may lead to increased production.

Chapter 2 provides background on the three most productive shale oil systems in the US, the motivation and goal of the proposed thermal stimulation process, as well as discusses efforts to improve recovery from shale reservoirs and thermal processes commonly applied. Chapter 3 describes in detail the approach taken to develop the fluid and reservoir models for a typical shale oil reservoir. Chapter 4 presents and discusses the results of a simplified preliminary study done to investigate the viability of the proposed thermal process. Chapter 5 builds on the work presented in Chapter 4 by excluding some of the simplifying assumptions made. Finally, Chapter 6 lists this study's conclusions and recommendations for future work.

Chapter 2: Background & Literature Review

2.1. BACKGROUND

This section contains information about the geologic and geographic setting of the three most productive shale oil producing regions in the US – the Eagle Ford, the Bakken and Spraberry in the Permian Basin as shown in Fig. 2-1. A description of kerogen, which is found in most shale reservoirs, is also provided.

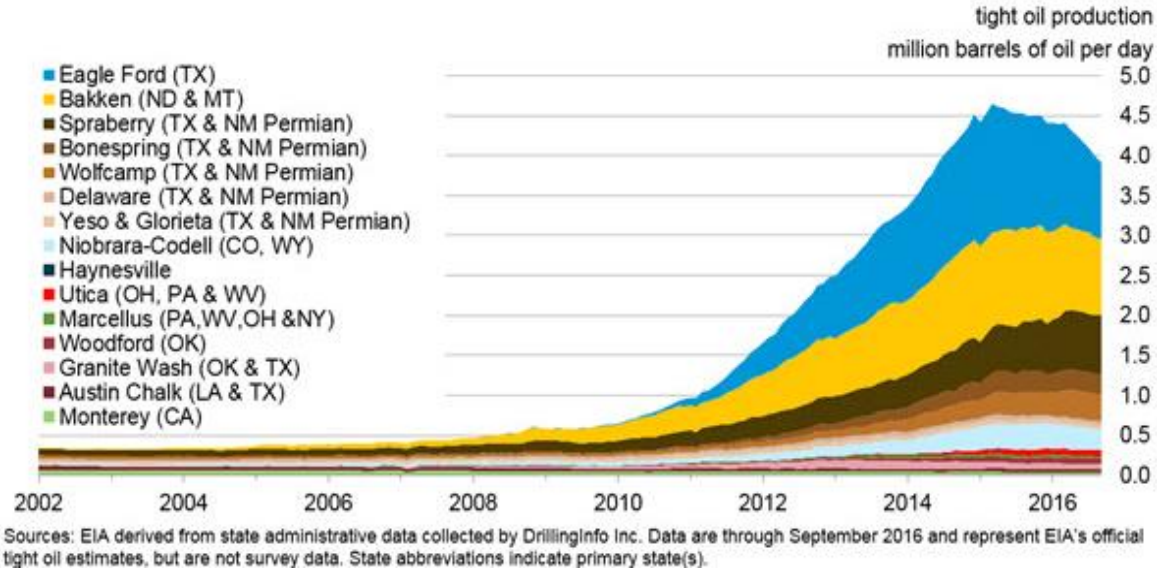

Figure 2-1: Most productive shale oil plays in the US (US EIA, 2016a)

2.1.1. The Eagle Ford Formation

The Eagle Ford shale formation was deposited during the late Cretaceous age over the region that is now Texas; it overlies the Buda limestone formation and is overlain by the Austin Chalk. Geographically, the Eagle Ford is 50 miles wide and 400 miles long, spanning 23 counties across Texas. It outcrops from the Mexican border north of the

Maverick basin through San Antonio, Austin and Dallas as shown in Fig. 2-2. The Eagle Ford shale consists of mudstone and carbonate with approximate mineral content of 20% quartz, 50% calcite, 20% clay and 10% kerogen (Martin et al., 2011).

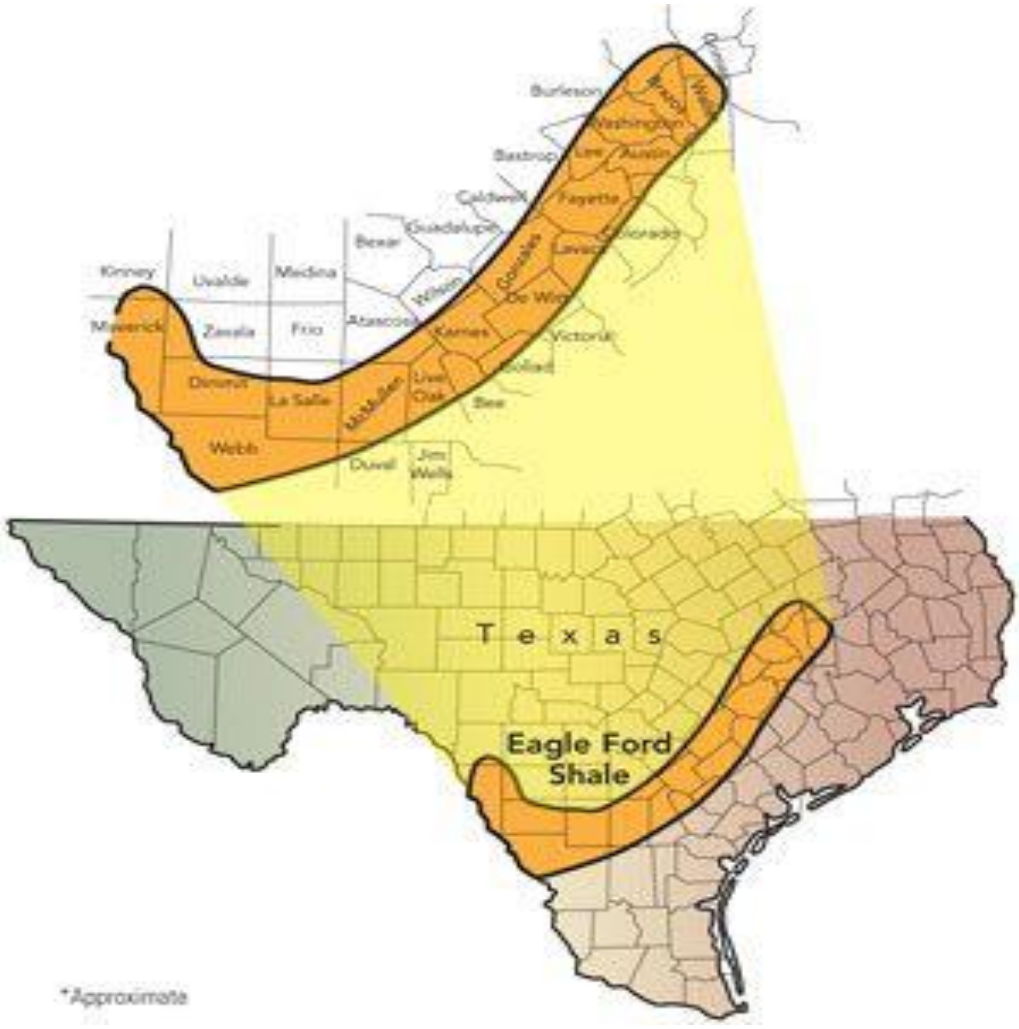

Figure 2-2: Map of part of Texas showing the Eagle Ford shale (Oil and Gas Journal)

The Eagle Ford shale consists of two components: upper and lower members or sections. The lower member consists of a marine interval with dark, well-laminated

organic rich shales. The upper member consists of interstratified calcareous shales, bentonites, limestones and quartzose siltstones. The thickness of both members combined varies between 50 ft. on the northeast side and 330 ft. on the southwest side with pay interval depth ranging between 1500 ft. and 14,000 ft. Porosity ranges between 3 and 10% and permeability is as low as 3 nD in certain parts of the Eagle Ford shale (Martin et al., 2011).

Production from horizontal wells in the Eagle Ford shale began in 2008 from a discovery well drilled by Petrohawk in southwest La Salle County. Oil production from the Eagle Ford is achieved by drilling horizontal wells with multiple hydraulic fracture stages. Early in Eagle Ford development, horizontal wells averaged 14 fracture stages per well; today, the average is 20 stages. The US EIA (2015) estimates oil and gas reserves in the Eagle Ford shale to be 5.17 billion barrels and 23.7 TCF respectively. Following the oil price decline at the end of 2014, rig count in the Eagle Ford fell from about 275 to fewer than 50. Consequently daily oil production fell from 1.75 MMbbls per day in 2014 to 0.9 MMbbls per day by the end of 2016. Similarly, daily natural gas production fell from 7.5 BCF per day to 5.5 BCF per day (EIA, 2016b).

2.1.2. The Bakken Formation

The Bakken formation was deposited around 360 million years ago during the late Devonian/early Mississippian age in the Williston Basin. It occupies about 225,000 square miles across Montana, North Dakota, South Dakota, and Manitoba and Saskatchewan in Canada. The Bakken formation overlies the Mississippian Lodgepole

Limestone and is overlain by the Devonian Three Forks Formation; together, these three components make up the Bakken Petroleum System. The Bakken Formation consists of three members: the Lower Bakken shale, the Middle Bakken and the Upper Bakken shale. The upper and lower members are organic rich marine shale (total organic carbon content can be as high as 36%) and serve as the source rock for the Middle Bakken member, which contains varying amounts of silt, sand, dolomite, limestone and clay. The Middle Bakken member has significantly lower total organic carbon content than its upper and lower counterparts; it is also believed to contain type II kerogen, which is oil prone (likely to generate oil during decomposition at elevated temperatures). The middle member has depths ranging from 9000 to 11,500 ft., thickness ranging from 10 to 92 ft. and permeability as low as 0.0003 mD in some regions. A map of the Williston Basin Province and the Bakken Petroleum System are shown in Fig. 2-3 (Theloy and Sonnenberg, 2013).

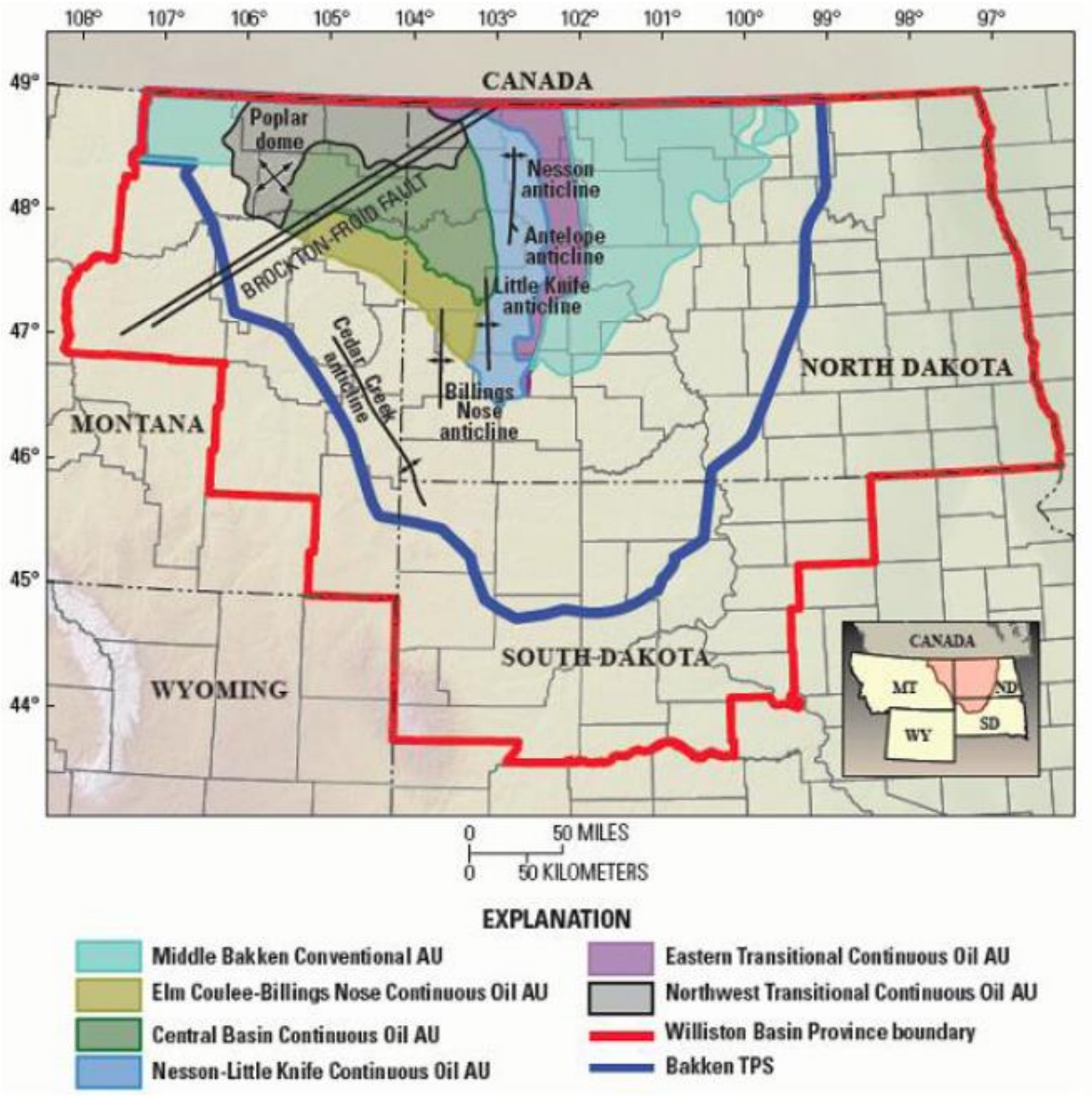

Figure 2-3: Map of the Williston Basin Province, showing the Bakken Total Petroleum System (US Geological Survey, 2013)

Oil production from the Bakken began in 1953 when the Antelope field was discovered. From 1953 to 1987 when the first horizontal well was drilled, 11.5 MMbbls of oil and 12.5 BCF of gas were produced from 165 vertical wells. In the 20 years after

the first horizontal well was drilled, 131.3 MMbbls of oil and 131 BCF of gas were produced. The EIA (2015) estimates oil reserves in the U.S. section of the Bakken shale to be 5.97 billion barrels. Following the oil price decline at the end of 2014, rig count in the Bakken fell from about 200 to fewer than 30, leading to a decline in oil production from 1.2 MMbbls per day to about 0.95 MMbbls per day (EIA, 2016b).

2.1.3. The Spraberry Formation

The Spraberry formation was deposited more than 250 million years ago during the Permian age. It is part of the Midland Basin within the Permian Basin and has a total area of approximately 2500 square miles spanning through portions of Irion, Reagan, Upton, Glasscock, Midland and Martin Counties in Texas. The Spraberry formation consists of three members: the upper Spraberry sand with average thickness of 250 ft., the middle Spraberry made up of calcareous shale with average thickness of 300 ft., and the lower Spraberry sandstone member with 450 ft. average thickness. Most wells in the Spraberry formation are completed in the upper Spraberry unit, which consists of fine sandstone and calcareous or silicate mudstone and siltstone deposited in a deep-water environment and interbedded with shaly non-reservoir rocks. The upper Spraberry unit has approximately 12.7% porosity, 0.1 – 0.5 mD permeability and 20 ft. pay thickness. The Spraberry trend is highlighted in Fig. 2-4 (Cather et al., 1998).

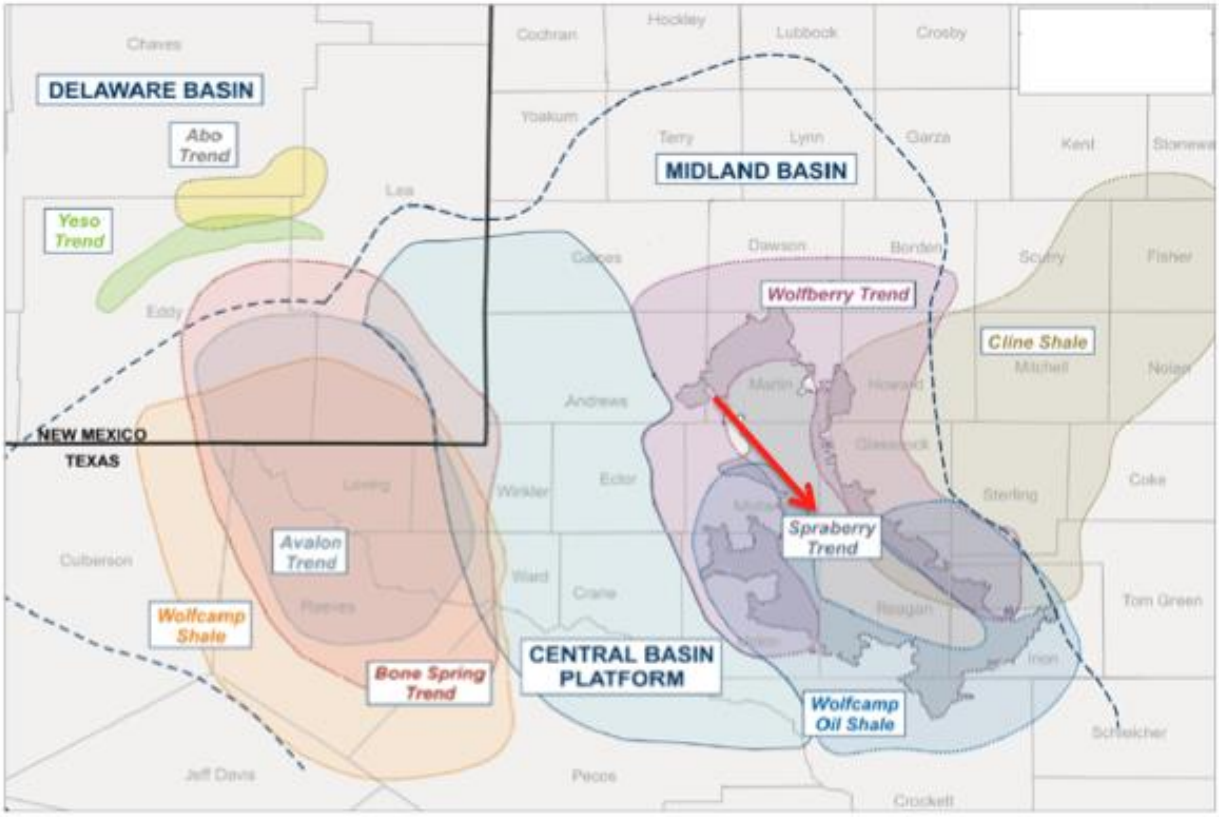

Figure 2-4: Map of the Permian Basin showing the Spraberry Trend (shaleexperts.com)

Oil production from the Spraberry formation began in 1943 but did not reach commercial quantities until 1949 when Seaboard Oil Company drilled a well that produced 320 bbls per day. By 1951, there were approximately 230 drilling rigs and 987 producing wells in the Spraberry formation, driving cumulative oil production to 12.1 MMbbls by the end of 1951 (Christie and Blackwood, 1952). As of 2009, there were more than 9000 wells producing 125 Mbbls per day from the Spraberry formation; today average daily oil production is more than 730 Mbbls per day (EIA, 2016a).

2.1.4. Kerogen

Kerogen is a solid mixture of organic matter found in source rock that produces oil when exposed to high pressures and temperatures encountered during burial over time. In cases where pressure and temperature are not sufficiently high to generate oil, the kerogen remains as part of the source rock and can be mined if shallow or converted to oil in the ground by heat injection. Kerogen can be classified into three groups depending on the hydrogen to carbon (H/C) ratio and oxygen to carbon (O/C) ratio. Type I kerogen is characterized by high aliphatic structure with H/C ratio greater than 1.5 and O/C ratio between 0.03 and 0.1. Type II kerogen is characterized by more cyclic aliphatic structure and large amount of aromatics with H/C ratio around 1.3 and O/C ratio around 0.15. Finally, Type III kerogen contains predominantly aromatic structures and long chain aliphatic structures with H/C ratio less than 0.8 and O/C ratio around 0.25. Type I and II kerogen are prone to oil generation at elevated temperatures over time, while Type III kerogen is gas prone.

Kerogen is commonly found in oil shale, as well as the shale oil reservoirs that are studied in the following chapters. Oil shale, such as in the Green River formation, is an organic-rich sedimentary rock containing significant amounts of kerogen (greater than 20% by weight) and no initial mobile oil. Oil production is achieved by heating the kerogen to convert it to oil. Shale oil reservoirs, such as the Bakken, Eagle Ford and Spraberry formations, are different in that they are low permeability reservoirs with initial mobile oil and low kerogen concentration (lower than 10% by weight).

2.2. Motivation For Enhanced Recovery In Shale Reservoirs

Despite the vast amount of oil present in shale reservoirs, recovery is limited by the extremely low permeability of the reservoir rock. Primary depletion only recovers 5 – 10% of oil in place, which is significantly lower than the 15 – 25% observed in conventional reservoirs. Adekunle and Hoffman (2014) estimate that the average Bakken well experiences a 75% two-year decline in oil production rate due to depletion of the natural reservoir drive (Fig. 2-5).

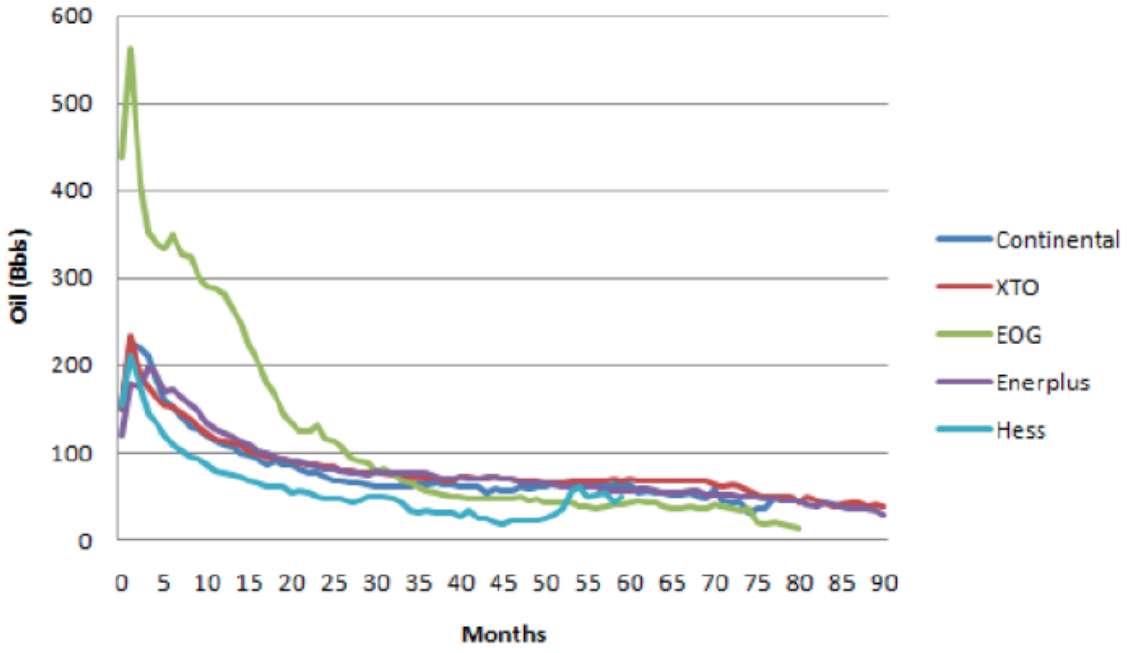

Figure 2-5: Steep production decline of different operators in the Bakken (Adekunle and Hoffman, 2014)

Similarly, Eagle Ford wells experience an 80% two-year decline in oil production rate (Martin et al., 2011). Fig. 2-6 illustrates this steep decline in average production rate for 38 wells in the Eagle Ford. Wells drilled in conventional reservoirs, such as the Gulf

of Mexico (GOM), experience a more gradual decline in production. Fig. 2-7 compares production for three classes of GOM wells: Class 15 wells with expected ultimate oil recovery (EUR) of approximately 900,000 bbls, Class 12 wells with EUR of about 450,000 bbls, and Class 9 wells with EUR around 270,000 bbls. A more gradual production decline is observed for GOM wells than for Bakken and Eagle Ford wells; moreover, class 15 GOM wells have fairly constant oil rate for the first four years of production (US Geological Survey, 1985).

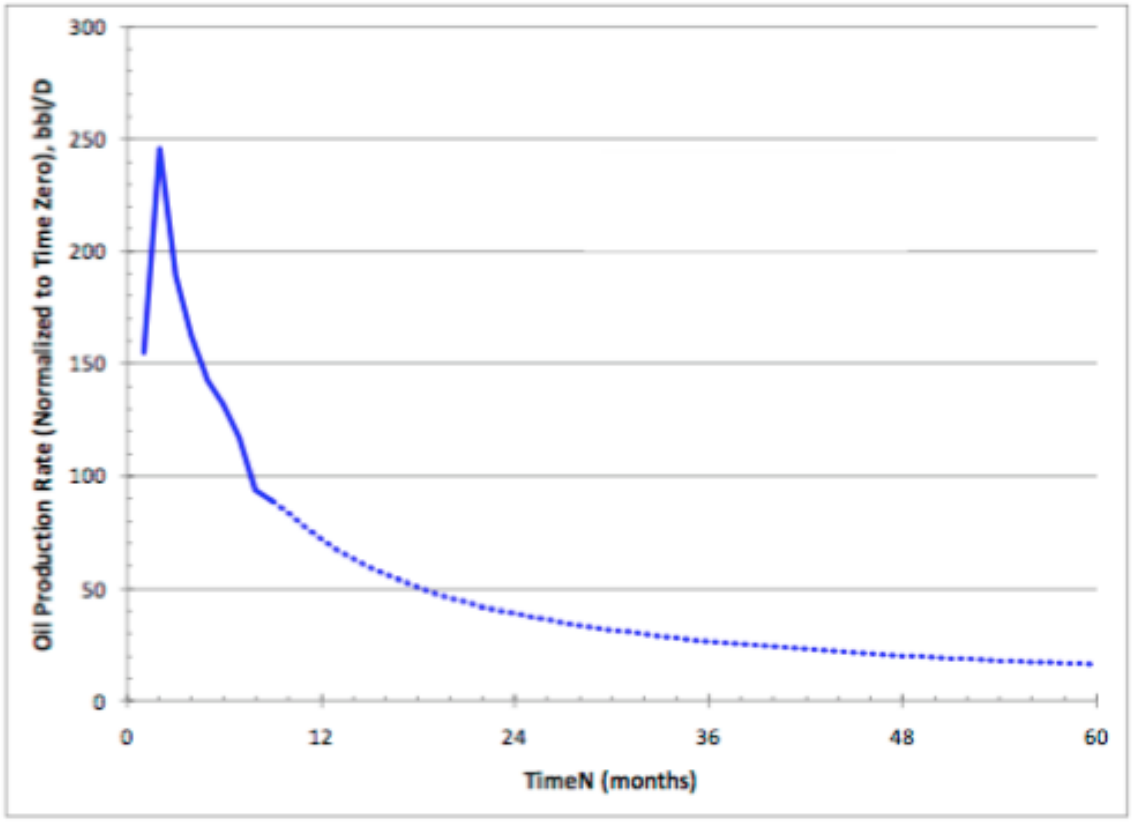

Figure 2-6: Steep average production decline for 38 Eagle Ford wells (Martin et al., 2011)

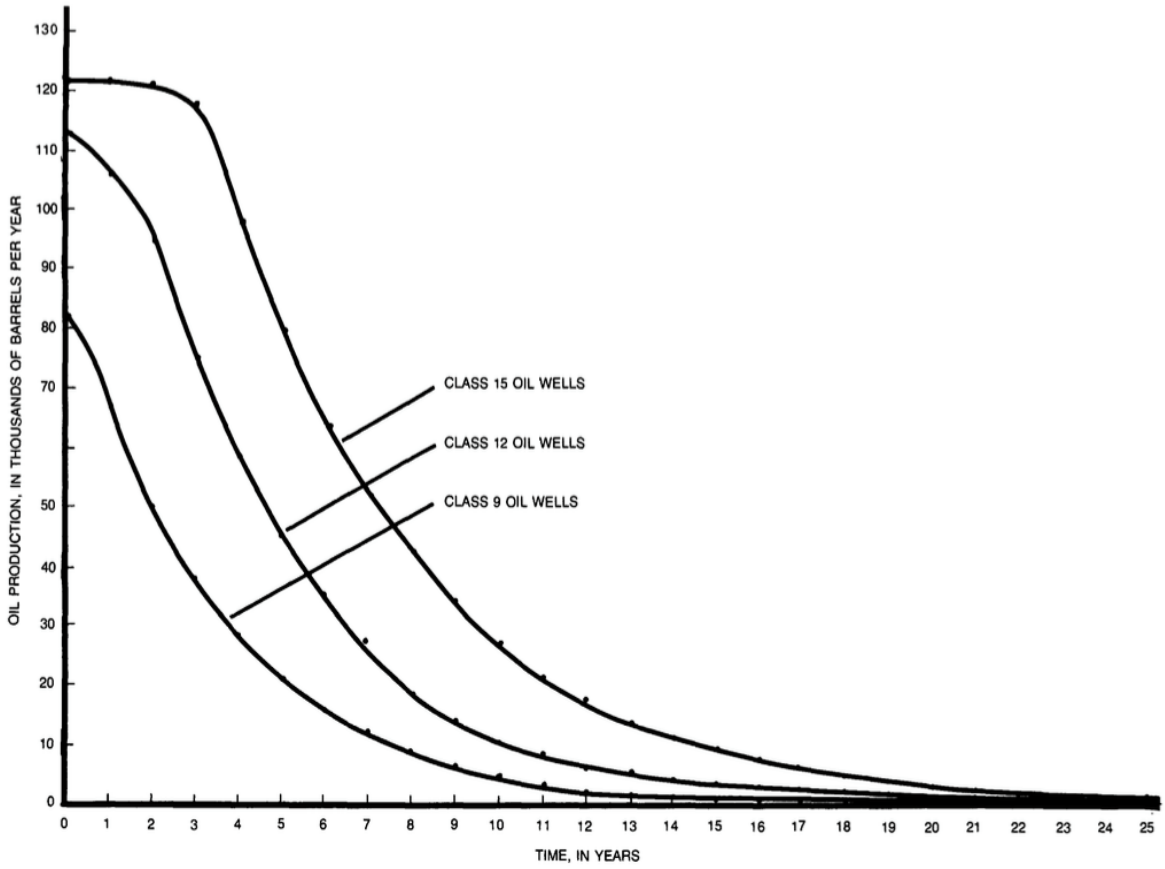

Figure 2-7: Production decline trend for wells in the Gulf of Mexico (US Geological Survey, 1985)

Furthermore, average oil production from the more than 10,000 wells operating in the Bakken is 87 bbls per day; average oil production from the more than 10,000 wells in the Eagle Ford is about 90 bbls per day, which is significantly lower than the average production rate of wells in the Gulf of Mexico (160 bbls of oil per day, with some wells producing as high as 90,000 bbls of oil per day) (EIA, 2016b).

There is potential for significant improvement in oil recovery from shale reservoirs. Because of the large amount of oil reserves in these shale reservoirs, a small increase in recovery could translate into millions of additional barrels of oil.

Waterflooding is not a viable strategy for improving recovery from shale reservoirs because of poor injectivity in these ultralow permeability formations, hence, enhanced recovery techniques must be considered.

2.3. OBJECTIVE

The objective of this study is to demonstrate the potential for thermal stimulation to improve oil recovery from shale reservoirs, and to optimize components of the thermal stimulation design. The proposed strategy involves a period of primary depletion, followed by a period of heat injection from the same well, and finally secondary depletion. The hypothesis is that temperature elevation over time will improve oil recovery by the following mechanisms:

1. Oil viscosity reduction.
2. Thermal pressurization (pore pressure increase resulting from heating a fluid in a fixed pore volume).
3. Increase in oil in place resulting from kerogen decomposition.
4. Increase in porosity and permeability as solid rock volume in the form of kerogen is converted to fluid pore volume.

Furthermore, a numerical reservoir model has been developed to study several components of the proposed thermal stimulation design, such as:

1. The length of the primary depletion period.
2. The length of the heat injection period.
3. The heat injection temperature.
4. The conductivity of the shale matrix.
5. The kerogen reaction parameters (activation energy and reaction frequency factor).

6. The relationship between reservoir thickness and heat loss.
7. Simultaneous heat injection and oil production.

Ultimately, the goal of any oil and gas project is to maximize revenue; thermal stimulation projects often require large amounts of energy and involve a significant amount of heat loss from the wellbore and to the overburden and underburden, consequently, special attention has been paid to minimizing energy cost per barrel of oil produced while investigating viability and optimizing the thermal stimulation design. The proposed method of heating is high frequency electromagnetic heating using downhole heaters.

2.4. LITERATURE REVIEW

This section reviews the existing literature on enhanced oil recovery from shale reservoirs, as well as, literature on thermal recovery from heavy oil reservoirs and oil shale.

2.4.1. Enhanced Oil Recovery In Shale Reservoirs

Chemical and gas enhanced recovery techniques have been extensively investigated as means of improving oil recovery from shale reservoirs. Gamadi et al. (2013) conducted an experimental study on Barnett, Marcos and Eagle Ford shale core plugs to verify and quantify the potential for cyclic gas injection (huff-and-puff) to improve oil recovery from shale oil reservoirs. Huff-and-puff involves injection of gas into a single well, followed by a shut-in period to allow the gas to dissolve into the oil, and finally production is resumed. The mechanisms involved in enhancing recovery during huff-and-puff include oil viscosity reduction, oil swelling, relative permeability hysteresis, wettability alteration, repressurization, diffusion, and interfacial tension reduction. Gamadi et al.'s (2013) experimental study found that cyclic gas injection using nitrogen could improve recovery from 10 to 50% depending on the shale core sample.

Song and Yang (2013) investigated the performance of four recovery schemes for tight reservoirs: waterflooding, immiscible CO_2 huff-and-puff, near-miscible CO_2 huff-and-puff, and miscible CO_2 huff-and-puff. The near-miscible and miscible CO_2 huff-and-puff resulted in the highest recovery efficiency – greater than 60% recovery for the core samples tested.

Wang et al.'s (2010) simulation results showed that CO_2 injection has the potential to improve Bakken oil recovery from 3.6 to 34% after 100 years of production. Furthermore, continuous CO_2 injection outperformed cyclic CO_2 injection but required a significantly greater amount of gas.

Hoffman (2012) used numerical simulations to study the impact of different gas injection schemes (CO_2, miscible hydrocarbon gas and immiscible hydrocarbon gas) on oil recovery from a 4-section area of the Elm Coulee field in the Bakken. He discovered that both miscible hydrocarbon gas and CO_2 have the potential to increase recovery from 6 to 20%. Hoffman (2012) also highlighted limitations to gas injection, including the unavailability of CO_2 in many basins and while miscible hydrocarbon gas is readily available, it is rarely used as injection gas because of its marketability.

Chen et al. (2014) studied the effect of reservoir heterogeneity on CO_2 huff-and-puff performance and found that reservoir heterogeneity leads to faster oil rate decline in the production stage. They also found that huff-and-puff recovery in a heterogeneous reservoir is lower than recovery from primary depletion because the incremental recovery in the production stage is not sufficient to compensate for lost production during injection and soaking.

Yu et al. (2014) found from simulation studies that CO_2 huff-and-puff works best with two effective hydraulic fractures within one perforation stage and that the most important design parameters for the process are CO_2 injection rate, injection time, number of cycles and CO_2 diffusivity. Sanchez-Rivera et al. (2015) also used simulation

studies to study various design components of the huff-and-puff process in order to identify the parameters with the largest impact on recovery and understand the reservoir's response to cyclical gas injection. The study found that huff-and-puff works best in reservoirs with extensive natural fracture networks to allow CO_2 to migrate deep into the formation; the study also found that starting huff-and-puff too early in the life of the reservoir and longer soaking periods diminish the effectiveness of the huff-and-puff process.

Zhu et al. (2015) proposed a recovery scheme for ultralow permeability shale where CO_2 is injected into a hydraulic fracture and oil is produced from an adjacent fracture propagating from the same well. Simulation results showed that this recovery scheme has the potential to recover an incremental 15.7% of original oil in place in low permeability oil reservoirs.

Shuler et al. (2011) conducted an experimental study on chemical improved oil recovery in Bakken shale core samples. They found that including specialized surfactant formulations in an aqueous phase, such as hydraulic fracturing fluid, promotes the spontaneous imbibition of the fluid into the mixed- to oil-wet rock matrix and microfractures containing high oil saturation, which forces trapped oil to migrate into the fracture network and flow into the wellbore. Lab tests showed that surfactant has the potential to improve oil recovery from a Bakken core sample from 3 to 40%.

Dawson et al. (2015) developed full scale models by incorporating field-scale fracture characterization into upscaled lab-based models to investigate the potential of

well-to-well surfactant flooding in the Bakken. The scheme involved primary depletion for 12.5 years, followed by conversion of a producer to a surfactant injector, while production uplift is monitored for the next 12.5 years. Dawson et al. (2015) suggest that nonionic surfactant production enhancer blended into a full chemical system has the potential to double oil recovery by permanently altering the wettability of the rock from oil- to water-wet. The mechanism of wettability alteration involves the hydroxyl functional group in alcohol-containing nonionic surfactant interacting with positive surface charges on the rock, reducing the electrostatic attractive forces between the rock and the oil and releasing the polar oil component from the surface of the rock.

Kim et al. (2016) used nuclear magnetic resonance detection and spontaneous water imbibition testing to investigate two effects of surfactants in Eagle Ford core samples: improved flow back to the surface resulting from reduced interfacial tension, and improved oil recovery resulting from wettability alteration. The Eagle Ford cores were treated with four surfactants – S1 (cationic microemulsion and flow back surfactant), S3 (nonionic microemulsion flowback additive), S4 (nonionic enhanced flowback surfactant), and S6 (nonionic enhanced oil recovery surfactant for carbonates). The core treated with S3 had the best ultimate recovery – 30.5% of original oil in place after 15 days, while the core treated with S1 had the best flowback performance, recovering 15.8% of treatment fluid.

Delamaide et al. (2014) highlight some issues with chemical enhanced oil recovery in low permeability reservoirs: chemical retention, chemical degradation and poor injectivity. In low porosity media, polymer retention as a result of adsorption, mechanical entrapment or hydrodynamic retention may completely or partially plug the reservoir. The use of surfactant can create high viscosity microemulsions, which cause injectivity problems.

2.4.2. Thermal Recovery

Thermal recovery has traditionally been used to reduce oil viscosity and improve recovery from heavy oil reservoirs. Additionally, thermal stimulation has been applied in oil shale to generate oil from kerogen.

Prats (1982) traces the development of thermal simulation to the 1950s and the advent of in-situ combustion. Ramey (1971) describes the in-situ combustion process as the injection of air or any suitable oxidizing gas into a formation, followed by the ignition of oil at the injection well, which creates a burning front that moves in the direction of gas flow. The oil is driven toward the producers by a combination of gas, steam and water drives.

Alvarez and Han (2013) describe another method of thermal stimulation called cyclic steam injection as the periodic injection of steam, in which one well serves as both producer and injector. Steam is injected into heavy oil reservoirs to elevate temperature and reduce oil viscosity, and to induce thermal and solution gas expansion drive. When enough steam has been injected to a point at which the oil flows, the well is shut-in to allow the steam to soak for a few days. Finally, the well is opened and the oil flows out through the producers. During production, reservoir temperature decreases and another steam injection cycle is repeated when oil flow rate is significantly reduced; cycles are repeated until steam injection becomes uneconomical. This method of thermal stimulation has been shown to improve heavy oil (greater than 10 API gravity, 1000 – 4000 cp viscosity) recovery in shallow, thick reservoirs from 15 to approximately 40%.

Steam flooding is another thermal recovery strategy used in heavy oil reservoirs. In steam flooding, steam is introduced through injection wells to reduce oil viscosity and displace the oil toward the production well. The steam, as well as the hot water that condenses from the steam, displaces the oil toward producers. Steam floods have been shown to improve oil recovery to 50 – 60% of original oil in place in the Kern River and Duri oil fields (Alavarez and Han, 2013). Furthermore, a number of companies, such as Imperial Energy, have demonstrated that a combination of steam flood with solvent injection results in 15 – 25% reduction in steam-oil ratio and improved oil production rates.

Butler et al. (1981) proposed a thermal recovery process for heavy oils by steam-assisted gravity drainage (SAGD), in which a pair of horizontal wells is drilled into the reservoir with one well (injector) a few meters above the other (producer). In SAGD, steam is injected into an expanding steam chamber formed above a horizontal production well. Steam flows to the edge of the chamber and condenses, heating the oil, which drains from around the chamber walls to the oil producer below. SAGD has been successfully applied in heavy oil reservoirs to recover 60 – 70% of original oil in place.

Steam assisted heating processes are limited to shallow and thick reservoirs because the heat loss from the wellbore and to the overburden and underburden are limited. If the reservoir depth is greater than about 4000 ft. (such as the shale reservoirs studied here), heat loss from the wellbore makes injection of steam from the surface uneconomical. Furthermore, as depth increases, the reservoir pressure increases and the

latent heat of the steam decreases. Thus, steam processes are typically not applied to deep reservoirs. It is possible to use down-hole steam generators for deeper reservoirs, but these generators are not commonly used because of high maintenance costs and combustion control problems downhole (Singh et al., 1988). Additionally, injected steam and water from condensation reduce relative permeability of oil in the pore space.

Thermal recovery techniques have also been used for in-situ conversion of kerogen in oil shale to generate oil at approximately 650 °F. Shell has tested this strategy in the Green River formation in Wyoming. Shell's in-situ conversion process (ICP) works by using a pattern of closely spaced electric heaters to gradually and uniformly heat the high kerogen concentration oil shale to about 650 °F, where kerogen conversion takes place; at this temperature, long chain kerogen molecules are cracked into smaller oil, water and gas molecules, which flow out from producers (Fowler and Vinegar, 2009). The shale oil reservoirs studied here are different from the heavy oil and oil shale reservoirs discussed in the literature in that shale oil reservoirs are low viscosity, low permeability reservoirs with low kerogen concentration.

The proposed heating method in this study is high-frequency electromagnetic heating. Carrizales et al. (2010) describe electromagnetic heating as the introduction of current in the kHz to MHz range into the reservoir from a radiating element located in the horizontal section of the wellbore; this energy is converted into heat within the formation through the absorption of electromagnetic energy by polar molecules such as connate water in the formation.

Chapter 3: Modeling Approach

The reservoir model built for this study was composed of three parts: a fluid characterization, a computational domain, and kerogen reaction parameters. This chapter describes the modeling approach taken to construct these components.

3.1. Fluid Characterization

A description of fluid behavior for varying pressure and temperature is an important component of the reservoir model in this study. PVT and compositional data for a Bakken fluid sample at pressure of 6840 psi and temperature of 241 °F were obtained and a fluid model was generated in CMG WinProp. This section details the generation and tuning of the fluid model to match experimental data.

Compositional simulations typically require a large number of flash calculations; in order to reduce computational effort, several individual components are lumped into pseudocomponents. Pedersen et al. (2007) define lumping as "deciding what carbon number fractions to group into the same pseudocomponents, and averaging the critical temperature (T_c), critical pressure (P_c) and acentric factor (ω) of the individual carbon number fractions into one T_c, P_c and ω representative of the whole lumped pseudocomponent." Generally, defined components, which are pure components whose properties have been experimentally measured, are reported as individual components; these include N_2, CO_2, C_1, C_2, C_3, iC_4, nC_4, iC_5, nC_5, and C_6. Zhu et al. (2015) obtained compositional data for a Bakken fluid sample taken at a depth of 5000 ft., pressure of 6840 psi and temperature of 241 °F. The compositional data for the fluid sample was

provided with defined components expressed as individual components and C_{7}+ fractions lumped into five pseudocomponents: $C_7 - C_{10}$, $C_{11} - C_{14}$, $C_{15} - C_{19}$, $C_{20} - C_{29}$ and C_{30}+. The data retrieved from Zhu et al. (2015), which includes molar fraction, molecular weight, critical properties and volumetric shift of components and pseudocomponents, is presented in Table 3-1.

Table 3-1: Compositional data for Bakken fluid sample

Component	Mole %	Mol. weight	Critical T, T_c (°F)	Critical P, P_c (psi)	Acentric factor, ω	Vol. shift (ft^3/lb-mol)
N2	1.509	28.014	-232.51	492.32	0.04	-0.0678
CO2	0.388	44.01	87.89	1069.87	0.225	-0.0263
C1	34.698	16.043	-116.59	667.2	0.008	-0.0833
C2	14.485	30.07	90.05	708.35	0.098	-0.0927
C3	9.327	44.097	205.97	615.76	0.152	-0.1
iC4	1.21	58.124	274.91	529.06	0.176	-0.12
nC4	4.536	58.124	305.69	551.1	0.193	-0.1
iC5	1.232	72.151	369.05	490.85	0.227	-0.0993
nC5	2.365	72.151	385.61	489.38	0.251	-0.082
C6	2.804	86.178	453.65	430.59	0.296	0.0223
C7-C10	12.245	111.803	572.26	401.11	0.3955	0.0977
C11-C14	5.983	165.572	718.62	306.93	0.56	0.19
C15-C19	3.787	231.329	862.53	254.08	0.7394	0.21
C20-C29	3.032	324.935	1040.44	219.26	0.9462	0.14
C30+	2.399	545.7	1389.95	190	1.0956	-0.24

The volumetric shift parameter is a correction introduced in order to improve the accuracy of volumetric predictions made from equations of state (EOS). CMG WinProp allows for creation of fluid models using either the Peng-Robinson or the Soave Redlich-Kwong EOS. Compositional data for the Bakken fluid sample was used to create a fluid model in CMG WinProp using the Peng-Robinson EOS (Eq. 3.1 – 3.5).

$$P = \frac{RT}{V_m - b} - \frac{a\alpha}{V_m^2 + 2bV_m - b^2} \tag{3.1}$$

$$a = \frac{0.457 R^2 T_c^2}{P_c} \tag{3.2}$$

$$b = \frac{0.0078 R T_c}{P_c} \tag{3.3}$$

$$\begin{aligned} \alpha &= \left(1 + \kappa\left(1 - T_r^{0.5}\right)\right)^2 \\ T_r &= T \big/ T_c \end{aligned} \tag{3.4}$$

$$\kappa = 0.375 + 1.542\omega - 0.269\omega^2 \tag{3.5}$$

where R is the universal gas constant, P is pressure, T is temperature, Z is compressibility factor, and V_m is molar volume.

Sanchez-Rivera et al. (2015) obtained experimental measurements of Bakken fluid properties at pressure of 6840 psi and temperature of 241 °F (initial reservoir conditions); these can be seen in Table 3-2. The fluid model created in CMG WinProp was tuned in order to match the provided fluid data at the given pressure and temperature.

Table 3-2: Experimental data for Bakken fluid sample at initial reservoir conditions

Property	Value
Oil viscosity (cp)	0.25
Fluid compressibility psi^{-1}	1.5×10^{-5}
Oil formation volume factor (rb/stb)	1.71
Oil density (lb/ft^3)	39.56
Bubble point (psi)	2872

CMG WinProp's regression tool for model tuning uses Agarwal regression procedure to tune selected EOS parameters to match experimental measurements. CMG Winprop's User Guide describes the procedure as follows: the specified list of EOS parameters is ordered such that the most sensitive parameter is used first, then regression is performed on a group of five parameters. Once a parameter reaches its maximum or minimum limit, or does not contribute to improving the match, it is replaced by the next parameter on the list. Table 3-3 compares the experimentally determined fluid properties to WinProp's pre-tuning predictions.

Table 3-3: Comparison of PVT behavior between fluid sample and initial fluid model

Property	Sample	WinProp Model	Error %
Oil viscosity (cp)	0.25	0.11	56.04
Fluid compressibility psi^{-1}	1.5×10^{-5}	1.3×10^{-5}	16.28
Oil formation volume factor (rb/stb)	1.71	1.71	1.72
Oil density (lb/ft^3)	39.56	40.3	2.25
Bubble point (psi)	2872	2600	12.01

In this study, the following parameters were selected for regression.

a. Critical pressure of pseudocomponents
b. Critical temperature of pseudocomponents
c. Acentric factor of pseudocomponents
d. Molecular weight of pseudocomponents
e. Volumetric shift parameter of all components
f. Exponent for calculating HC-HC binary interaction coefficients

We chose to optimize critical properties of the pseudocomponents because critical properties for the pure components have been experimentally determined, while the pseudocomponents are uncertain and must have been calculated by Zhu et al. (2015) from correlations and with specific assumptions. Table 3-4 compares the experimentally determined fluid properties to WinProp's tuned predictions.

Table 3-4: Comparison of PVT behavior between fluid sample and tuned fluid model

Property	**Sample**	**WinProp Model**	**Error %**
Oil viscosity (cp)	0.25	0.31	24.11
Fluid compressibility psi^{-1}	1.5×10^{-5}	1.3×10^{-5}	15.38
Oil formation volume factor (rb/stb)	1.71	1.71	0.00
Oil density (lb/ft^3)	39.56	40.3	1.84
Bubble point (psi)	2872	2600	10.46

WinProp was able to generate a good match to the fluid sample data. The discrepancy between the WinProp model and experimental fluid sample data is a result of

using compositional data from Zhu et al. (2015) to match experimental fluid sample data from Sanchez-Rivera et al. (2015); the fluid samples could have been obtained from different parts of the Bakken.

WinProp also generates viscosity versus temperature tables at different pressures using the WinProp viscosity model. The WinProp viscosity model locates two temperatures for each fluid component at which the component is in its liquid state; the viscosities at these two temperatures are extrapolated over all temperatures in the viscosity-temperature table. Fig. 3-1 illustrates variation of oil viscosity with temperature at initial reservoir pressure.

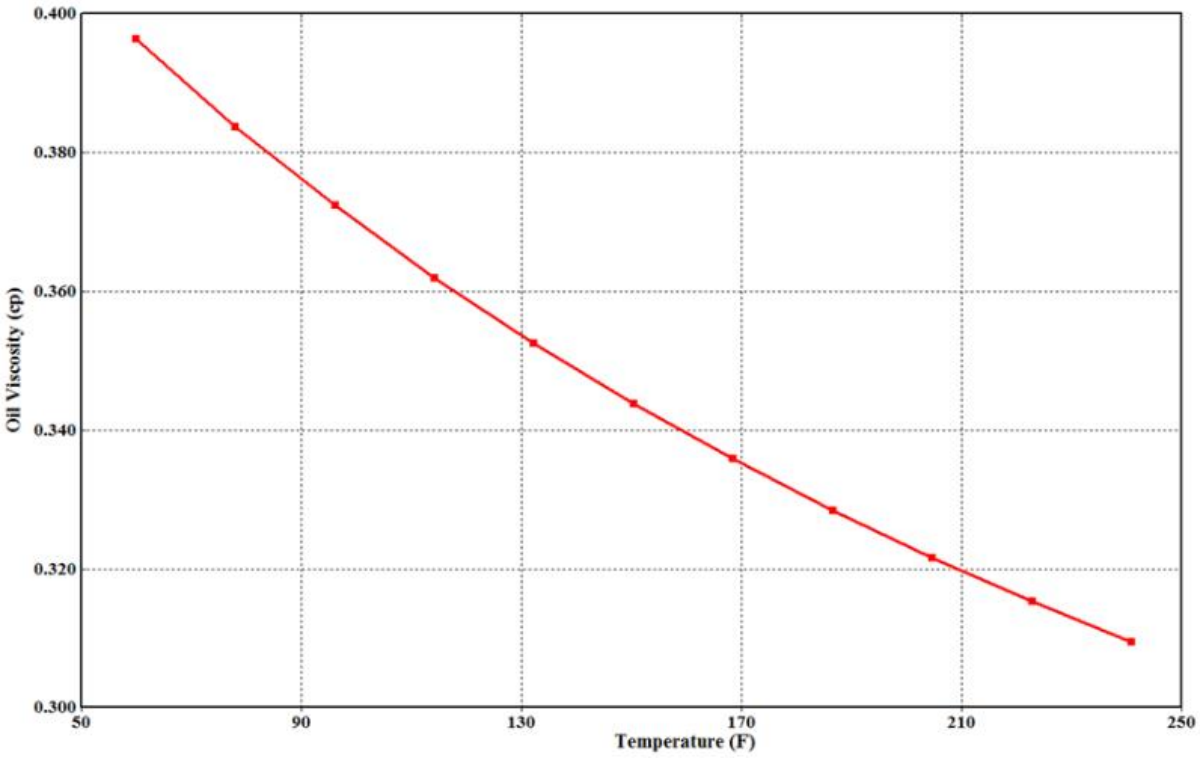

Figure 3-1: Lower oil viscosity at higher temperatures

3.2. COMPUTATIONAL DOMAIN

Defining a computational domain is an important step in reservoir modeling; the computational domain is a representative section of the reservoir to be analyzed. Conclusions drawn from studying the computational domain can be extrapolated to understand/predict field behavior. In this section, reservoir properties of the Bakken were assumed to be typical of most shale reservoirs.

This study's domain, illustrated by the shaded area in Fig. 3-2, is centered around one wing of a hydraulic fracture propagating from a horizontal well; in the x-direction, the domain runs along the wellbore, with left and right boundaries located halfway between two adjacent fractures; in the y-direction, the domain runs from the wellbore to the midpoint between the wellbore and an adjacent well. The domain is at a single-fracture stage scale, incorporating near wellbore activity and fluid behavior in the near fracture region, while also allowing for the application of field operating conditions and extrapolation of results to a larger field scale.

Fig. 3-2 shows a section of two horizontal wells with well spacing of 500 ft. and fracture half-length of 200 ft. The wells have a 6000 ft. lateral with 30 single-cluster fracture stages, giving a fracture spacing of 200 ft. The domain has no-flow boundaries on the sides and bottom, allowing for symmetry when extrapolating results to the larger field scale.

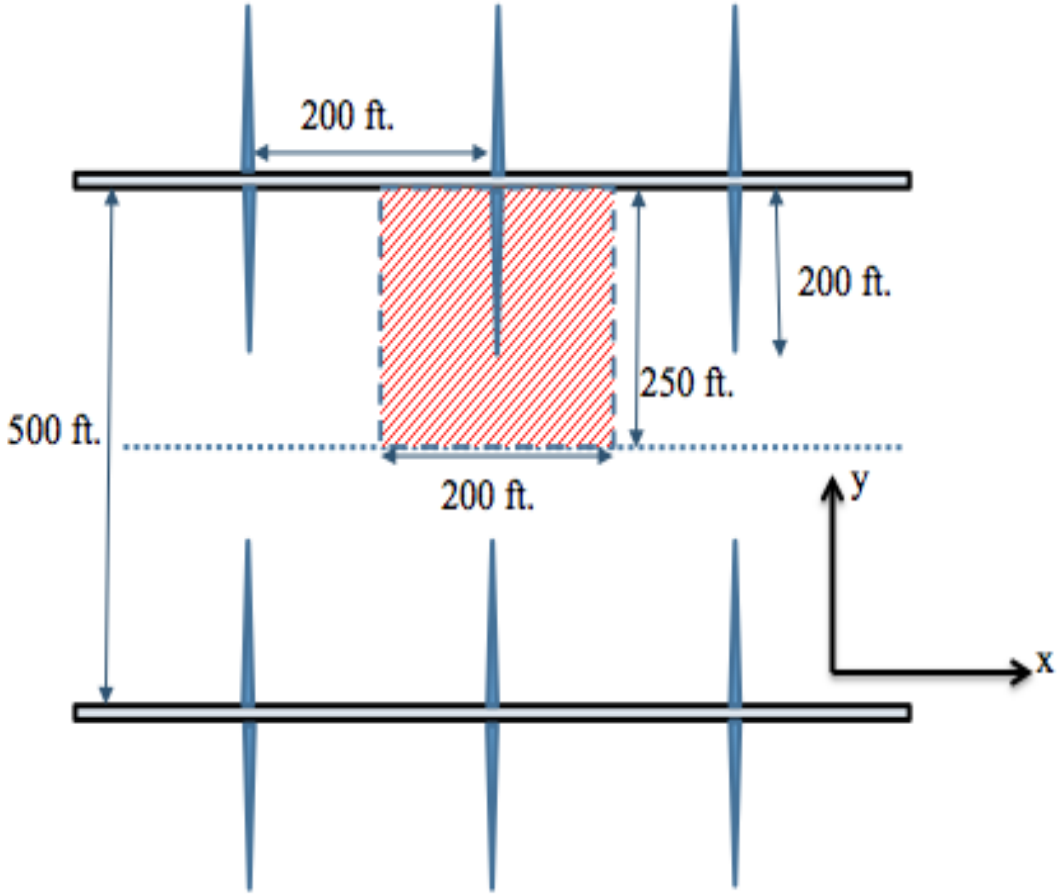

Figure 3-2: Computational domain (shaded area) between two horizontal wells and symmetric around a hydraulic fracture

The thickness of the Bakken formation varies from 0 to 70 ft. across the Williston Basin, so we assign a thickness (z-direction) of 10 ft. similar to the thickness implemented in Sanchez-Rivera et al. (2014) and Chen et al.'s (2013) studies. The depth of the Bakken (9500 ft.) gives rise to high reservoir temperatures in the 240 °F range and initial pressure of 6840 psi (Adekunle and Hoffman, 2014). Kerogen concentration from pyrolysis studies on Bakken samples reported by Vernik et al. (1990) is in the 6 – 15 wt-

% range. The following subsections discuss the modeling of key reservoir properties such as porosity, permeability, relative permeability, thermal properties and fractures.

3.2.1. Reservoir Porosity and Permeability

Most studies performed in the Bakken have measured or determined similar formation porosity. Li et al. (2015) used nuclear magnetic resonance (NMR) and Dean-Stark core analysis to determine 4 – 9% porosity for Bakken rock. Vargas et al. (2015) measured the porosity of over 200 core samples using nuclear magnetic resonance, gas expansion, radius of investigation, pressure build-up and pressure pulse-decay methods, giving an average porosity of 4.1%. Sanchez-Rivera et al. (2015) used 8% porosity in their Bakken huff-and-puff optimization study. Shoaib and Hoffman (2009), Chen et al. (2013) and Wang et al. (2010) also used similar porosity values in their Bakken studies (7.5%, 8% and 7.5% respectively). A porosity value of 8% was used in this study. Table 3-5 summarizes different porosity values used in previous studies.

Table 3-5: Comparison of porosity from various Bakken studies

Study	**Porosity**
Shoaib and Hoffman (2009)	7.5%
Wang et al. (2010)	7.5%
Chen et al. (2013)	8%
Sanchez-Rivera et al. (2015)	8%
Li et al. (2015)	4 – 9%
Vargas et al. (2015)	4.1%

Permeability in the Middle Bakken, as reported by various studies, varies between 0.0003 and 0.05 mD. Li et al. (2015) found the Klinkenberg-corrected permeability to be in the range of 0.0003 to 0.002 mD using pulse-decay and steady state permeability measurements for various Bakken core samples. In their Bakken CO_2 huff-and-puff studies, Chen et al. (2013) and Yu et al. (2014) used 0.01 mD and 0.005 mD respectively. Kurtoglu and Kazemi (2012) postulate that field measurements of permeability in the 0.01 mD range likely include the effect of natural fractures, which are important flow paths for fluids in the Bakken. A permeability value of 0.0015 mD, within the range given by Li et al. (2015), was used in this study. The porosity and permeability assigned to natural and hydraulic fractures will be discussed in a later section. Table 3-6 summarizes different permeability values used in previous studies.

Table 3-6: Comparison of porosity from various Bakken studies

Study	**Permeability (mD)**
Shoaib and Hoffman (2009)	0.015
Wang et al. (2010)	0.04
Chen et al. (2013)	0.01
Sanchez-Rivera et al. (2015)	0.01
Yu et al. (2014)	0.005
Li et al. (2015)	0.0003 – 0.05

3.2.2. Relative Permeability

Relative permeability is an important component of reservoir models. Because of the ultralow permeability of shale reservoirs, it is difficult to measure relative permeability in shale core samples by conventional methods. Previous studies in Bakken shale have estimated relative permeability by different means. Yu et al. (2014) obtained water-oil and liquid-gas relative permeability curves for the Bakken by tuning the curves to match production history. Wang et al. (2010) calculated Bakken relative permeability curves based on correlations for water-wet dolomite rocks, followed by tuning to match production history. Shoaib and Hoffman (2009) and Chen et al. (2013) make assumptions about Bakken relative permeability curves in their studies but do not describe how the curves were determined.

Sanchez-Rivera et al. (2015) combined relative permeability curves from previous Bakken studies into a single plot for comparison. Figs. 3-3 and 3-4 show water-oil and liquid-gas relative permeability curves, respectively.

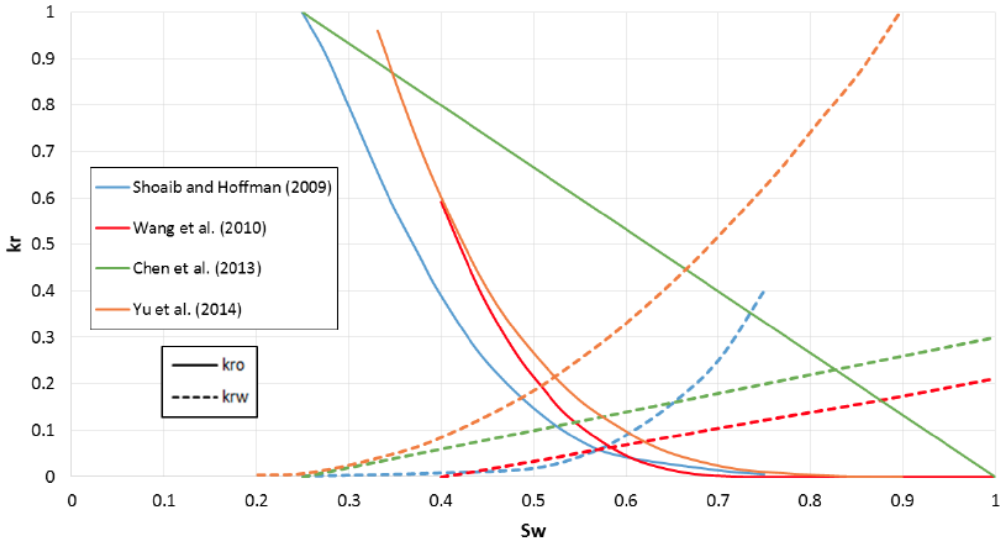

Figure 3-3: Oil-water relative permeability curves used in different studies (Sanchez-Rivera et al., 2015)

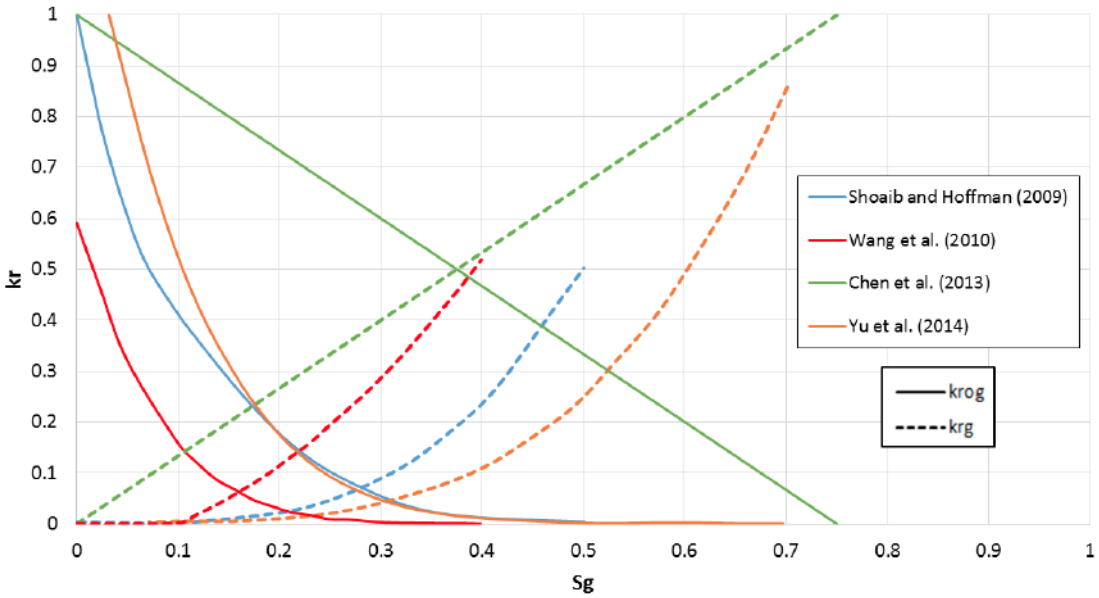

Figure 3-4: Gas-liquid relative permeability curves used in different studies (Sanchez-Rivera et al., 2015)

Sanchez-Rivera et al. (2015) deemed Yu et al.'s (2014) relative permeability curves the most reliable owing to their origin from history matching production and pressure data, so the curves were fit to the Corey-Brooks model (Eq. 3.6 – 3.8).

$$k_{rw} = k_{rw}{}^{o} S^{n} \tag{3.6}$$

$$k_{ro} = k_{ro}{}^{o} (1-S)^{m} \tag{3.7}$$

$$S = \frac{S_w - S_{wr}}{1 - S_{or} - S_{wr}} \tag{3.8}$$

Where k_{rw} and k_{ro} are water and oil endpoint relative permeabilities respectively, S_{wr} and S_{or} are water and oil residual saturations and S_w is water saturation. Analogous equations to Eq. 3.6 – 3.8 can be used to fit gas-liquid relative permeability data. Table 3-7 shows the Corey-Brooks constants used in this study, determined from curve fitting.

Table 3-7: Corey-Brooks constants for relative permeability curves

Water-Oil Relative Permeability Corey-Brooks Constants	
Residual water saturation, S_{wr}	0.2
Critical water saturation, S_{wcrit}	0.325
Residual oil saturation, S_{or}	0.1
Endpoint water relative permeability, $k_{rw}{}^{o}$	1
Endpoint oil relative permeability, $k_{ro}{}^{o}$	1
Exponent for calculating water relative permeability, n_w	2
Exponent for calculating oil relative permeability, n_{ow}	3.5
Liquid-Gas Relative Permeability Corey-Brooks Constants	

Residual gas saturation, S_{gr}	0.03
Critical gas saturation, S_{gcrit}	0.07
Endpoint gas relative permeability, k_{rog}^{o}	1
Endpoint liquid relative permeability, k_{rg}^{o}	0.85
Exponent for calculating oil relative permeability to gas, n_{og}	5.75
Exponent for calculating gas relative permeability, n_{g}	3.15

3.3.3. Fracture Modeling

In ultralow permeability shale reservoirs, the fracture network, composed of interconnected hydraulic and natural fractures is the main conduit through which reservoir fluids flow to the wellbore. Chen et al. (2013) assigned porosity and permeability of 43% and 10,000 mD to 0.005 ft. wide hydraulic fractures while modeling the Bakken; the same values are used in this study

Sanchez-Rivera et al. (2015) showed that modeling hydraulic fractures as pseudo-fractures can greatly reduce convergence issues and increase simulation speed. Pseudo-fractures allow for the significant contrast between fracture and matrix permeability to be decreased with no effect on simulation results; flow conductivity is kept constant while decreasing pseudo-fracture permeability and increasing fracture width as given by:

$$k_{pseudo} w_{pseudo} = k_{frac} w_{frac} \tag{3.9}$$

where k_{pseudo} and w_{pseudo} are pseudo-fracture permeability and width respectively, while k_{frac} and w_{frac} are the hydraulic fracture permeability and width. Fig. 3-5, taken from Sanchez-

Rivera et al. (2015), shows that modeling hydraulic fractures as pseudofractures does not introduce significant error into model results.

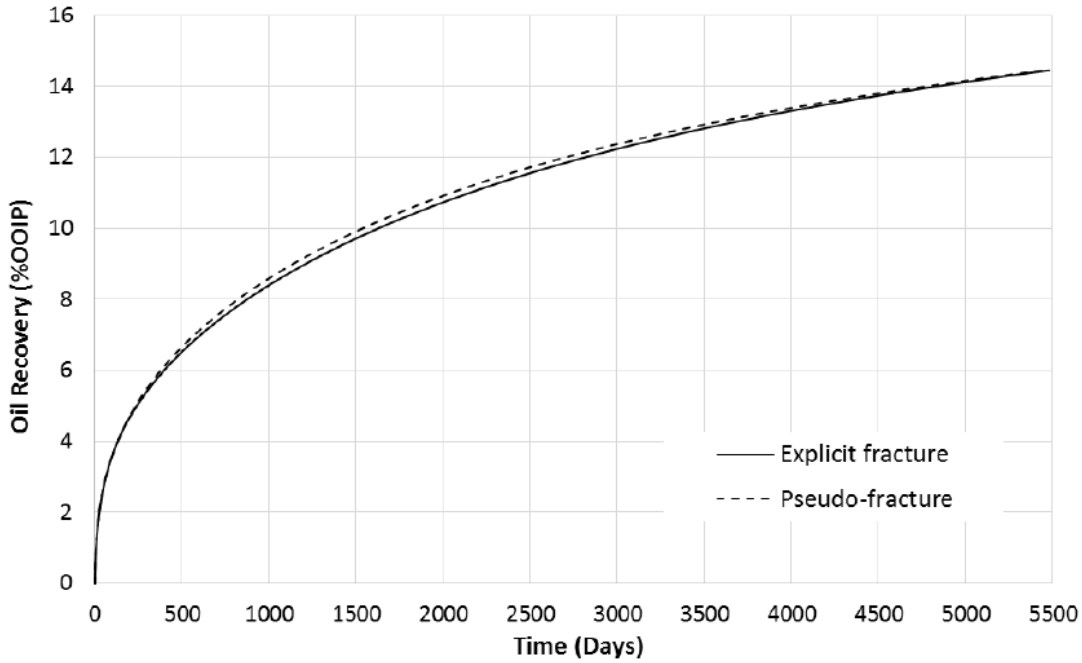

Figure 3-5: Oil recovery comparison for pseudo and explicit fractures (Sanchez-Rivera et al., 2015)

For example, a 10,000 mD, 0.005 ft. wide hydraulic fracture was modeled as a 50 mD, 1 ft. wide pseudo-fracture in this study. To study the effect of micro fractures in a simple way, 5 natural micro fractures, spaced 28 ft. apart, were incorporated in the domain with an effective permeability of 1.6 mD and effective width of 1.25 ft. 25 × 50 × 1 grids were used in the reservoir model, with fine scale gridding around the hydraulic fracture. Natural micro fractures were connected perpendicularly to the hydraulic fracture as depicted in the permeability field (Fig. 3-6).

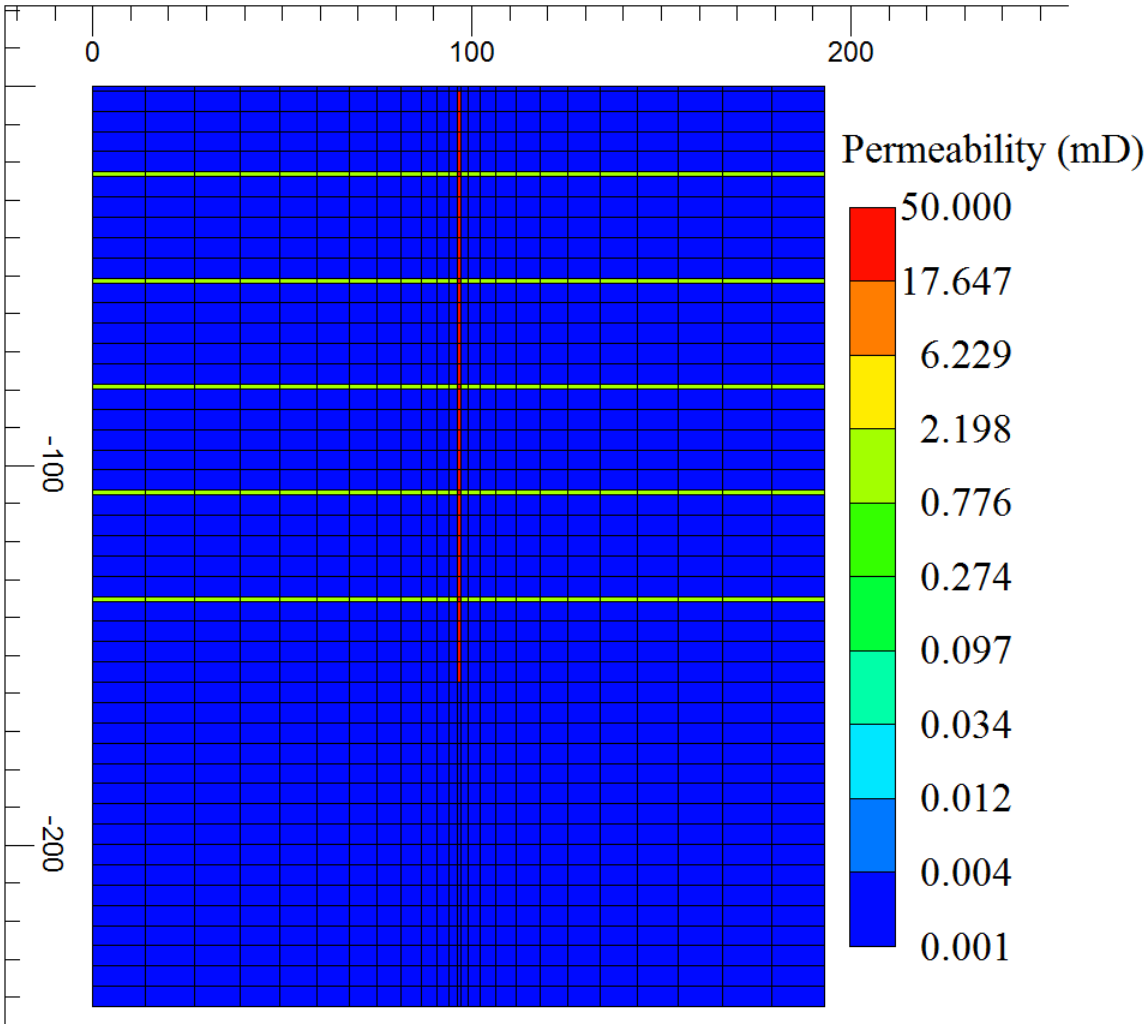

Figure 3-6: Domain gridding showing hydraulic fracture (red line) and natural fractures

3.3.4. Thermal Properties

Due to low shale permeability, heat transfer through the rock matrix is likely dominated by thermal conduction, rather than convection. Gilliam and Morgan (1987) studied the thermal properties of samples from Devonian shale, Pierre shale, and oil shale from the Green River formation. They used a DuPont Model 1090 differential scanning

calorimeter to measure heat capacity and a Dynatech Corporation Model TCFM-N20 comparative thermal conductivity analyzer in conjunction with a Hewlett-Packard Model 3052A automatic data acquisition and control system to measure thermal conductivity. Gilliam and Morgan (1987) report thermal conductivity in the 37 – 41 Btu/ft.-day-°F range and heat capacity between 0.2 and 0.3 Btu/lb °F as illustrated in Figs. 3-7 and 3-8. The USGS (1988) reports thermal conductivity of shale values between 20.8 – 41.6 Btu/ft.-day-°F depending on quartz content. In this study, thermal conductivity of 30 Btu/ft. day °F and heat capacity of 0.25 Btu/lb °F were assigned to the shale matrix.

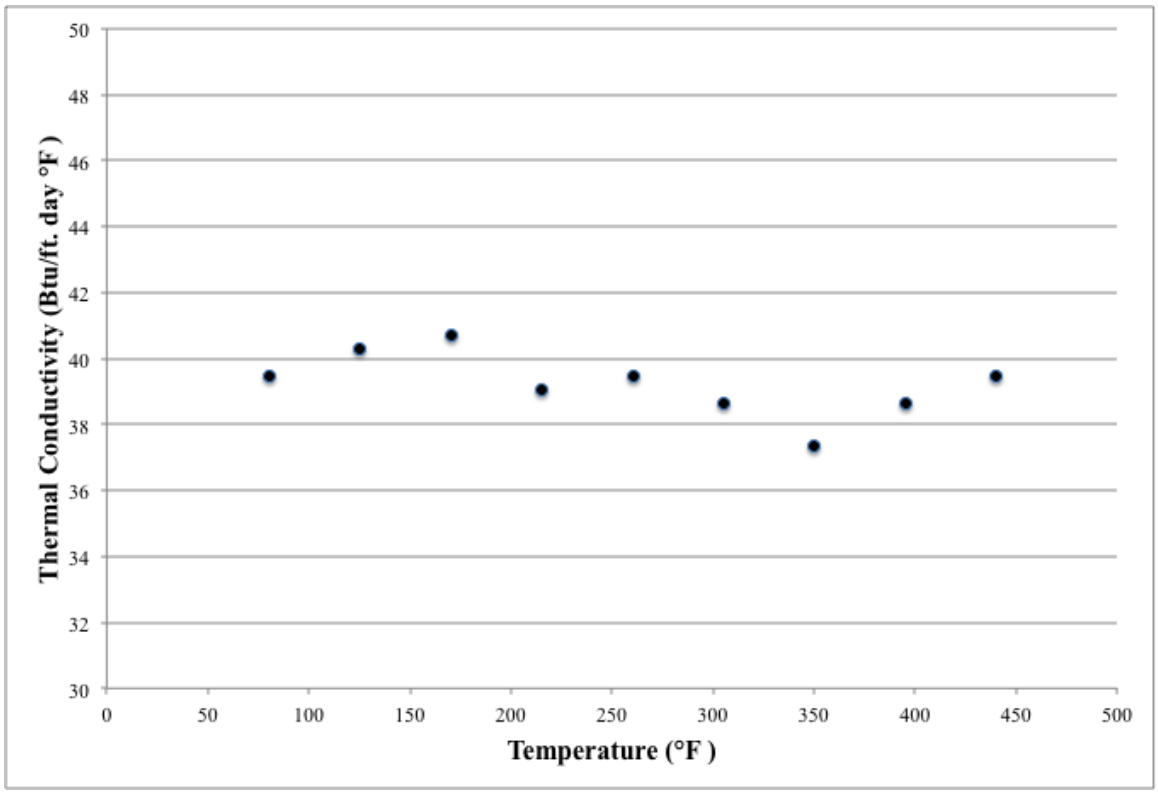

Figure 3-7: Thermal conductivity variation with temperature (Gilliam and Morgan, 1987)

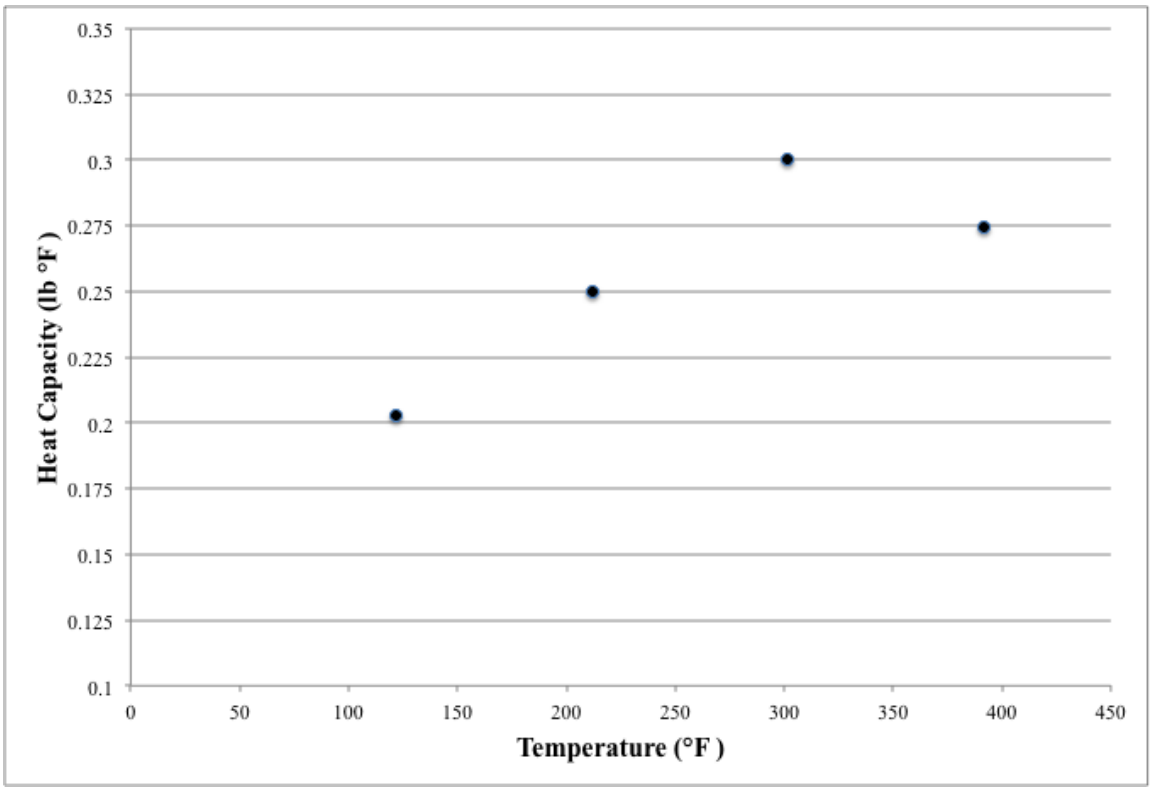

Figure 3-8: Heat capacity variation with temperature at constant pressure (Gilliam and Morgan, 1987)

3.3. KEROGEN REACTION PARAMETERS

At elevated temperatures, solid kerogen can be converted through a series of chemical reactions into oil and gas; the reaction actively begins at 554 °F.

1 mole kerogen → 0.0269 mole H_2O + 0.00959 mole heavy oil + 0.0178 mole light oil + 0.0448 mole HC gas + 0.0105 mole H_2 + 0.00541 mole CO_2 + 0.583 mole coke

The products of the initial kerogen decomposition reaction are cracked into lighter components in subsequent reaction steps as follows: cracking of heavy oil in gaseous phase, cracking of light oil in gaseous phase, cracking of heavy oil in liquid phase, cracking of light oil in liquid phase, and finally coking of hydrocarbon gas in gaseous phase (Lee et al., 2015). These reactions actively start at 608°F, 608°F, 608°F, 608°F, and 626°F, respectively.

1 mole heavy oil (gas phase) → 1.853 mole light oil + 0.045 mole HC gas + 2.4515 mole coke

1 mole light oil (gas phase) → 5.730 mole HC gas

1 mole heavy oil (liquid phase) → 0.206 mole light oil + 2.365 mole HC gas + 17.497 mole coke

1 mole light oil (liquid phase) → 0.5730 mole HC gas + 10.904 mole coke

1 mole HC gas → 2.8 mole H_2 + 1.671 mole coke

The chemical formula of kerogen can be defined as $CH_{1.5}N_{0.026}O_{0.02}$. In the cracking reactions, heavy oil is represented as ducosane ($C_{22}H_{46}$), light oil is represented

as undecane ($C_{11}H_{24}$), and hydrocarbon gas as ethane (C_2H_6). The molecular weights, critical properties and acentric factor of these fluid components are provided in Table 3-8 (Lee et al., 2015).

Table 3-8: Properties of kerogen decomposition products

Properties	**$C_{22}H_{46}$**	**$C_{11}H_{24}$**	**C_2H_6**
Molecular weight (lbm/lbmol)	311.27	156.63	30.14
Critical pressure (psia)	181	285	707
Critical temperature (°F)	964.7	690.1	90.1
Critical compressibility	0.215	0.243	0.279
Acentric factor	0.972	0.536	0.099

Oba et al. (2002) have determined the frequency factor and activation energy for the decomposition of various samples of kerogen recovered from sediments. The samples were heated from room temperature to 1472 °F using a thermo-gravimetric analyzer and heating rates (H_r) of 40 – 140 °F/min. During the pyrolysis of kerogen samples, the temperature peaks (T_{max}), corresponding to hydrocarbon release from kerogen, were recorded and Eq. 3.10 was used to determine activation energy (E_a) and frequency factor (A), where R is the universal gas constant:

$$\ln\left(\frac{H_r}{T_{max}^{\ 2}}\right) = -\frac{E_a}{RT_{\max}} + \ln\left(\frac{AR}{E_k}\right) \tag{3.10}$$

The kerogen samples that Oba et al. (2002) analyzed varied from type I – III. Type 1 kerogen is characterized by its abundance of hydrogen, making it highly oil prone

during decomposition. Type II kerogen has a moderate amount of hydrogen and forms oil and gas, while type III kerogen contains enough hydrogen to generate gas but not oil. Results for all three kerogen types in the samples analyzed by Oba et al. (2002) are listed in Table 3-9.

Table 3-9: Kerogen reaction parameters

Kerogen Type	A **(day^{-1})**	E_a **(Btu/lbmole)**
Type I	$8.64 \times 10^{18} - 8.64 \times 10^{22}$	87,000 – 100,000
Type II	$9.5 \times 10^{16} - 4.5 \times 10^{19}$	81,500 – 100,000
Type III	$8.64 \times 10^{17} - 8.64 \times 10^{20}$	83,500 – 107,000

Although the experiments carried out by Oba et al. (2002) were for kerogen samples obtained from oil shale, we assume that the kerogen contained in shale reservoirs such as the Bakken, Eagle Ford and Spraberry formations, has similar properties.

Chapter 4: Development of a Multiphase Thermal Simulator for Preliminary Studies

This chapter describes preliminary work performed to determine the viability of the proposed thermal recovery process. A 2D black oil, thermal, reactive transport reservoir simulator was developed in MATLAB to study the effect of steam injection on oil recovery from shale reservoirs. Specifically, viscosity change at elevated temperatures, as well as, changes in oil in place, porosity and permeability during kerogen decomposition is studied. Furthermore, we assume no thermal fluid expansion or vaporization of volatile components of the oil and we ignore coke, a solid product of kerogen decomposition. Additionally, because the developed simulator is a two-phase (oil and water) black oil model, we assume all injected steam condenses into hot water on contact with the reservoir. The following subsections discuss simulator development, input parameters, results and effect of kerogen reaction rate on recovery. A later section will extend the results of this section by using a commercial thermal compositional simulator (CMG STARS) to account for thermal fluid expansion and coke production.

4.1. Model Development

The reservoir simulation scheme employed in this study consists of discretizing the reservoir into gridblocks and overall time into time steps. At each time step, pressure and water/oil saturation for each grid block are determined by solving material balance, then the temperature of each grid block is determined from the energy balance. Reaction rate is calculated as a function of temperature, porosity is updated based on the amount of

kerogen lost to the reaction, permeability is updated as a function of porosity and finally, fluid properties are updated as a function of new pressure and temperature, before the simulation moves to the next time step. The simplified kerogen reaction that will be modeled in this preliminary study neglects coke and gas products of kerogen decomposition and assumes that the oil generated is a black oil as represented by the following relationship:

1 mole kerogen → 0.0274 mole black oil

The equations used in the simulator are presented in the following subsection.

4.1.1. Governing Equations

In a black oil reservoir model, the mass balance for each phase in a gridblock, is stated as the accumulation of mass is a combination of the net mass in/out of that block and the mass generated or consumed in a chemical reaction during each time step. Eq. 4.1 expresses this relationship for oil phase in block *i* in Fig. 4-1.

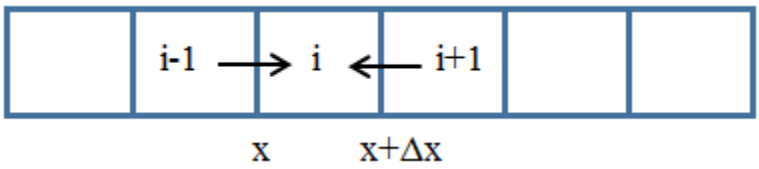

Figure 4-1: 1D material balance illustration

$$\left[\rho_o q_o\right]_x \Delta t + \left[\rho_o q_o\right]_{x+\Delta x} \Delta t + (b-a) r \Delta x \Delta t + \rho_{osc} q_{o,well} A \Delta x \Delta t = \left[A \Delta x \phi S_o \rho_o\right]_{t+\Delta t} - \left[A \Delta x \phi S_o \rho_o\right]_t \quad (4.1)$$

$$q_o = -\frac{kk_{ro}A}{\mu_o}\frac{\Delta P}{\Delta x} \tag{4.2}$$

$$\rho_o = \frac{\rho_{osc}}{B_o} \tag{4.3}$$

where ρ_o is oil phase density, q_o is flow into block i from neighboring blocks at x and $x+\Delta x$, Δt is time step size, b and a are product and reactant stoichiometric coefficients of the oil phase respectively (from the kerogen reaction balance), r is reaction rate, ρ_{osc} is oil phase density at standard conditions (14.7 psi and 60 °F), $q_{o,well}$ is oil well flux if there is a well in block i, A is cross-sectional area, ϕ is porosity, S_o is oil saturation, k is rock permeability, k_{ro} is oil relative permeability, μ_o is oil viscosity, B_o is oil formation volume factor, and P is pressure; we assume no capillary pressure, so water and oil phase pressures are equal.

Substituting q_o and ρ_o in Eq. 4.1 with expressions in Eq. 4.2 and 4.3, and dividing by $A\Delta x\Delta t$ before taking the limits as Δx and Δt go to zero, gives:

$$\frac{\partial}{\partial t}\left(\frac{\phi S_o}{B_o}\right) = \frac{\partial}{\partial x}\left(\lambda_o \frac{\partial P}{\partial x}\right) + q_{o,well} + (b-a)r \tag{4.4}$$

$$\lambda_o = \frac{kk_{ro}}{\mu_o B_o} \tag{4.5}$$

The time derivative in Eq. 4.4 can be expanded using the chain and product rules and simplified using the definitions of fluid and rock compressibilities.

$$\frac{\phi}{B_o}\frac{\partial S_o}{\partial t}+\left(\frac{\phi S_o}{B_o}c_o+\frac{\phi S_o}{B_o}c_f\right)\frac{\partial P}{\partial t}=\frac{\partial}{\partial x}\left(\lambda_o\frac{\partial P}{\partial x}\right)+q_{o,well}+(b-a)r \tag{4.6}$$

$$c_o=B_o\frac{\partial}{\partial P}\left(\frac{1}{B_o}\right) \tag{4.7}$$

$$c_f=\frac{1}{\phi}\frac{\partial \phi}{\partial P} \tag{4.8}$$

where c_o and c_f are oil and rock compressibility. Although, Eq. 4.6 was derived for the oil phase, a similar equation can be derived for water phase, assuming that water is neither a product nor reactant in the kerogen reaction.

$$\frac{\phi}{B_w}\frac{\partial S_w}{\partial t}+\left(\frac{\phi S_w}{B_w}c_w+\frac{\phi S_w}{B_w}c_f\right)\frac{\partial P}{\partial t}=\frac{\partial}{\partial x}\left(\lambda_w\frac{\partial P}{\partial x}\right)+q_{w,well} \tag{4.9}$$

$$\lambda_w=\frac{kk_{rw}}{\mu_w B_w} \tag{4.10}$$

where B_w is water formation volume factor, S_w is water saturation, c_w is water compressibility, $q_{w,well}$ is water well flux if there is a well in block i, μ_w is water viscosity and k_{rw} is water relative permeability. A combined mass balance absent of phase saturations is derived by multiplying the oil equation (Eq. 4.6) by B_o/B_w and adding to the water equation (Eq. 4.9) to give:

$$\left(\frac{\phi c_t}{B_w}\right)=\frac{B_o}{B_w}\frac{\partial}{\partial x}\left(\lambda_o\frac{\partial P}{\partial x}\right)+\frac{\partial}{\partial x}\left(\lambda_w\frac{\partial P}{\partial x}\right)+\frac{B_o}{B_w}\left(q_{o,well}+(b-a)r\right)+q_{w,well} \tag{4.11}$$

$$c_t = S_o c_o + S_w c_w + c_f \tag{4.12}$$

where c_t is total compressibility. Pressure can be determined from the balance in Eq. 4.11 by using finite differences to discretize the balance and expanding to 2D.

$$\frac{\phi_i c_{t_i}}{B_w}\frac{P_i^{n+1}-P_i^n}{\Delta t} = Dx_{oil_i} + Dx_{water_i} + Dy_{oil_i} + Dy_{water_i} + \frac{B_o}{B_w}\left(q_{o,well_i} + (b-a)r_i\right) + q_{w,well_i} \tag{4.13}$$

$$Dx_{oil_i} = \frac{1}{\Delta x_i}\frac{B_o}{B_w}\left[\lambda_{o_{i,i-1}}\frac{P_{i-1}^{n+1}-P_i^{n+1}}{\Delta x_{i,i-1}} + \lambda_{o_{i,i+1}}\frac{P_{i+1}^{n+1}-P_i^{n+1}}{\Delta x_{i,i+1}}\right] \tag{4.14}$$

$$Dx_{water_i} = \frac{1}{\Delta x_i}\left[\lambda_{w_{i,i-1}}\frac{P_{i-1}^{n+1}-P_i^{n+1}}{\Delta x_{i,i-1}} + \lambda_{w_{i,i+1}}\frac{P_{i+1}^{n+1}-P_i^{n+1}}{\Delta x_{i,i+1}}\right] \tag{4.15}$$

$$Dy_{oil_i} = \frac{1}{\Delta y_i}\frac{B_o}{B_w}\left[\lambda_{o_{i,i-Nx}}\frac{P_{i-Nx}^{n+1}-P_i^{n+1}}{\Delta y_{i,i-Nx}} + \lambda_{o_{i,i+Nx}}\frac{P_{i+Nx}^{n+1}-P_i^{n+1}}{\Delta y_{i,i+Nx}}\right] \tag{4.16}$$

$$Dy_{water_i} = \frac{1}{\Delta y_i}\left[\lambda_{w_{i,i-Nx}}\frac{P_{i-Nx}^{n+1}-P_i^{n+1}}{\Delta y_{i,i-Nx}} + \lambda_{w_{i,i+Nx}}\frac{P_{i+Nx}^{n+1}-P_i^{n+1}}{\Delta y_{i,i+Nx}}\right] \tag{4.17}$$

In the above equations, subscript *(i,j)* represent flow between blocks *i* and *j*, where *j* can be *i+1*, *i-1*, *i+Nx* or *i-Nx* as shown in Fig. 4-2. *Nx* is the number of gridblocks in the x-direction (3 in Fig. 4-2). Similar equations can be derived for every gridblock in the reservoir and solved simultaneously for pressures at the *n+1* time step.

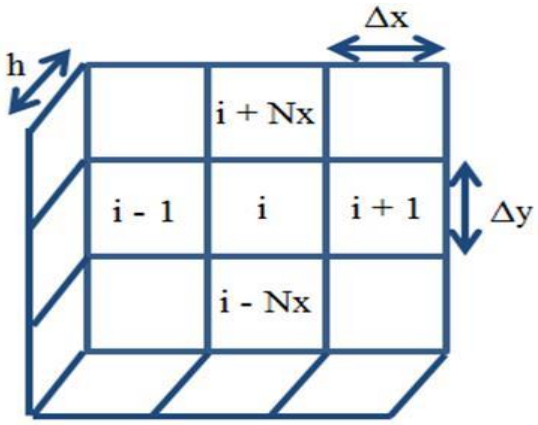

Figure 4-2: 2D grid representation

After solving for gridblock pressures, the water balance (Eq. 4.9) can be expanded using finite differences and saturation at the $n+1$ time step can be determined.

$$\frac{\phi_i}{B_w}\frac{S_{w_i}^{\,n+1}-S_{w_i}^{\,n}}{\Delta t}+\left(\frac{\phi_i S_{w_i}^{\,n}}{B_w}c_w+\frac{\phi_i S_{w_i}^{\,n}}{B_w}c_f\right)\frac{P_i^{n+1}-P_i^{n}}{\Delta t}=Dx_{water_i}+Dy_{water_i}+q_{w,well_i} \tag{4.18}$$

The energy balance for each gridblock, which governs temperature distribution, is stated as the accumulation of internal energy is a combination of flow into the gridblock by convection and conduction from neighboring gridblocks and energy flow into/out of the block from a well source. Pan et al. (1984) showed that the reaction enthalpy is negligible compared to other energy terms in the balance, therefore we omit the reaction enthalpy term from our balance equation.

$$\begin{aligned}\phi S_o\rho_o U_o A\Delta x+\phi S_w\rho_w U_w A\Delta x+(1-\phi)\rho_r U_r A\Delta x&=\left[\rho_o q_o H_o\Delta t\right]_x-\left[\rho_o q_o H_o\Delta t\right]_{x+\Delta x}\\&+\left[\rho_w q_w H_w\Delta t\right]_x-\left[\rho_w q_w H_w\Delta t\right]_{x+\Delta x}+\left[KA\frac{\partial T}{\partial x}\Delta t\right]_x-\left[KA\frac{\partial T}{\partial x}\Delta t\right]_{x+\Delta x}\\&+\rho_o q_{o,well}H_o\Delta t\Delta x+\rho_w q_{w,well}H_w\Delta t\Delta x\end{aligned} \tag{4.19}$$

where U_o, U_w and U_r are the specific internal energy of oil, water and rock respectively, ρ_r is rock density, H_o and H_w are oil and water specific enthalpies respectively, K is total conductivity (i.e. combination of the conductivity of water, oil and rock) and T is temperature. If we divide Eq. 4.19 by $A\Delta x\Delta t$, take limits as Δx and Δt go to zero and substitute in expressions for q_o and q_w from Eq. 4.2, we get the following differential equation.

$$\frac{\partial}{\partial t}\left(\phi S_o \rho_o U_o + \phi S_w \rho_w U_w + (1-\phi)\rho_r U_r\right) = -\frac{\partial}{\partial x}\left(\varphi_o \frac{\partial P}{\partial x} + \varphi_w \frac{\partial P}{\partial x}\right) + \frac{\partial}{\partial x}\left(K \frac{\partial T}{\partial x}\right) - \left(\rho_o q_{o,well} H_o + \rho_w q_{w,well} H_w\right) \tag{4.20}$$

$$\varphi_{phase} = \rho_{phase} H_{phase} \frac{k k_{r_{phase}}}{\mu_{phase}} \tag{4.21}$$

$$U_{phase} = C_{v_{phase}} T \tag{4.22}$$

$$H_{phase} = C_{p_{phase}} T \tag{4.23}$$

where C_p and C_v are the constant-pressure and constant-volume heat capacities respectively. Expanding the time derivative using chain and product rules and expressing both spatial and time derivatives using finite differences gives an expression that can be solved for temperature at the $n+1$ time step.

$$A_{oil_i} + A_{water_i} + A_{rock_i} = G_{o_i} + G_{w_i} + F_i - \left(\rho_{o_i} q_{o,well_i} H_{o_i} + \rho_{w_i} q_{w,well_i} H_{w_i}\right) \tag{4.24}$$

$$A_{oil_i} = \phi_i {S_{o_i}}^n \rho_o^n \frac{U_{o_i}^{n+1} - U_{o_i}^n}{\Delta t} + \phi_i {U_{o_i}}^n \rho_o^n \frac{S_{o_i}^{n+1} - S_{o_i}^n}{\Delta t} + \phi_i {S_{o_i}}^n {U_{o_i}}^n \rho_o^n (c_o + c_r) \frac{P_i^{n+1} - P_i^n}{\Delta t} \quad (4.25)$$

$$A_{water_i} = \phi_i {S_{w_i}}^n \rho_w^n \frac{U_{w_i}^{n+1} - U_{w_i}^n}{\Delta t} + \phi_i {U_{w_i}}^n \rho_w^n \frac{S_{w_i}^{n+1} - S_w^n}{\Delta t} + \phi_i {S_{w_i}}^n {U_{w_i}}^n \rho_w^n (c_w + c_r) \frac{P_i^{n+1} - P_i^n}{\Delta t} \quad (4.26)$$

$$A_{rock_i} = (1 - \phi_i) \rho_r^n \frac{U_{r_i}^{n+1} - U_{r_i}^n}{\Delta t} \quad (4.27)$$

$$G_{o_i} = \frac{\varphi_{o_{i,i-1}}^{n+1}}{\Delta x_i} \left(\frac{P_{i-1}^{n+1} - P_i^{n+1}}{\Delta x_{i,i-1}} \right) + \frac{\varphi_{o_{i,i+1}}^{n+1}}{\Delta x_i} \left(\frac{P_{i+1}^{n+1} - P_i^{n+1}}{\Delta x_{i,i+1}} \right) + \frac{\varphi_{o_{i,i-Nx}}^{n+1}}{\Delta y_i} \left(\frac{P_{i-Nx}^{n+1} - P_i^{n+1}}{\Delta y_{i,i-Nx}} \right) + \frac{\varphi_{o_{i,i+Nx}}^{n+1}}{\Delta y_i} \left(\frac{P_{i+Nx}^{n+1} - P_i^{n+1}}{\Delta y_{i,i+Nx}} \right) \quad (4.28)$$

$$G_{w_i} = \frac{\varphi_{w_{i,i-1}}^{n+1}}{\Delta x_i} \left(\frac{P_{i-1}^{n+1} - P_i^{n+1}}{\Delta x_{i,i-1}} \right) + \frac{\varphi_{w_{i,i+1}}^{n+1}}{\Delta x_i} \left(\frac{P_{i+1}^{n+1} - P_i^{n+1}}{\Delta x_{i,i+1}} \right) + \frac{\varphi_{w_{i,i-Nx}}^{n+1}}{\Delta y_i} \left(\frac{P_{i-Nx}^{n+1} - P_i^{n+1}}{\Delta y_{i,i-Nx}} \right) + \frac{\varphi_{w_{i,i+Nx}}^{n+1}}{\Delta y_i} \left(\frac{P_{i+Nx}^{n+1} - P_i^{n+1}}{\Delta y_{i,i+Nx}} \right) \quad (4.29)$$

$$F_i = \frac{K_{i,i-1}^n}{\Delta x_i} \left(\frac{T_{i-1}^n - T_i^n}{\Delta x_{i,i-1}} \right) + \frac{K_{i,i+1}^n}{\Delta x_i} \left(\frac{T_{i+1}^n - T_i^n}{\Delta x_{i,i+1}} \right) + \frac{K_{i,i-Nx}^n}{\Delta y_i} \left(\frac{T_{i-Nx}^n - T_i^n}{\Delta y_{i,i-Nx}} \right) + \frac{K_{i,i+Nx}^n}{\Delta y_i} \left(\frac{T_{i+Nx}^n - T_i^n}{\Delta y_{i,i+Nx}} \right) \quad (4.30)$$

where A_{oil}, A_{water} and A_{rock} represent energy accumulation in oil, water and rock respectively, which shows up as an increase in temperature. G_{o} and G_{w} are oil and water convection terms and F_{i} is the energy conduction term.

The rate of kerogen decomposition is dependent on temperature and is governed by the following equation.

$$r_i = Ae^{\frac{-E_a}{k_b T_i}} C_{\ker_i} \tag{4.31}$$

where r is reaction rate, A is reaction frequency factor, which is the frequency of reactant molecule collisions, E_a is activation energy, which is the minimum energy required by reactants for the reaction to occur, k_b is Boltzmann's constant and C_{ker} is kerogen concentration. Over time, kerogen concentration decreases as kerogen is consumed in the reaction.

$$C_{\ker_i}^{n+1} = C_{\ker_i}^{n} - r_i \Delta t \tag{4.32}$$

Consequently, porosity increases as solid rock volume in the form of kerogen is converted to fluid pore volume (Eq. 4.33). Additionally, we assume that rock permeability is related to porosity by the Carmen-Kozeny relationship (Eq. 4.34).

$$\phi_i^{n+1} = \phi_i^n - \frac{C_{\ker_i}^{n+1} - C_{\ker_i}^{n}}{\rho_{\ker}} \tag{4.33}$$

$$k_i^{n+1} = k_i^n \left(\frac{\phi^{n+1}}{\phi^n} \right) \left(\frac{1-\phi^n}{1-\phi^{n+1}} \right)^2 \tag{4.34}$$

Finally, oil viscosity decreases with increasing temperature as follows:

$$\mu = \mu_{ref} \exp\left(\frac{1}{T} - \frac{1}{T_{ref}} \right) \tag{4.35}$$

where μ_{ref} and T_{ref} are viscosity and temperature at some reference point (initial reservoir conditions. Putting it all together, the solution steps are as follows:

1. Solve for pressure implicitly using Eq. 4.13
2. Solve for saturation using Eq. 4.18
3. Using updated pressures and saturation, solve for temperature using Eq. 4.24
4. Calculate reaction rate using Eq. 4.31
5. Update porosity and permeability as a function of lost kerogen volume using Eq. 4.33 and 4.34
6. Update oil viscosity using Eq. 4.35
7. Proceed to the next time step and repeat the previous steps.

4.1.2. Model Verification

CMG STARS was used to verify that the simulator developed in MATLAB correctly solves the flow and energy equations for pressure and temperature. Kerogen decomposition was neglected in this verification because reaction kinetics are modeled in a more complex way in CMG STARS than in the MATLAB model. Fig. 4-3 compares pressure field in a square reservoir, with a well at its center, after 600 days of cyclic steam stimulation. There is a 350 day pre-heating period, where steam is injected with no production before cycling begins; each cycle consists of 20 days of steam injection, followed by 10 days of soaking and finally 20 days of fluid production. Similarly, Fig. 4-4 compares temperature field. We observe that the simulator developed in MATLAB produces identical pressure and temperature fields to CMG STARS results.

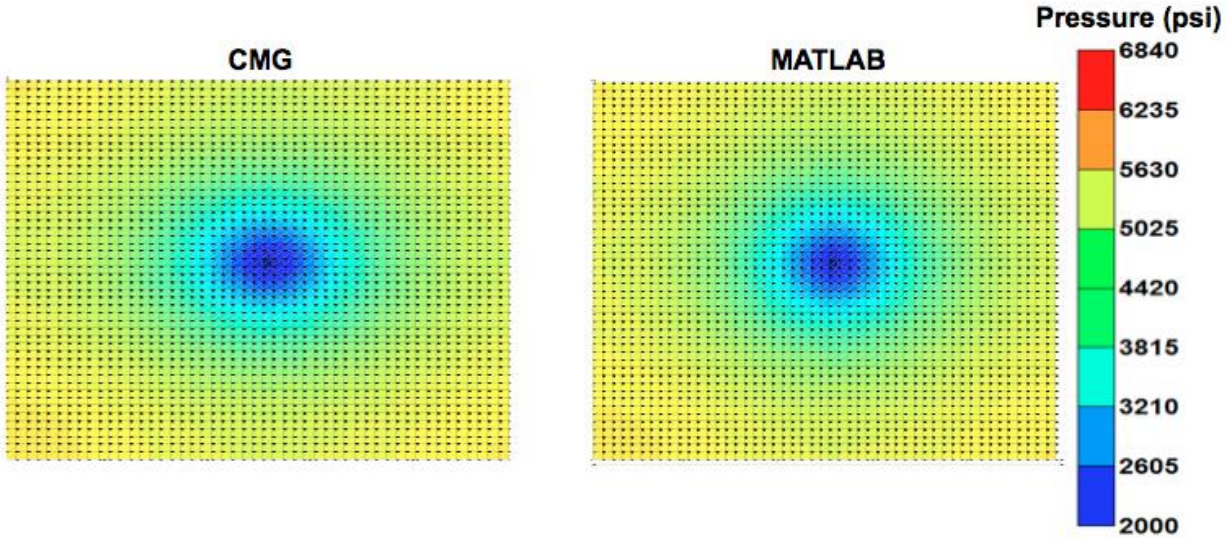

Figure 4-3: Pressure distribution is similar for CMG and MATLAB models

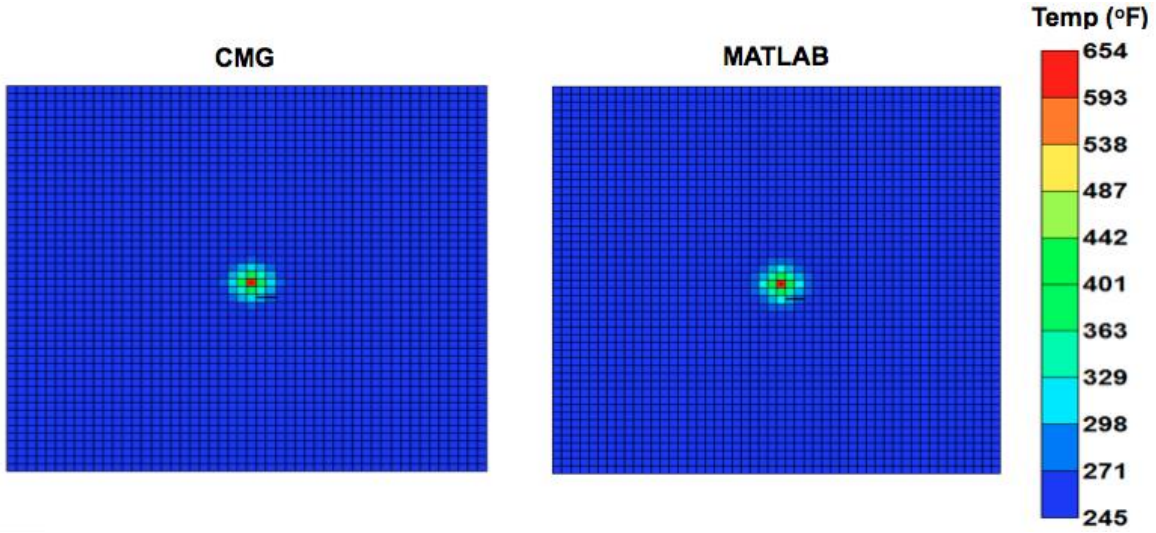

Figure 4-4: Temperature distribution is similar for CMG and MATLAB models

Furthermore, Fig. 4-5 below shows that oil production rate predicted by the developed MATLAB simulator closely matches CMG STAR's result.

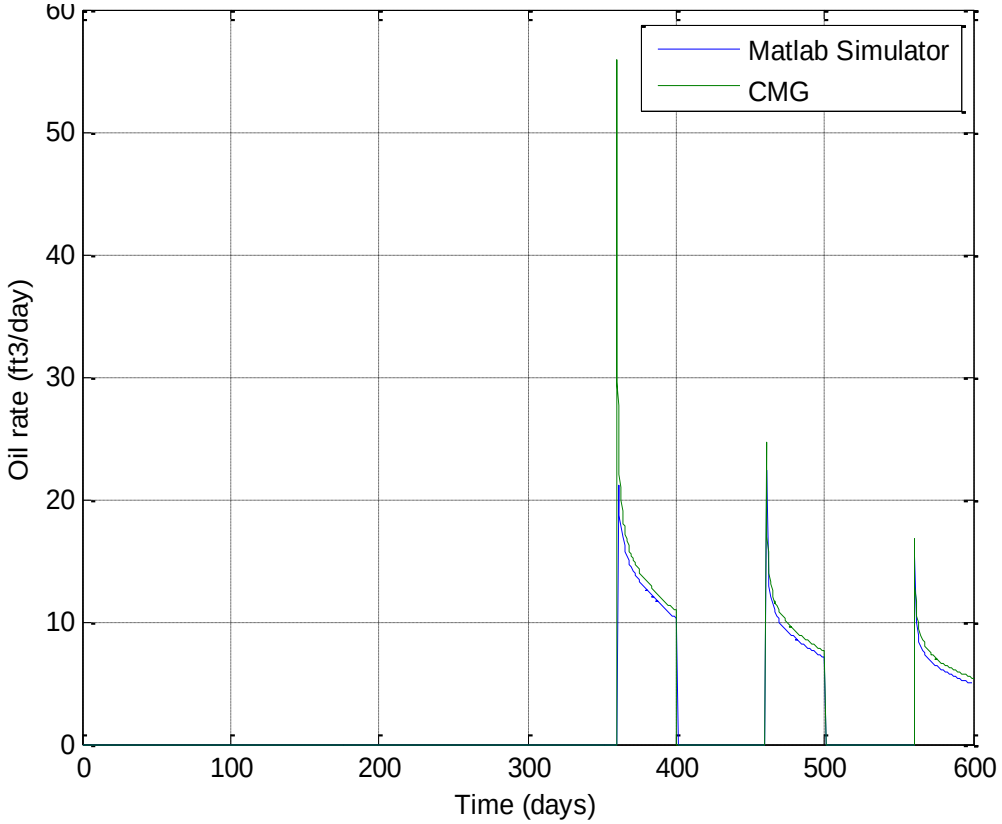

Figure 4-5: Oil production rate is similar for CMG and MATLAB models

After simulator development, model inputs were defined, as will be discussed in the following subsection, and oil recovery during cyclic steam stimulation was studied.

4.1.3. Model Inputs

A more detailed analysis of the reservoir and fluid properties used in this study is provided in Chapter 3; a brief summary of relevant properties is presented in the following table. Injection pressure and production pressure are 7000 psi and 1000 psi respectively.

Table 4-1: Summary of initial reservoir and fluid properties

PROPERTY	VALUE	UNITS
Fracture width	0.005	ft.
k_{matrix}	0.001	mD
k_{frac}	10,000	mD
$k_{natural\ frac}$	1	mD
ϕ_{matrix}	0.08	[ ]
Initial oil saturation	0.7	[ ]
Initial reservoir pressure	6840	psi
Production pressure	1000	psi
Injection pressure	7000	psi
Reservoir temperature	248	°F
Steam temperature	750	°F
Formation compressibility	$1x10^{-6}$	psi^{-1}
Initial oil viscosity	0.31	cp
Initial oil density	40.3	lb/ft^3

4.2. RESULTS & DISCUSSION

The developed reservoir simulation model was used to study recovery from the computational domain for 1500 days of primary production, followed by 2500 days of steam cycling (4000 days total well life). Each steam cycle consists of 100 days of 750 °F steam injection, 5 days of thermo-capillary soaking and 100 days of production from the same well. Thermo-capillary soaking is a period during which the well is shut in to allow

the steam to diffuse into the formation and propagate heat into the reservoir. 50% of heat from injected steam is assumed to be lost to the overburden and underburden.

Fig 4-6 shows temperature distribution after 4000 days, made up of 1500 days of primary depletion, followed by 2500 days of steam cycling. The injected steam penetrates the reservoir through the fracture network and because of the low permeability of the formation, heat is primarily transferred from the fractures to the rock matrix by conduction. Additionally, heat from steam in the wellbore is also transferred to the matrix by conduction, resulting in increased temperature around the wellbore.

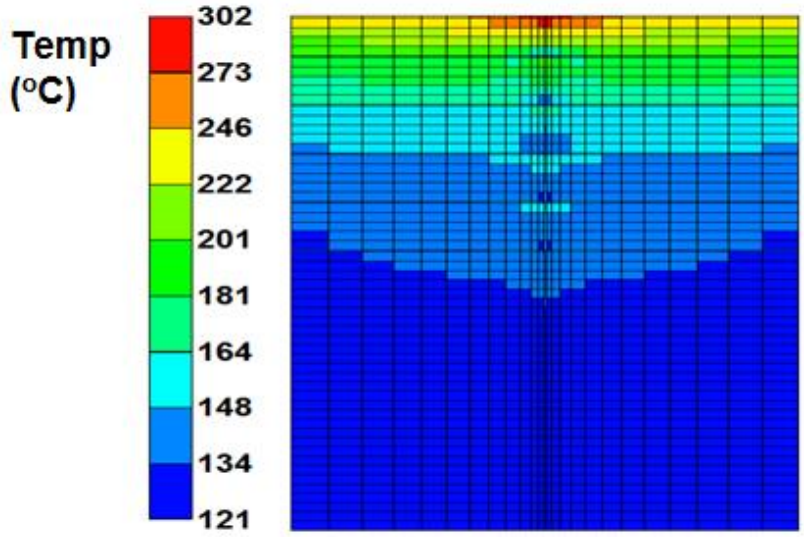

Figure 4-6: Temperature field at 4000 days

As a result of temperature elevation, Fig. 4-7 shows that viscosity is reduced from to as low as 0.02 cp around the wellbore, however, the average viscosity is still about 0.15 cp, which is not significantly lower than initial fluid viscosity.

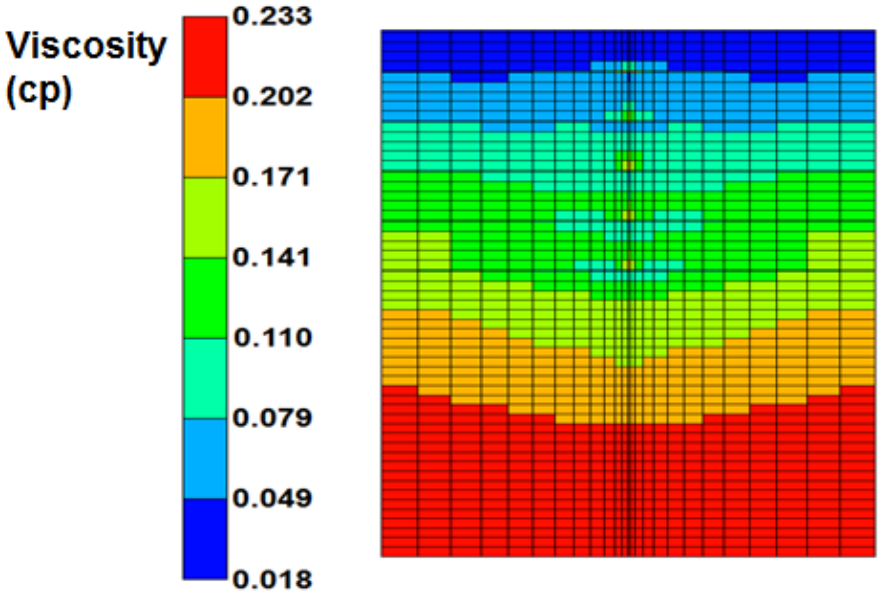

Figure 4-7: Oil viscosity field at 4000 days

An important consequence of temperature elevation in kerogen-containing reservoirs is the generation of oil from kerogen decomposition. Increased oil in place from kerogen decomposition is accompanied by an increase in porosity, and consequently permeability. Fig. 4-8 shows porosity and permeability increase around the wellbore, where the maximum temperature increase occurs; porosity increased from 8 to 15%, while permeability doubled from 0.001 to about 0.002 mD. It is important to note that as a result of neglecting coke production in this preliminary study, porosity is overestimated. In reality, produced coke would occupy some of the new pore space.

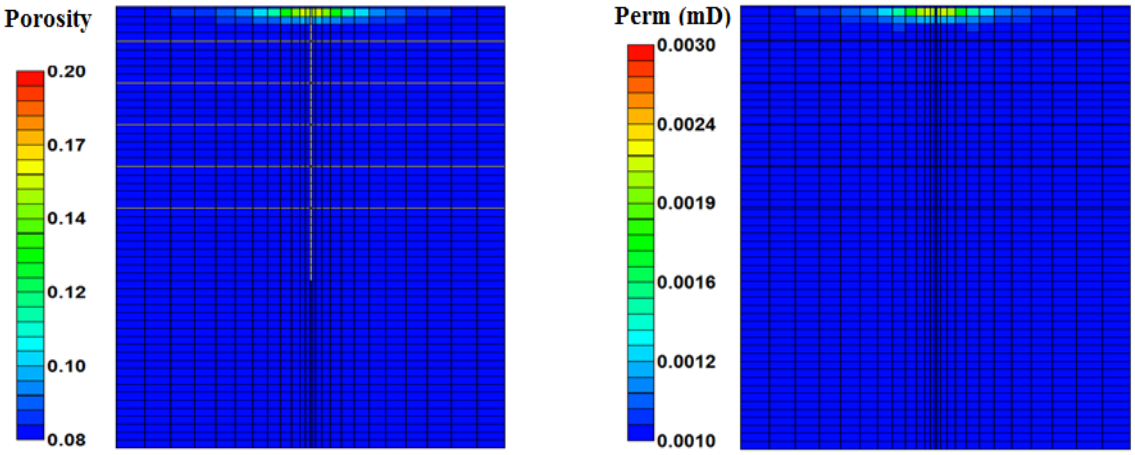

Figure 4-8: Porosity and permeability fields at 4000 days

Fig. 4-9 below shows that oil recovery from shale reservoirs can be increased by steam injection, from 8.8% to about 10.1%, for a shale reservoir absent of kerogen and to about 12.8% for a kerogen-containing reservoir. The increase in recovery for the reservoir without kerogen is a result of reduced viscosity at elevated temperatures during steam injection, while the increase in recovery for the kerogen-containing reservoir is a combination of reduced viscosity and oil generation during kerogen decomposition.

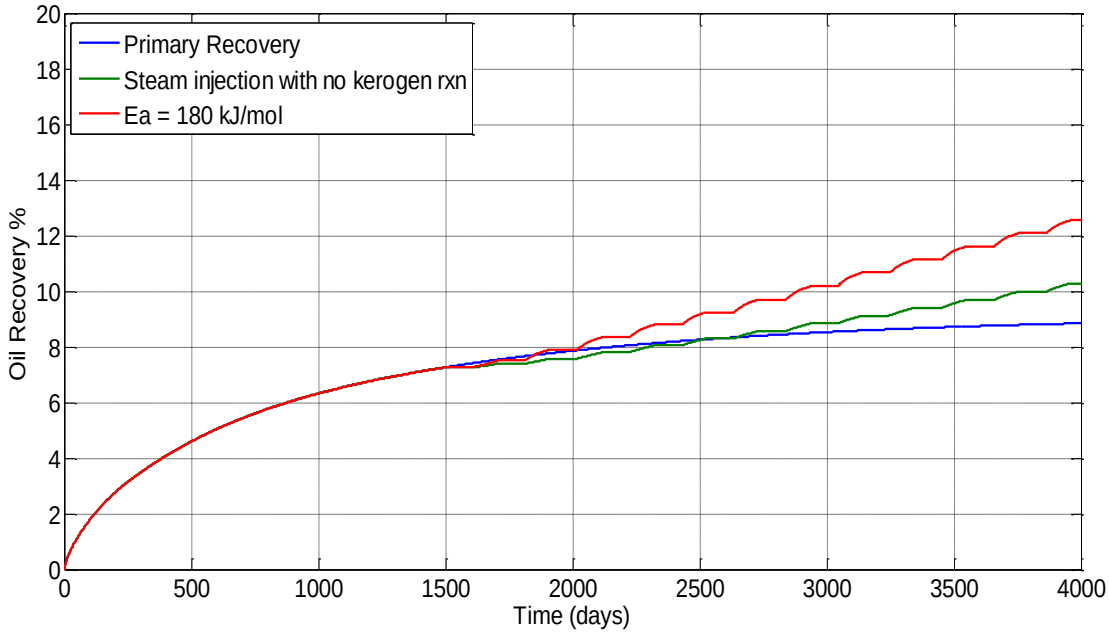

Figure 4-9: Steam injection improves recovery

Original oil in place for the computational domain was 5700 bbls; therefore, an increase in recovery from 8.8% during primary depletion to 12.8% with steam injection represents an additional 270 bbls of oil, while 1200 bbls of steam were injected, giving a cost of 4.4 barrels of steam per incremental barrel of oil produced.

Kerogen decomposition rate is governed by the activation energy and frequency factor of the reaction. Eq. 4.31 shows that lower activation energy results in higher kerogen reaction rate. Consequently, greater oil generation and recovery are expected for reservoirs containing kerogen with low reaction activation energy, as illustrated in Fig. 4-10. Similarly, as a result of higher kerogen decomposition rate at higher reaction frequency factors, oil recovery is greater in reservoirs containing kerogen with high reaction frequency factor, as illustrated in Fig. 4-11.

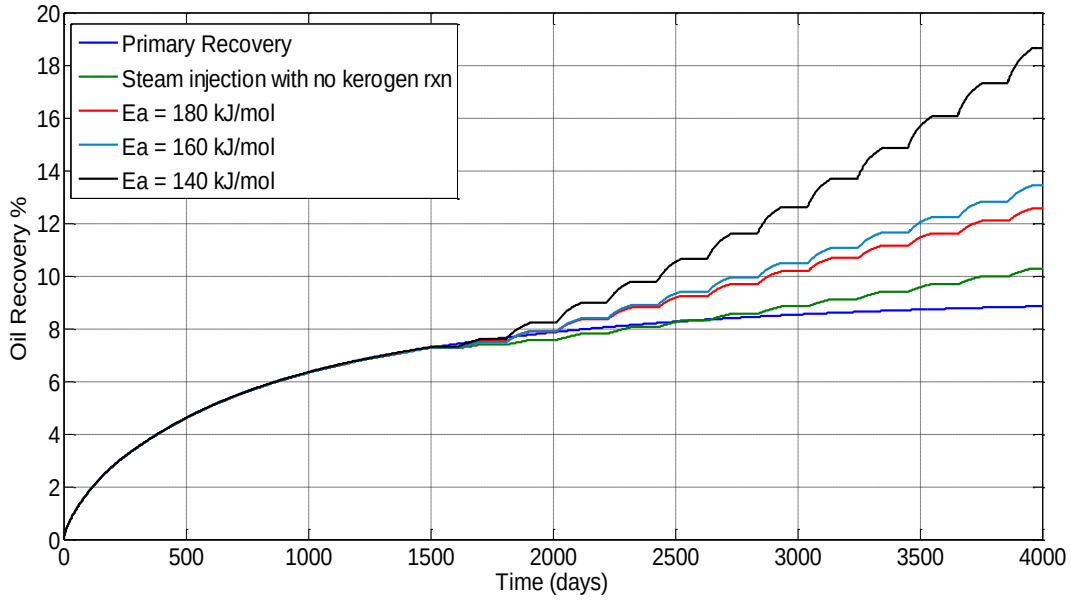

Figure 4-10: Higher oil recovery for lower activation energy kerogen

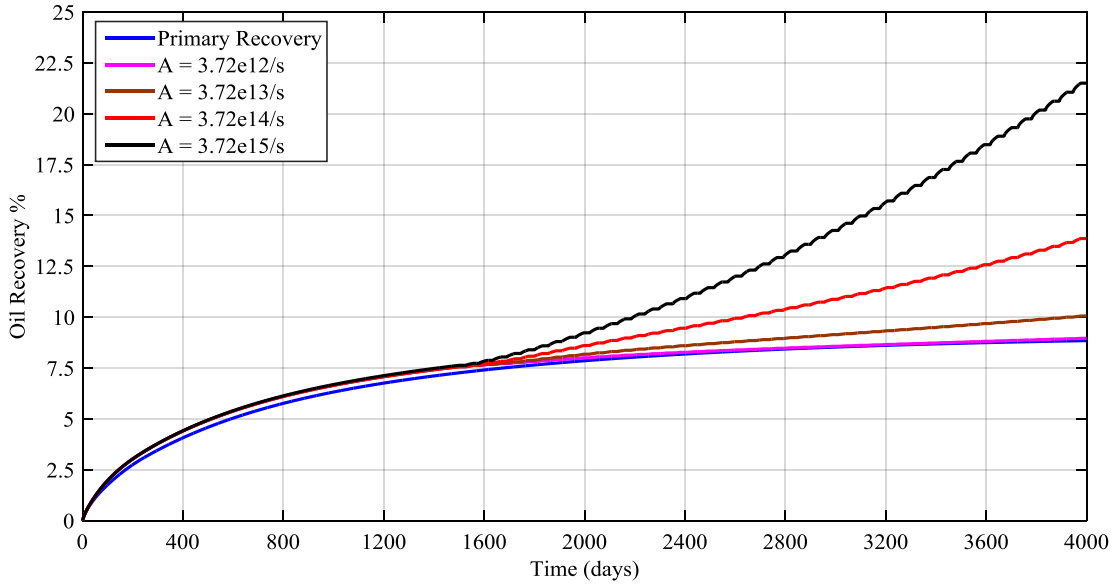

Figure 4-11: Higher oil recovery for higher frequency factor kerogen

Although this preliminary study shows the potential for steam injection to significantly improve oil recovery from kerogen-containing reservoirs by oil generation during kerogen decomposition, assumptions such as no thermal fluid expansion or vaporization of volatile oil components and no coke production during kerogen decomposition weaken the validity of results. Model results can be improved by replacing our black oil model with a compositional model. Furthermore, shale reservoirs are usually found in deep formations (depths greater than 5000 ft.); at these depths, heat loss from the wellbore makes injection of steam from the surface uneconomical and downhole steam generators are not recommended because of high maintenance costs and combustion control problems downhole.

In the next section, we include thermal expansion and coke production in our reservoir model and replace steam injection with downhole electromagnetic heating.

Chapter 5: Thermal Stimulation in Unconventional Shale Reservoirs

This chapter presents and discusses thermal simulation results derived from CMG STARS. It begins with a brief description of the equations solved in CMG STARS, followed by some key model inputs. Finally, an in-depth discussion of the thermal stimulation results is presented and the effects of several reservoir and design parameters are investigated.

5.1 Model Development

Thermal stimulation of shale oil reservoirs was simulated in CMG STARS, incorporating mass transport, heat transfer, phase equilibrium at elevated temperatures and reaction kinetics for the following kerogen decomposition reaction (Fan et al., 2010):

1 mole kerogen → 0.009588 mole heavy oil + 0.0178 mole light oil + 0.04475 mole HC gas + 0.00541 mole CO2 + 0.5827 mole coke

The kerogen and coke are considered components of the organic solid phase, heavy oil is considered the C_{20}-C_{29} components of the oil, light oil consists of C_{11}-C_{29} components and HC gas stands for the ethane in this work.

5.1.1. Governing Equations

The mass balance equation in compositional simulations can be expressed for each fluid component *i* and for each organic solid component s (either kerogen or coke) as follows (Fan et al., 2010):

$$\frac{\partial}{\partial t}\left(\phi\sum_j S_j\rho_j X_{ij}\right)-\sum_j\left(a_{ij}-b_{ij}\right)r+\nabla\sum_j\rho_j X_{ij}u_j+\sum_j\rho_j X_{ij}q_j=0 \tag{5.1}$$

$$\frac{\partial C_s}{\partial t}-\left(a_s-b_s\right)r=0 \tag{5.2}$$

where ϕ is reservoir porosity, S_j is the saturation of phase j, ρ_j is density of phase j, X_{ij} is the mole fraction of component i in phase j, a_{ij} and a_s are product stoichiometric coefficients for component i in phase j and for organic solid component s, respectively, b_{ij} and b_s are reactant stoichiometric coefficients for component i in phase j and for organic solid component s, respectively, q_j is the rate of phase j as source/sink, C_s is the organic solid concentration, r is reaction rate. Velocity, u_j, is computed by Darcy's law:

$$u_j=-\boldsymbol{K}\frac{k_{rj}}{\mu_j}(\nabla P_j+\rho_j gz) \tag{5.3}$$

where $\boldsymbol{K}$ is permeability tensor, k_{rj} is relative permeability of phase j, μ_j is viscosity of phase j, g is the gravitational constant (g = 32ft/s^2), z is reservoir depth and P_j is phase j pressure. The first group of terms in Eq. 5.1 accounts for mass accumulation, while the other groups of terms represent mass change in each phase resulting from the reaction, mass flow and well source/sink. The first term in Eq. 5.2 represents the change in organic solid component (e.g., kerogen) concentration, while the second group of terms accounts for mass evolved/consumed during the reaction. The mass of each component evolved or consumed during the reaction is governed by reaction rate (r) expressed as (Fan et al., 2010):

$$r = Ae^{\frac{-E_a}{k_b T}} \prod_{i,j} C_{ij}^{b_{ij}} \prod_{s} C_s^{b_s} \tag{5.4}$$

where A is frequency factor, E_a is activation energy, k_b is the Boltzmann constant and C_{ij} is the concentration of component i in phase j. The kerogen decomposition reaction converts organic solid reactants into fluid products, increasing pore volume and consequently, permeability. Eq. 5.5 below relates porosity to the change in kerogen concentration with time, while the Carmen-Kozeny equation (Eq. 5.6) relates rock permeability to changing fluid porosity.

$$\phi^{n+1} = \left(C_s^{n+1} - C_s^n\right)\frac{1}{\rho_s} + \phi^n \tag{5.5}$$

$$K^{n+1} = K^n \left(\frac{\phi^{n+1}}{\phi^n}\right)^{ck} \left(\frac{1-\phi^n}{1-\phi^{n+1}}\right)^2 \tag{5.6}$$

where ρ_s is solid density, superscript n is a time marker and ck is the Carmen-Kozeny coefficient, which we assume to be 0.95 in this study.

As a result of the temperature dependence of phase density, composition and reaction rate, the mass balance equation is coupled with the energy balance equation given by (Fan et al., 2010):

$$\frac{\partial}{\partial t}\left[\phi\left(\sum_j U_j \rho_j S_j\right) + (1-\phi)U_r\right] - \nabla\left(\sum_j H_j \rho_j u_j\right) - \nabla\left(\kappa \nabla T\right) + \sum_j H_j \rho_j q_j + q_h = 0 \tag{5.7}$$

where U_j and U_r are the internal energies of phase j and the rock respectively, H_j is the enthalpy of phase j, κ is thermal conductivity, T is temperature and q_h is heat input/output from a well. The first group of terms in Eq. 5.7 represents energy accumulation, the second and third groups are convection and conduction respectively, while the fourth and fifth groups account for heat input and output. Additionally, Eq. 5.7 assumes reaction enthalpy is negligible in comparison with heat input (Pan et al., 1984).

5.1.2. Model Inputs

A more detailed analysis of the reservoir and fluid properties used in this study is provided in Chapter 3; a brief summary of relevant properties is presented in the following table. Injection temperature and production pressure are 700 °F and 2000 psi respectively.

Table 5-1: Summary of reservoir and fluid properties at initial conditions

PROPERTY	**VALUE**
Fracture permeability (mD)	10,000
Fracture width (ft.)	0.005
Rock permeability (mD)	0.0015
Rock porosity	0.08
Reservoir thickness (ft.)	10
Shale thermal conductivity (Btu/ft. day °F)	30
Initial oil saturation	0.7
Initial pressure (psi)	6840
Initial temperature (°F)	248
Initial kerogen concentration (weight %)	10
Oil viscosity (cp)	0.31
Fluid compressibility psi^{-1}	1.3×10^{-5}
Oil formation volume factor (rb/stb)	1.71
Oil density (lb/ft^3)	40.3
Bubble point (psi)	2600

5.2. RESULTS & DISCUSSION

In the following sections, the proposed thermal recovery method is discussed, as well as sensitivity to key parameters such as heating temperature, time and kerogen reaction properties that affect the viability of the proposed process. A key consideration in thermal recovery processes is the cost of energy input; therefore the economics of the proposed recovery method is also assessed.

5.2.1. The Thermal Recovery Process

The proposed method consists of a primary depletion period operated at 2000 psi bottomhole pressure, followed by thermal stimulation using 700 °F heater wells, and finally a secondary depletion period operated at 2000 psi bottomhole pressure. A single well serves as both the producer and the heater. Fig. 5-1 illustrates pressure decline from an initial average reservoir pressure of 6840 psi to 3300 psi during 3000 days of primary depletion; increased reservoir temperature during the following 1000 days of thermal stimulation leads to an increase in average reservoir pressure to 7000 psi. When a fluid is heated in a fixed pore volume, the pore pressure increases; we refer to this mechanism here as "thermal pressurization." Pressure continues its decline during the final 3000 days of secondary depletion observed in this study. 7000 days (20 years) well life was chosen for this study based on the study by Clark (2009), which found that Bakken wells produce less than 10 bbls/day after about 7000 days.

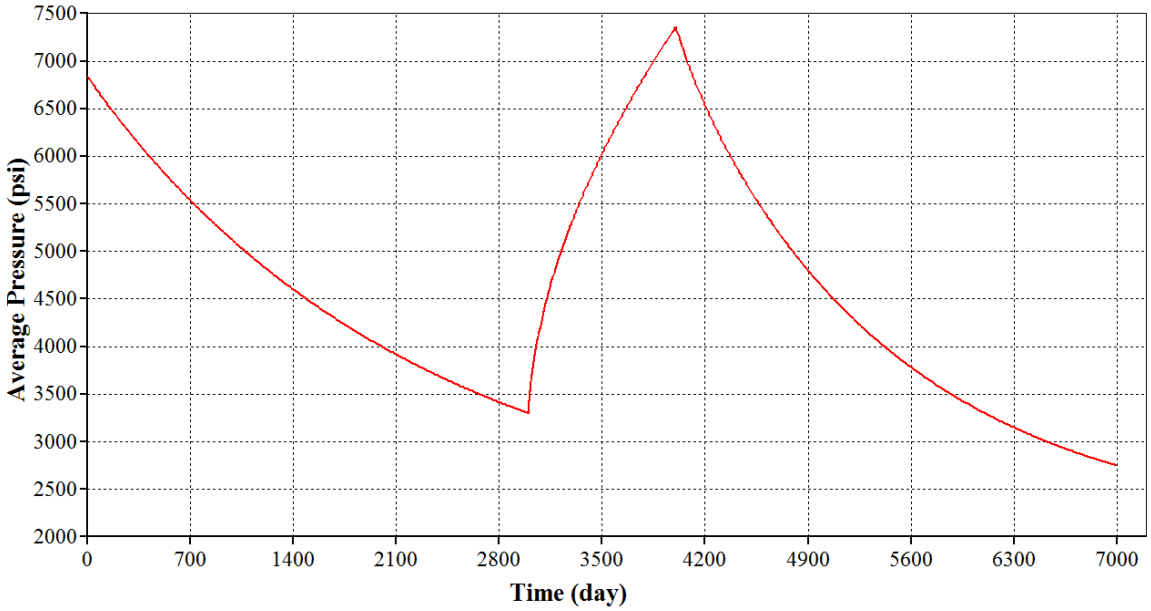

Figure 5-1: Average reservoir pressure versus time for the base case. 3000 days of production were followed by 1000 days of heating and then 3000 days of secondary recovery

Fig. 5-2 shows that after heating, pressure varies from a maximum of 7650 psi close to the wellbore to about 6600 psi farther away. As expected, there is greater thermal pressurization close to the heat source.

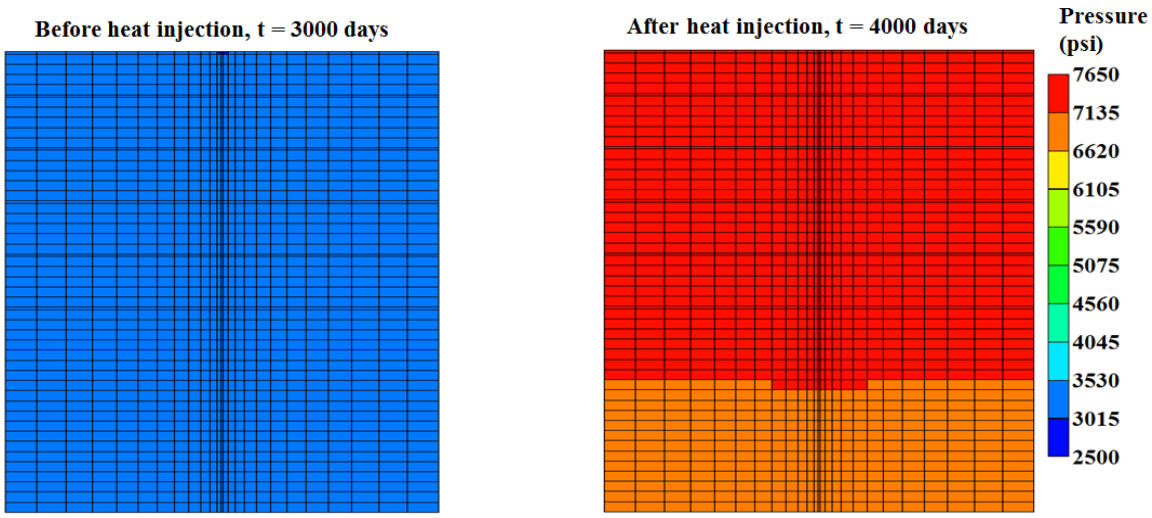

Figure 5-2: Pressure increase after heating

The temperature and the oil viscosity distributions in the reservoir at the end of the thermal stimulation period are illustrated in Fig. 5-3; the temperature increased from about 240 to 680 °F around the wellbore which leads to a slight decrease in oil viscosity from 0.3 to 0.23 cp. This decrease is significant, but not enough to significantly improve recovery as will be shown later in this section.

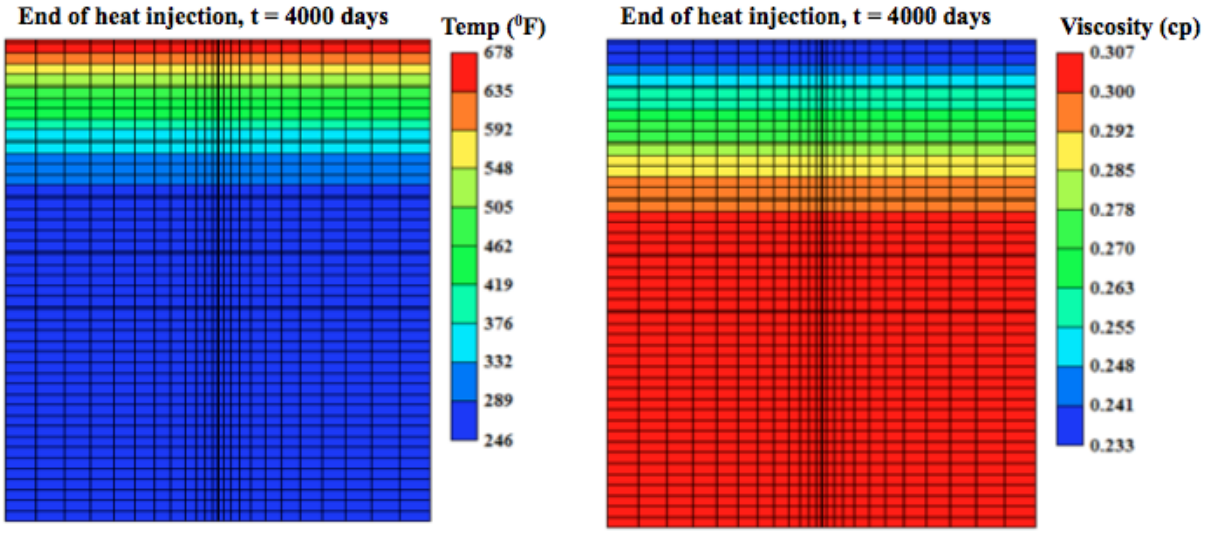

Figure 5-3: Increased temperature (on the left) and reduced viscosity (on the right) around the wellbore after heating

The high reservoir temperature around the wellbore resulting from heat injection accelerates kerogen decomposition into oil and gas, increasing the fluid content; Eq. 5.4 shows the temperature dependence of kerogen decomposition rate. Additionally, rock volume (i.e. kerogen) is converted to pore volume during kerogen decomposition, resulting in increased porosity. The Carmen-Kozeny relationship in Eq. 5.6 shows a positive relationship between porosity and permeability; consequently, permeability increases during kerogen decomposition. Figs. 5-4a to 5-4c show decreased kerogen concentration around the wellbore from 1.0 lbmol/ft^3 (10 wt-%) to no kerogen, increased porosity from 8 to 10% and increased permeability from 0.0015 to 0.002 mD.

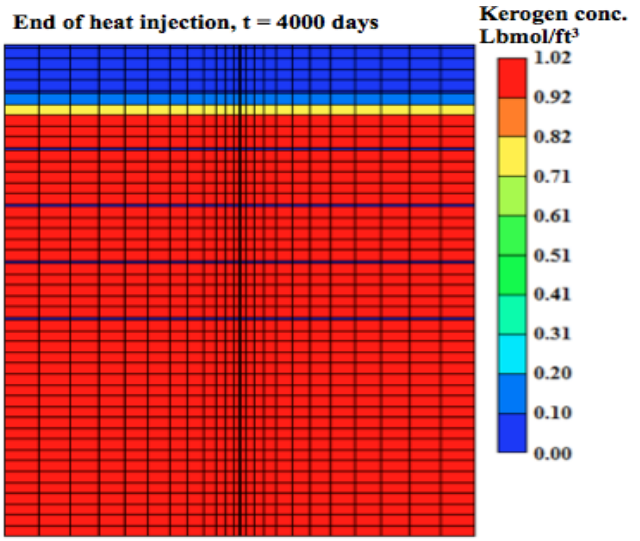

Figure 5-4a: Kerogen conc. after heating

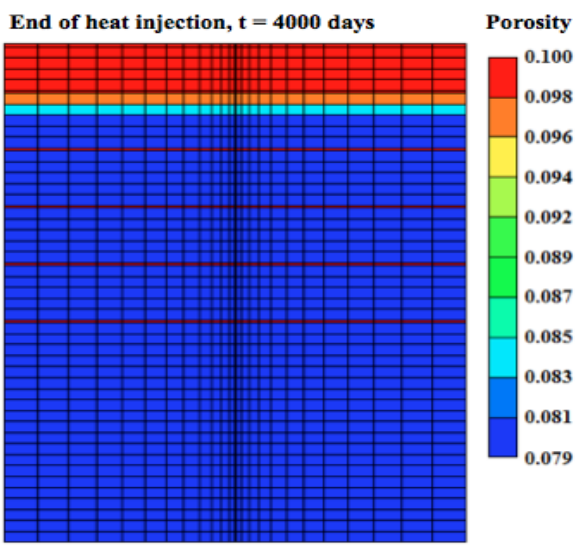

Figure 5-4b: Porosity after heating

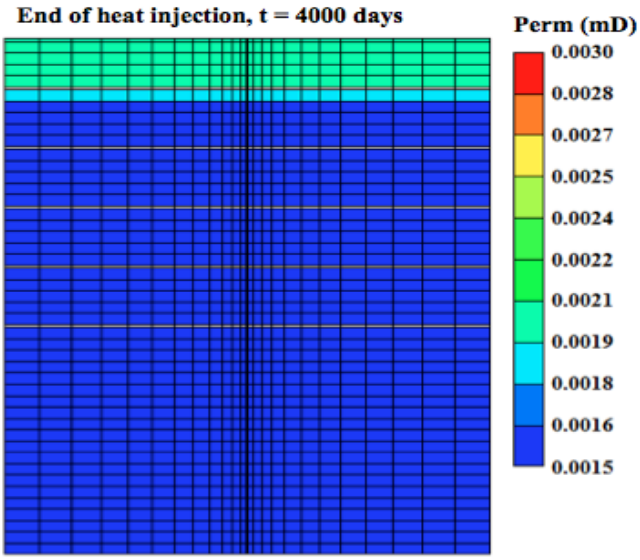

Figure 5-4c: Permeability after heating

In order to determine the impact of thermal stimulation on recovery, this study compared four cases: primary depletion for the entire reservoir life (7000 days), primary

depletion with a shut-in period midway through the well life, thermal recovery assuming no kerogen in the reservoir shale and thermal recovery in a shale reservoir with 10 wt-% of kerogen. Fig. 5-5 shows an oil recovery of below 7.2% for both primary depletion cases, which is consistent with the 7% estimated by Clark (2009) from material balance and decline curve analyses and the 8 – 10% recovery estimated by Breit et al. (1992). Thermal stimulation results in improved recovery – 11.5% and 10.5% overall recovery with and without kerogen, respectively. Interestingly, thermal recovery for the case of a kerogen-containing shale reservoir is only slightly greater than thermal recovery from a shale reservoir with no kerogen, implying that increased oil in place from kerogen decomposition in the kerogen-containing reservoir is not the primary reason for the improved recovery. Fig. 5-4a explains kerogen decomposition's minor impact on recovery; the region with the highest kerogen decomposition is not well connected with the fractured region, therefore, the generated oil is not produced. The slight increase in thermal recovery with kerogen compared to recovery without kerogen can be partially attributed to the increase in permeability around the wellbore during kerogen decomposition (Fig. 5-4c). A better connection between the fracture and the heated region would enhance the impact of kerogen decomposition on recovery.

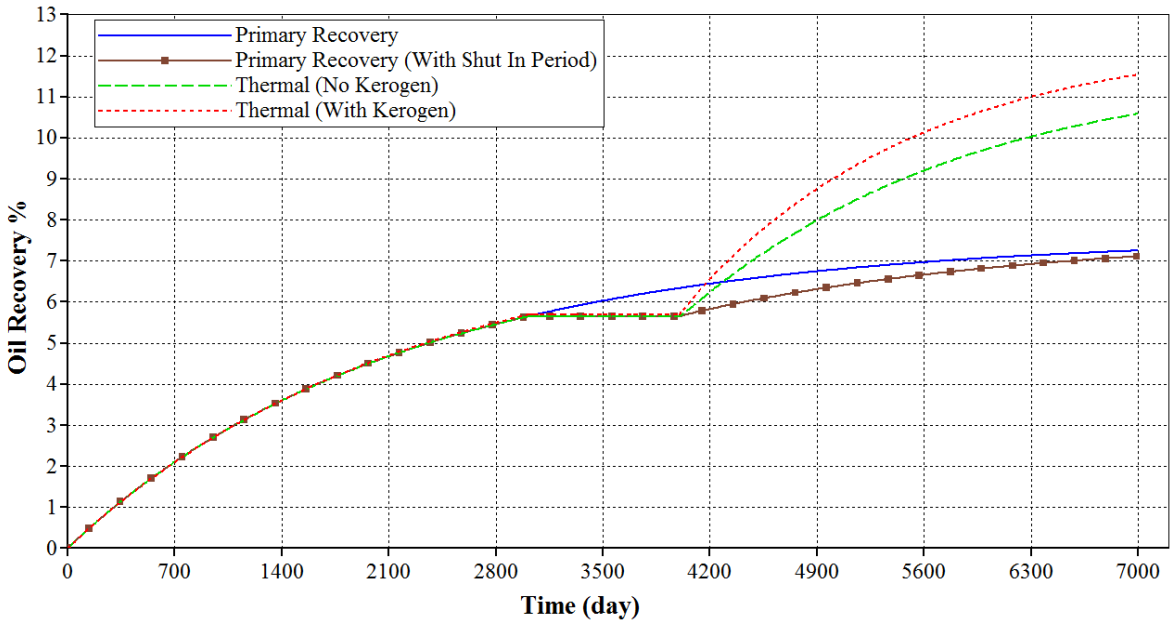

Figure 5-5: Oil recovery for primary recovery and thermal stimulation with and without kerogen

As previously stated, viscosity decreased from 0.3 to 0.23 cp during heating. In order to determine the effect of this viscosity change on recovery, viscosity was modified to 0.23 cp, while everything else, including temperature, was kept constant. Fig. 5-6 shows that recovery (7.7%) of 0.23 cp oil is only slightly greater than recovery (7.2%) of 0.3 cp oil, therefore, the viscosity reduction does not significantly improve recovery.

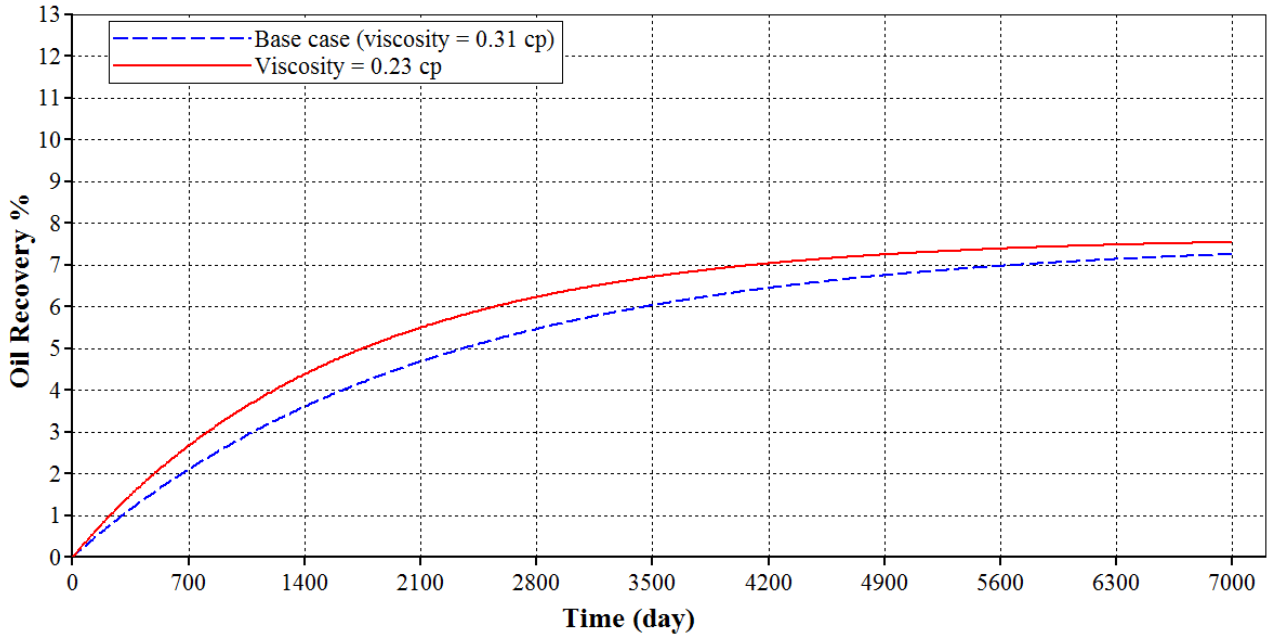

Figure 5-6: Oil viscosity reduction does not significantly affect recovery

Fig. 5-7 shows that average reservoir pressure after heating is slightly higher for the case of a reservoir with kerogen, contributing to the observed slightly higher oil recovery for the kerogen-containing reservoir compared to the reservoir absent of kerogen.

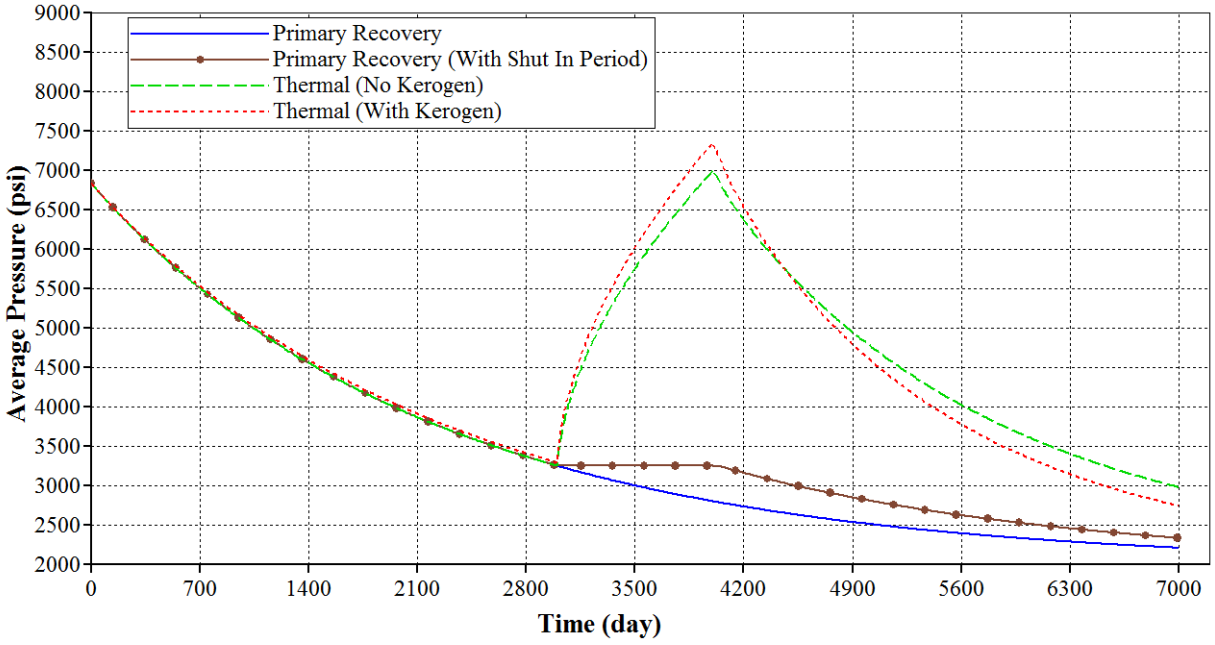

Figure 5-7: Average reservoir pressure for primary recovery and thermal stimulation with and without kerogen

The slightly higher pressure observed in the kerogen-containing reservoir is a result of the difference between the volume of hydrocarbons generated and the amount of pore space created during kerogen decomposition. Because kerogen is denser than hydrocarbon fluids, the volume of fluids produced during decomposition of a given mass of kerogen is greater than the volume of pore space created by the consumption of that mass of kerogen in the reaction, resulting in increased pore pressure.

The following subsections discuss parameters that may influence thermal recovery from shale oil reservoirs.

5.2.2. Primary Production Duration

The length of the primary depletion period is an important parameter in the proposed thermal stimulation process. Previous secondary recovery studies, particularly gas injection in shale oil reservoirs, have assumed primary depletion periods ranging from 0 days (Chen et al., 2013) to 1825 days (Yu et al., 2014).

The length of primary recovery was varied while heat injection into a kerogen-containing shale oil reservoir was maintained at 700 °F and for 1000 days in all cases. As Fig. 5-8 shows, the length of the primary depletion period has a significant effect on recovery. Starting heat injection after 4000 days leads to 11% recovery, but recovery can be increased by reducing the primary depletion period. In fact Fig. 5-8 suggests that the optimal scenario is beginning heat injection without any primary depletion, resulting in greater than 12.5% recovery. Fig. 5-9 shows that maximum reservoir pressure after heat injection can be as high as 11,900 psi when heat injection begins early in the life of the reservoir. From DFIT data, Yang et al. (2013) determined fracture pressure in the Bakken to be 7500 – 8100 psi. Therefore, starting early can lead to additional fracturing which may increase oil recovery more than what is modeled here. We have not included thermally-driven fracturing in these simulations and have limited our evaluation to the schemes that stay under the fracture pressure. Including thermally-driven fracturing in future simulations is recommended.

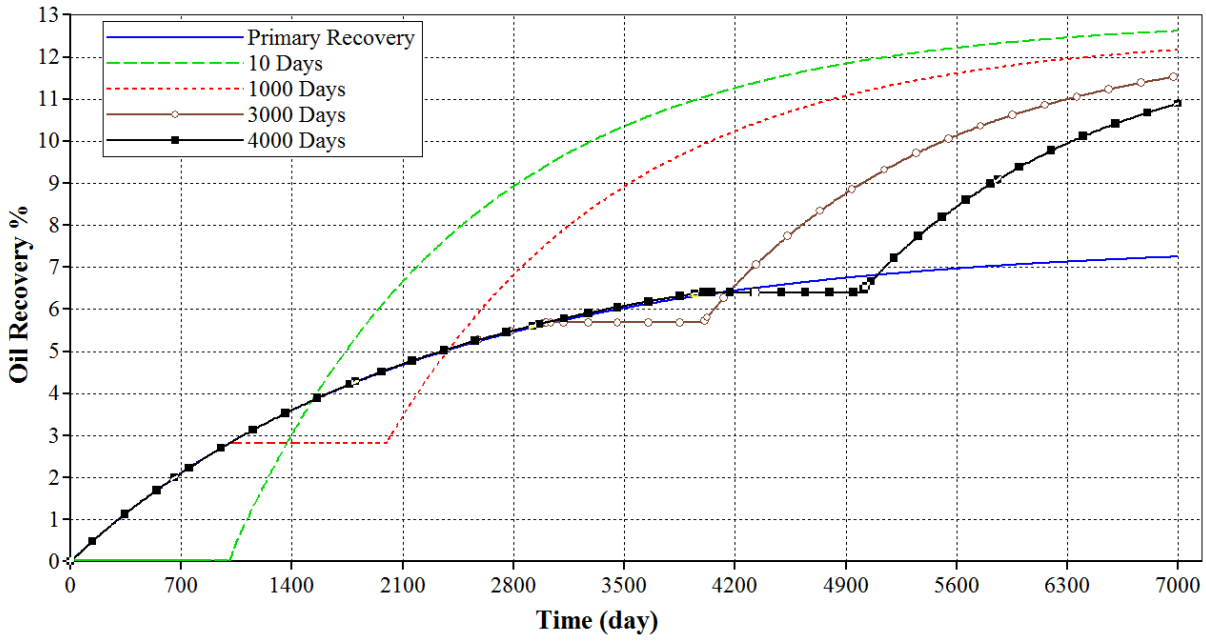

Figure 5-8: Early heat injection leads to more favorable recovery

Primary depletion period of 3000 days was selected as the base case in this study because Fig. 5-9 shows that the (spatially) maximum reservoir pressure after heating does not exceed the fracture pressure range given by Yang et al. (2013). For cases with shorter primary depletion periods, maximum reservoir pressure after heating can be decreased if heat is injected for a shorter duration and at a lower temperature.

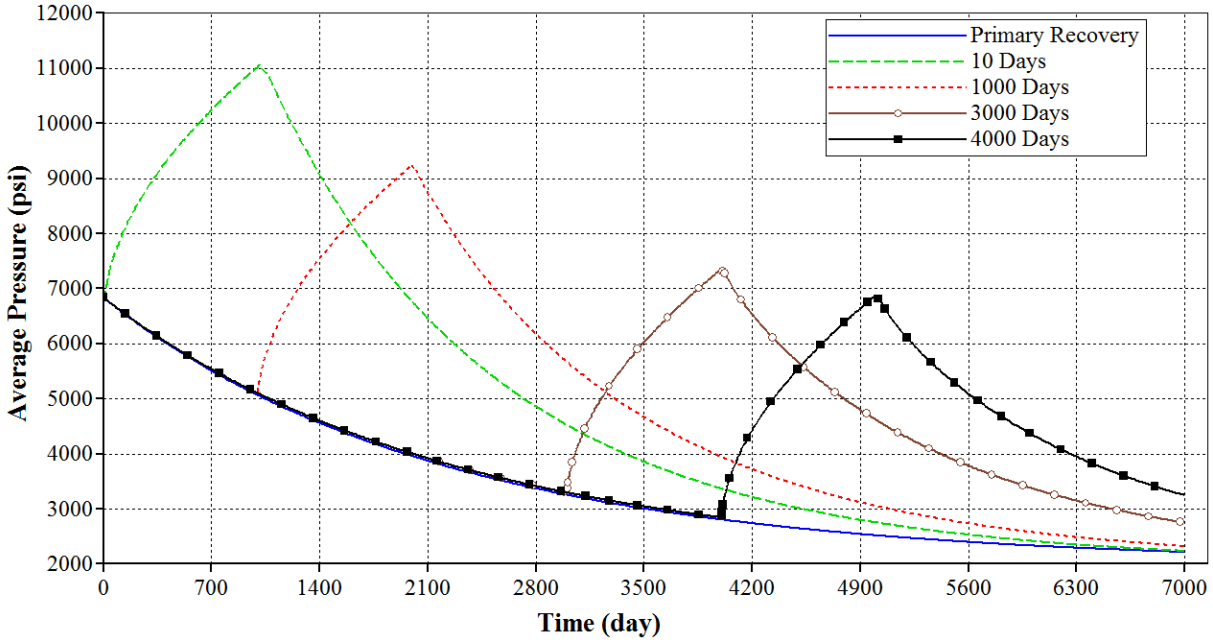

Figure 5-9: Maximum reservoir pressure for different heat injection start times

5.2.3. Heating Temperature and Time

Heating temperature and time are important parameters when designing a thermal stimulation process. Longer heating times and higher heating temperatures result in higher energy input into the reservoir, leading to greater thermal pressurization and viscosity reduction. Furthermore, kerogen decomposition rate is temperature dependent; at elevated temperatures, more kerogen decomposes into oil and gas, increasing porosity and permeability evolution. As expected, Figs. 5-10 and 5-11 show that higher temperatures and longer heat injection periods, respectively, result in greater oil recovery.

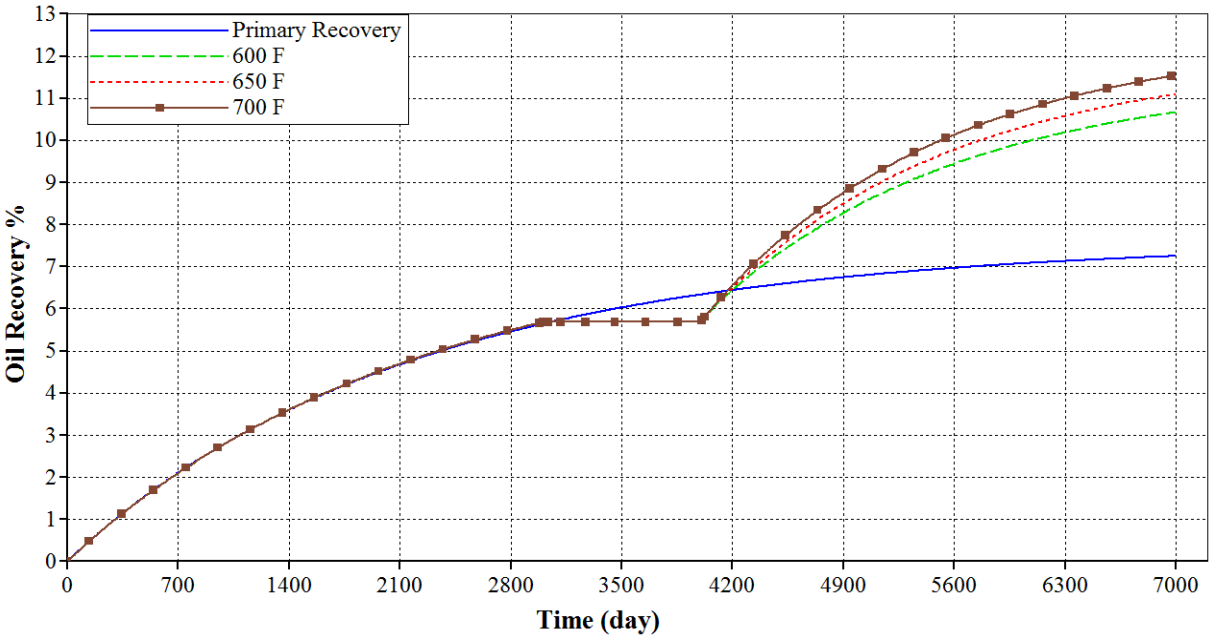

Figure 5-10: Higher injection temperature leads to more favorable recovery

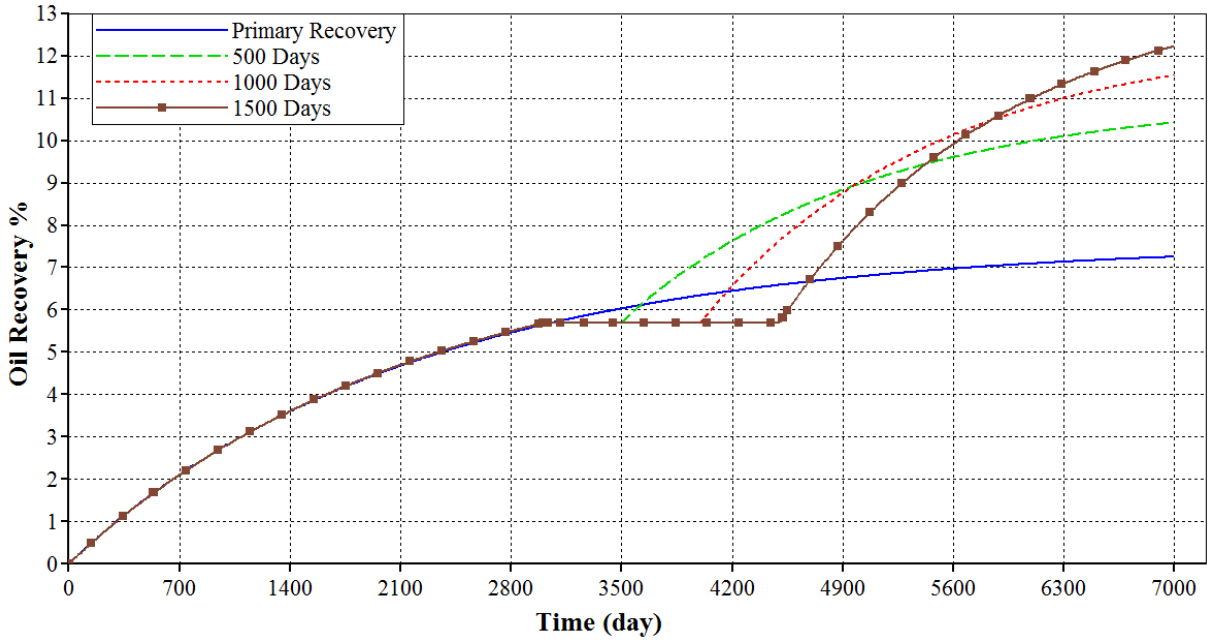

Figure 5-11: Longer heat injection period leads to more favorable recovery

However, longer heating times and higher temperatures increase cost. Fig. 5-12 shows that a 700 °F heater requires about 33% more energy than a 600 °F heater and Fig. 5-13 shows that longer heating times require significantly more energy than shorter heating periods. The optimal heating temperature and time must be based on the resulting lowest energy cost per incremental barrel of oil produced. A later section discusses the economics of the thermal recovery process.

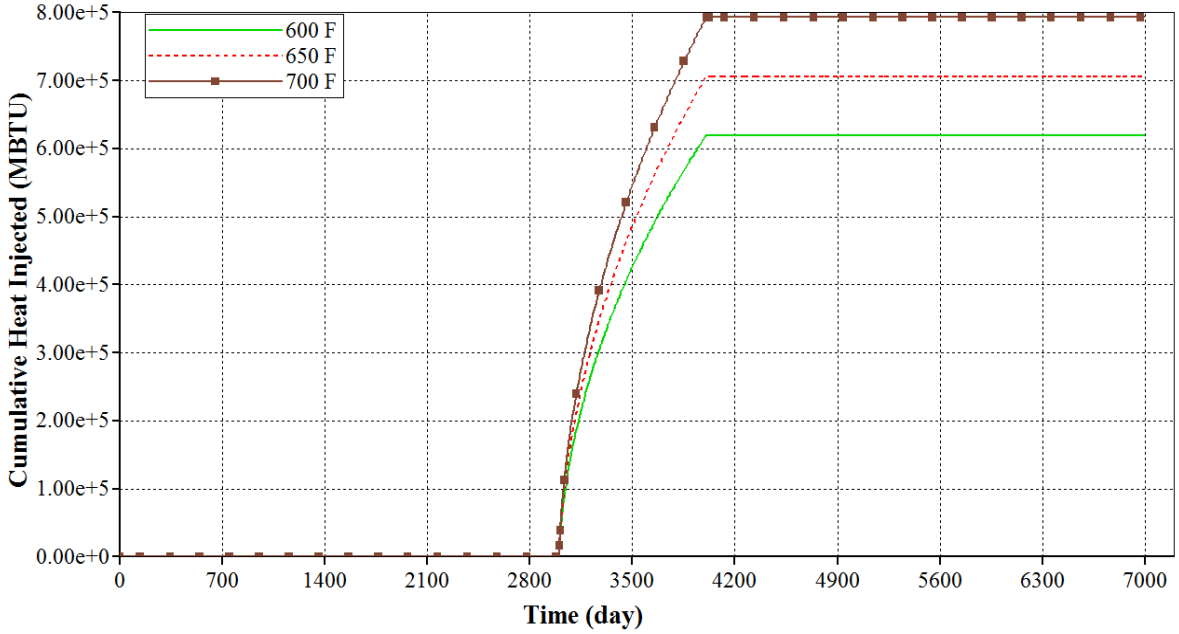

Figure 5-12: Higher injection temperature requires more energy input

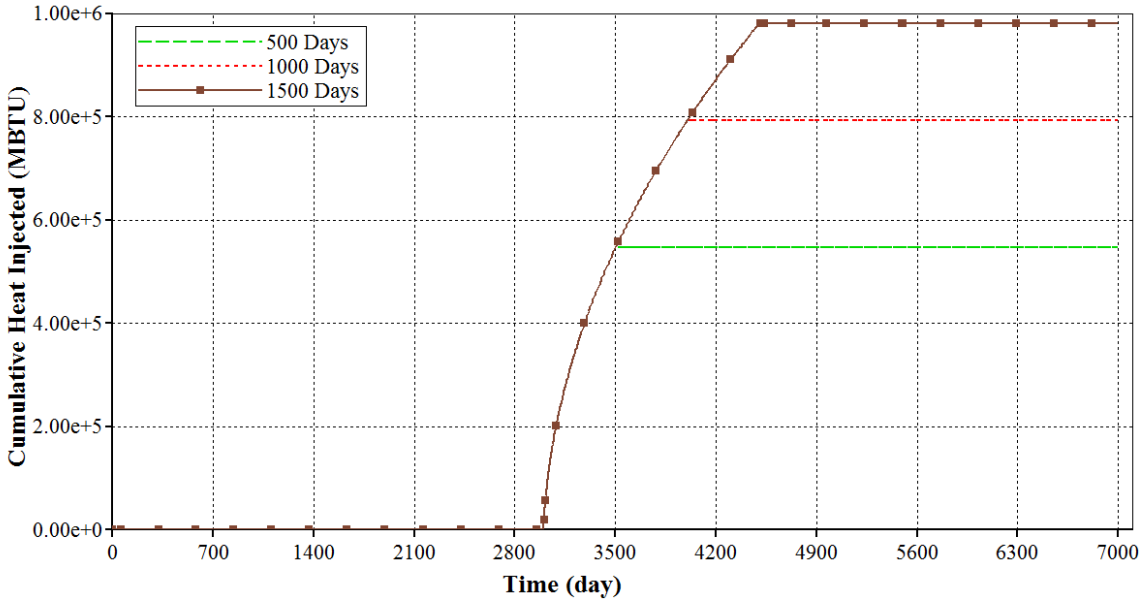

Figure 5-13: Longer heat injection periods require more energy input

5.2.4. Shale Conductivity

A USGS (1988) report states that shale thermal conductivity is in the 20.8 – 41.6 Btu/ft-day-°F range. Because the heat source in this study is a heater well, rather than steam or hot water, the main mechanism of heat transfer is conduction through the rock matrix. Consequently, the conductivity of shale determines how far the temperature field propagates. Fig. 5-14 illustrates that higher conductivity leads to more effective temperature propagation.

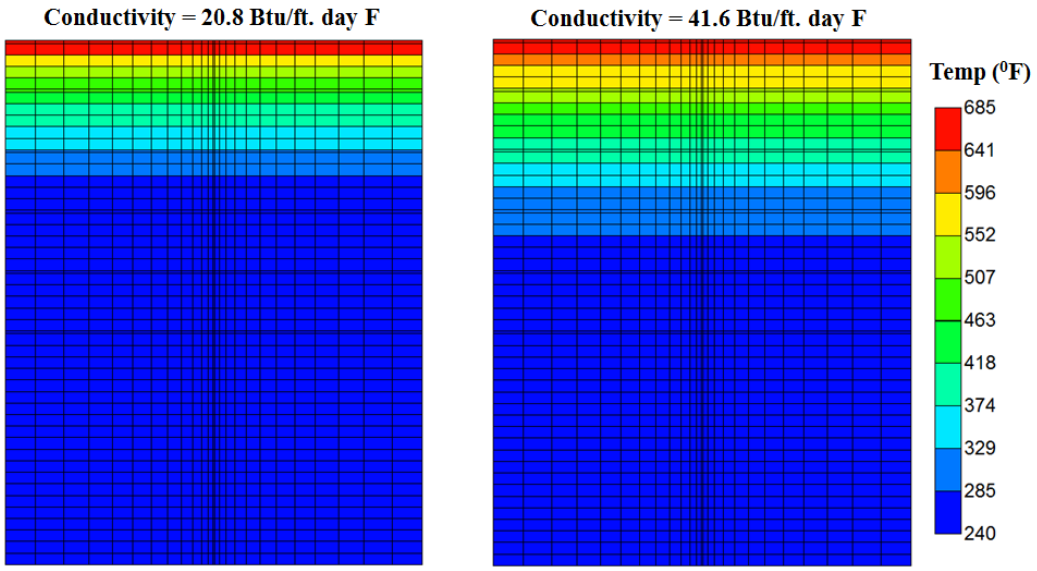

Figure 5-14: Temperature field for different conductivities after heating, t = 4000 days

Farther temperature propagation implies that more of the reservoir fluid is at an elevated temperature encouraging larger thermal pressurization and recovery – 12.3% for the high conductivity case versus 10.9% for the low conductivity case, as shown in Fig. 5-15.

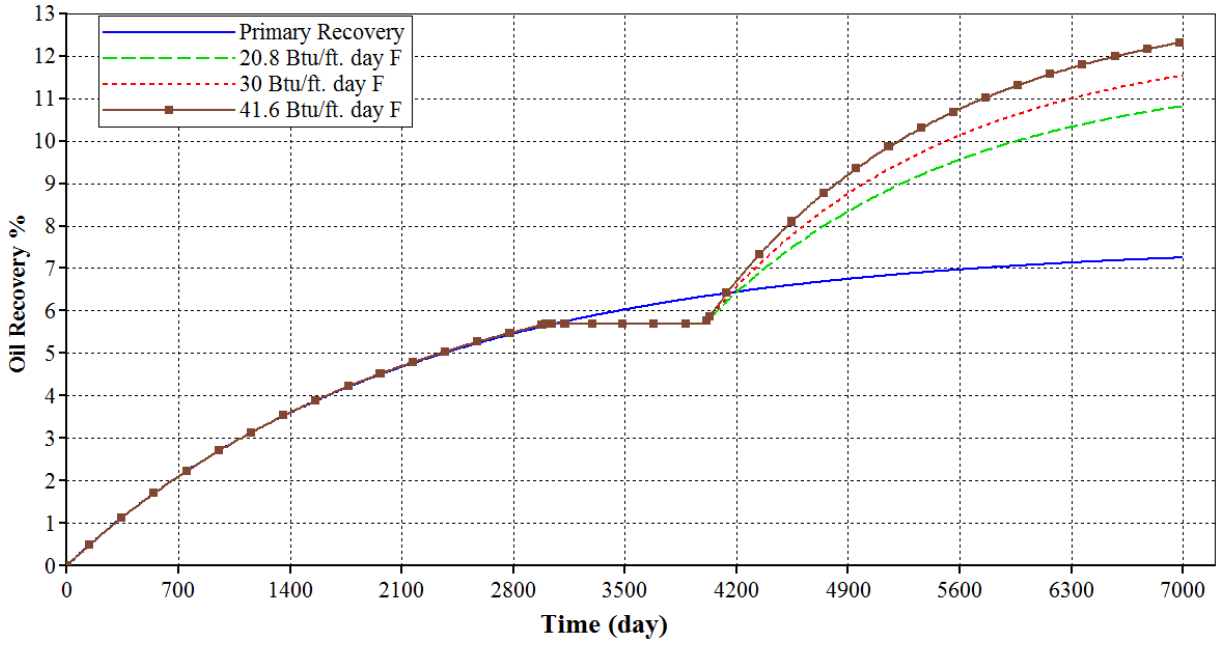

Figure 5-15: Greater oil recovery in more conductive shale formation

5.2.5. Kerogen Reaction Activation Energy and Frequency Factor

Kerogen reaction rate is inversely proportional to activation energy and directly proportional to frequency factor. Activation energy is the minimum energy that must be available to reactants for a reaction to occur; Oba et al. (2002) determined that activation energy for kerogens varies between 81,500 and 107,000 Btu/lbmol. Frequency factor is a measure of the frequency of reactant molecule collisions; Oba et al. (2002) determined that frequency factor for kerogen is in the $9.5 \times 10^{16} – 9.5 \times 10^{22}$ per day range. Fig. 5-16 illustrates the direct relationship between frequency factor and kerogen reaction rate – greater increase of oil in place (OIP) during the heating period implies faster kerogen

decomposition. Conversely, Fig. 5-17 shows an inverse relationship between oil generation and activation energy; more oil is generated in low activation energy kerogen.

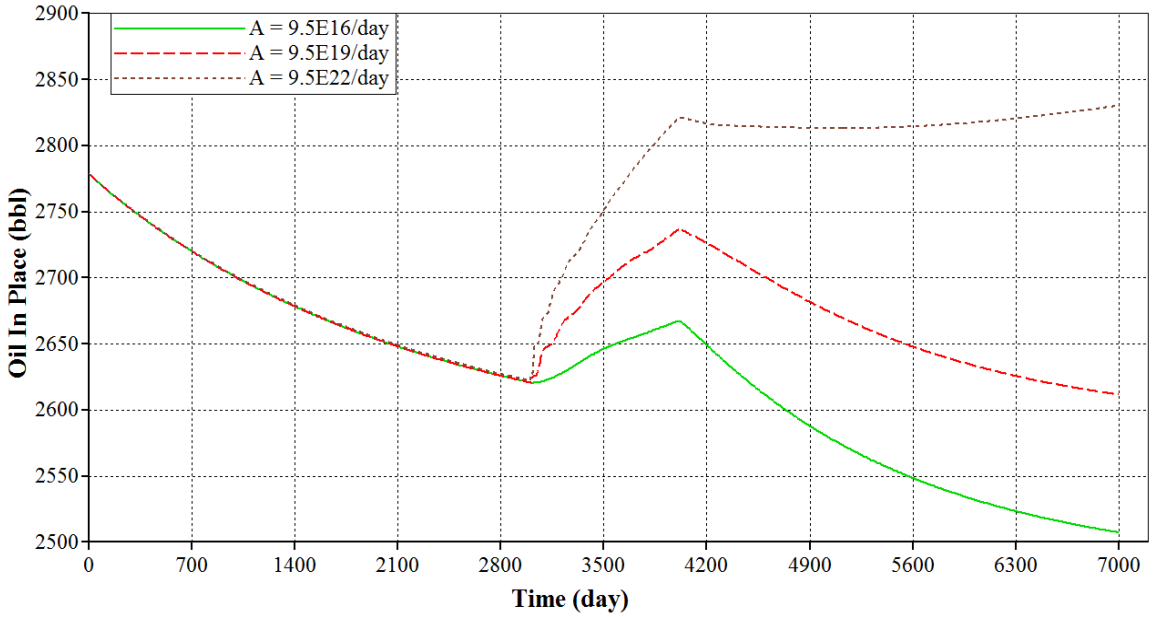

Figure 5-16: Oil in place for different kerogen reaction frequency factors

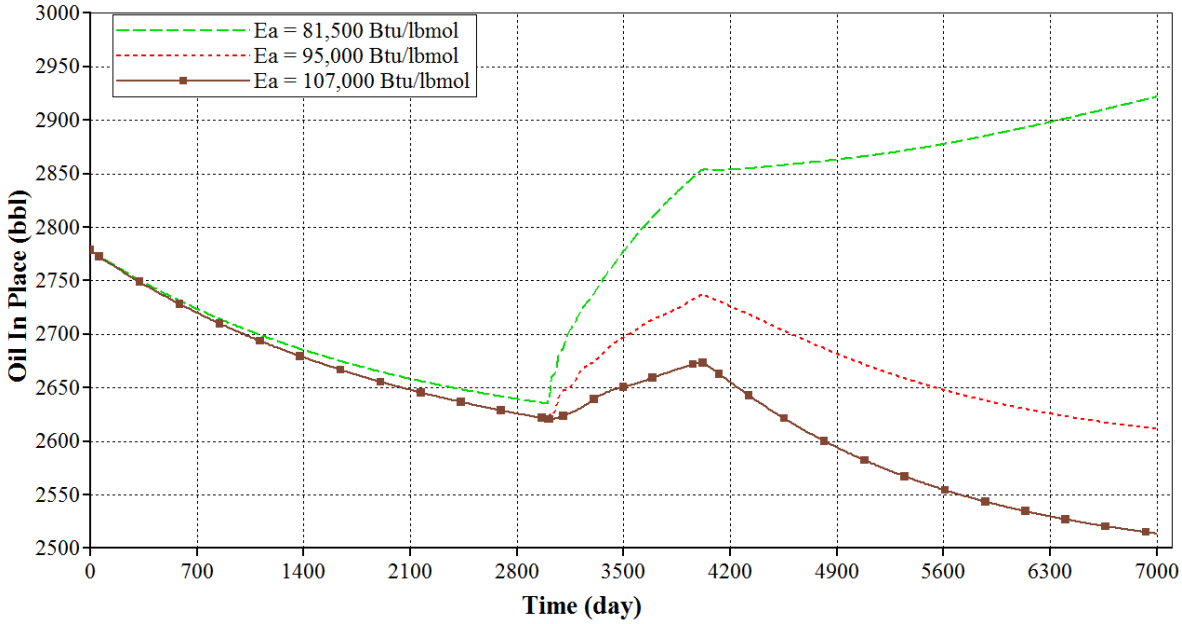

Figure 5-17: Oil in place for different kerogen reaction activation energies

For the three cases in Fig. 5-16, decline in OIP is identical during primary depletion. However, during the heating period, higher frequency factor leads to greater kerogen decomposition and larger increase in oil in place. After heating, oil in place for the 9.5×10^{22} frequency factor case is more than 5% greater than for 9.5×10^{16}. Interestingly, for the kerogen with a high frequency factor, oil in place continues increasing even after heating is stopped, implying that oil is being generated from kerogen faster than it can be produced at the wellbore.

Figs. 5-18 and 5-19 below show that higher frequency factors and lower activation energies, which both imply faster kerogen decomposition, result in higher recovery but not significantly. Recovery for the high frequency factor kerogen reservoir is greater than for the low frequency factor kerogen by only 0.5% because although there

is more oil, low permeability in the region of kerogen decomposition limits recovery. The heating scheme may be improved to better connect the region of kerogen decomposition with the fracture network by using a conductive proppant or injecting hot gas.

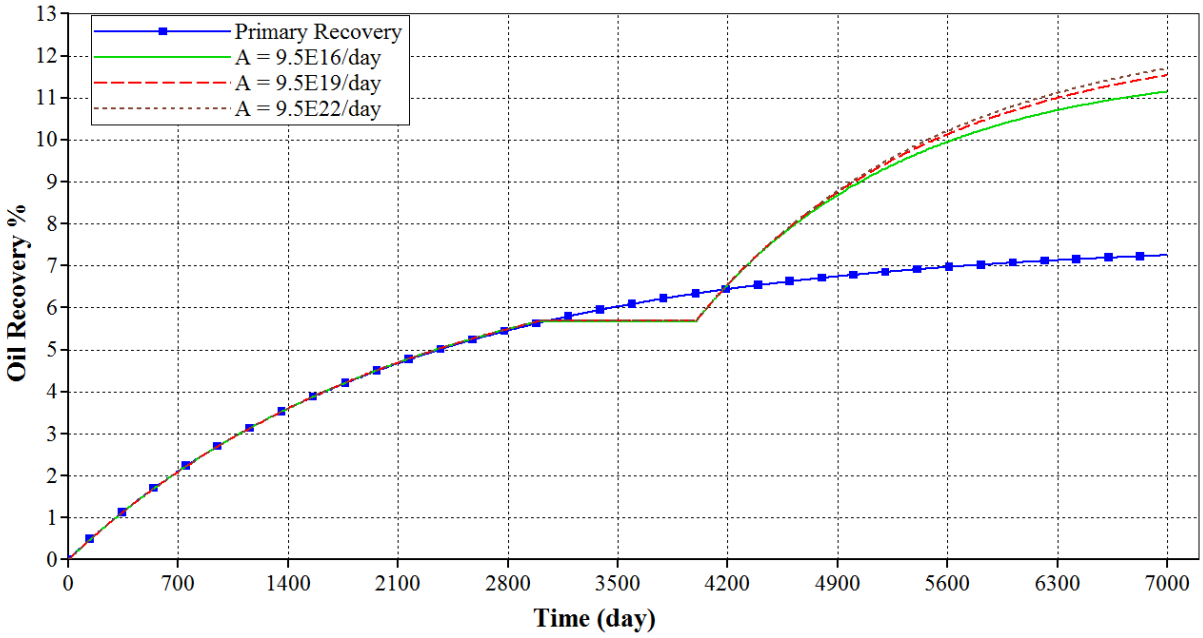

Figure 5-18: Oil recovery for different kerogen reaction activation energies

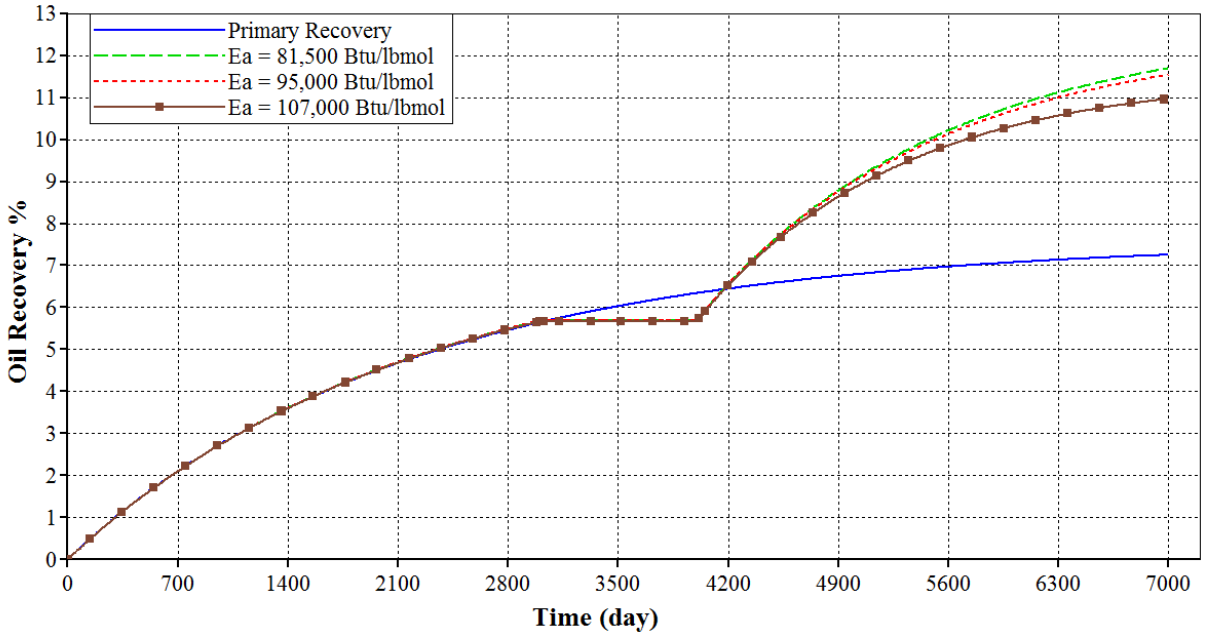

Figure 5-19: Oil recovery for different kerogen reaction frequency factors

5.2.6. Configuration with Simultaneous Production and Injection

The work done in this study has involved injecting heat and producing oil from the same well in cycles. In this section, the effect of producing oil while injecting heat through an adjacent well as shown in Fig. 5-20 is investigated.

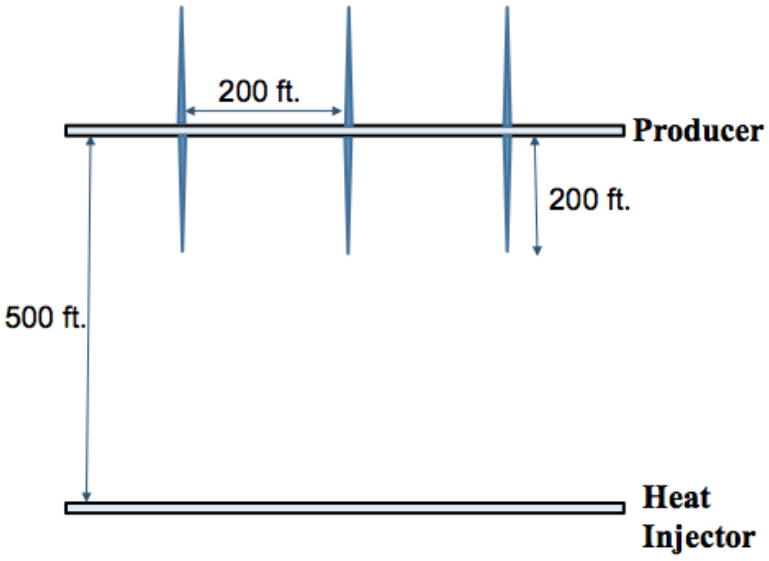

Figure 5-20: Illustration of modified configuration with separate injector and producer

Thermal pressurization during heat injection is expected to act as pressure support and reduce the rate of pressure decline during production. Fig. 5-21 shows that initially, pressure around the wellbore increases, however, pressure gradually declines over time. After 7000 days, average reservoir pressure reaches about 4000 psi from an initial pressure of 6840 psi. Although we observe pressure decline with simultaneous production and heat injection, Fig. 5-22 shows that this pressure decline is not as rapid as is observed with no thermal stimulation or with cyclic thermal stimulation, as was studied in earlier parts of this work.

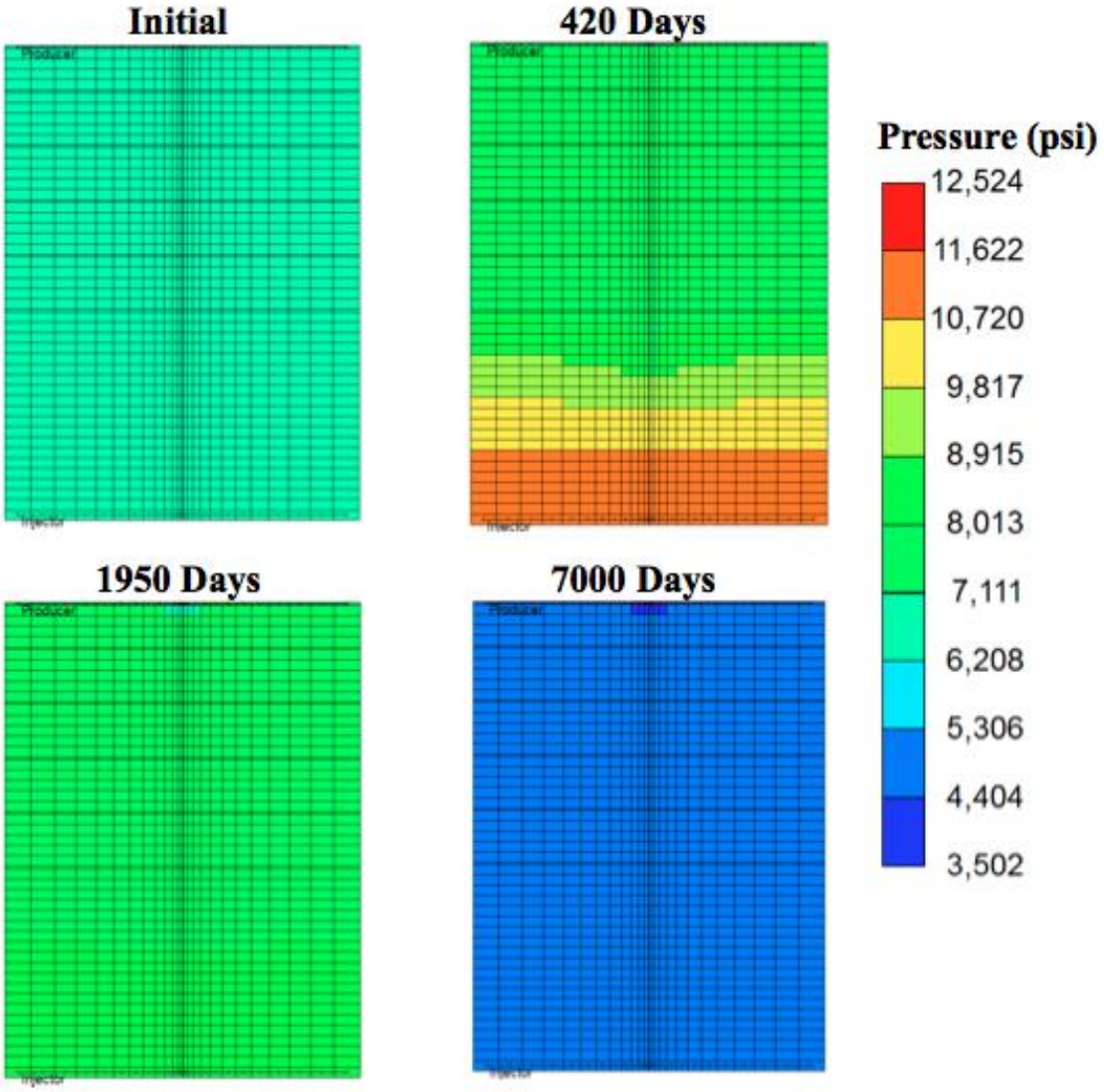

Figure 5-21: Pressure field at different times

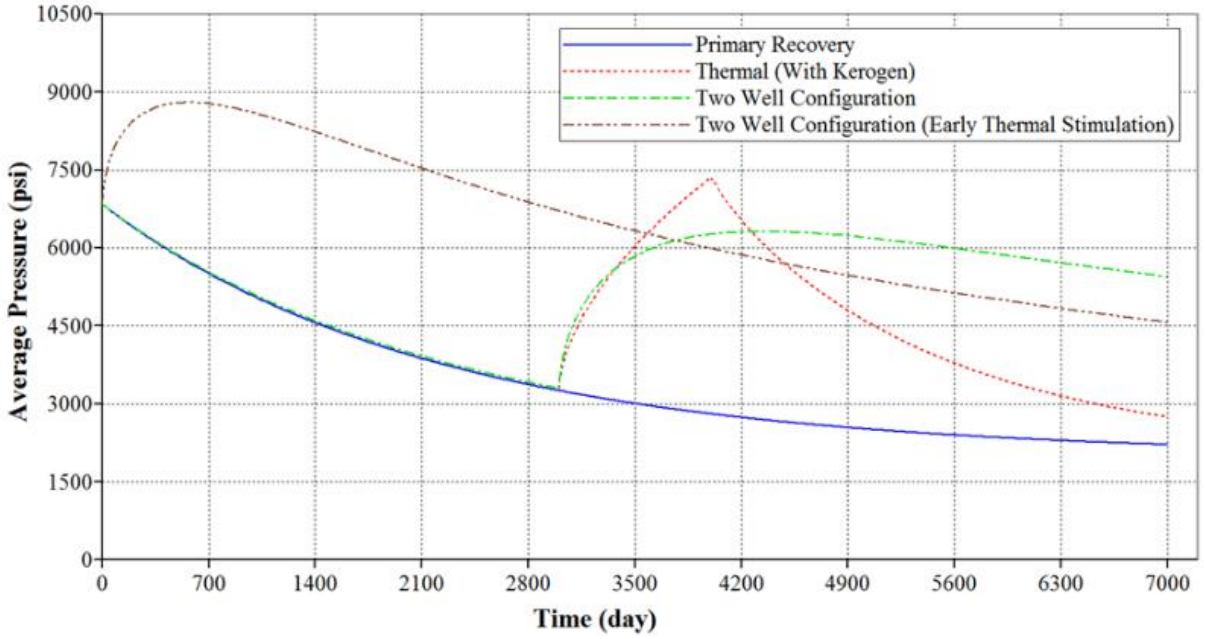

Figure 5-22: Gradual pressure decline for two-well configuration

Consequently, oil recovery is greater with simultaneous heat injection and production than with cyclic thermal stimulation as shown in Fig. 5-23 – 20.5% recovery when simultaneous injection and production begins on day 1 or 15.5% recovery when simultaneous injection and production begin after 3000 days of primary depletion compared to 11.5% for cyclic heat injection and 7.2% for primary depletion for the entire reservoir life.

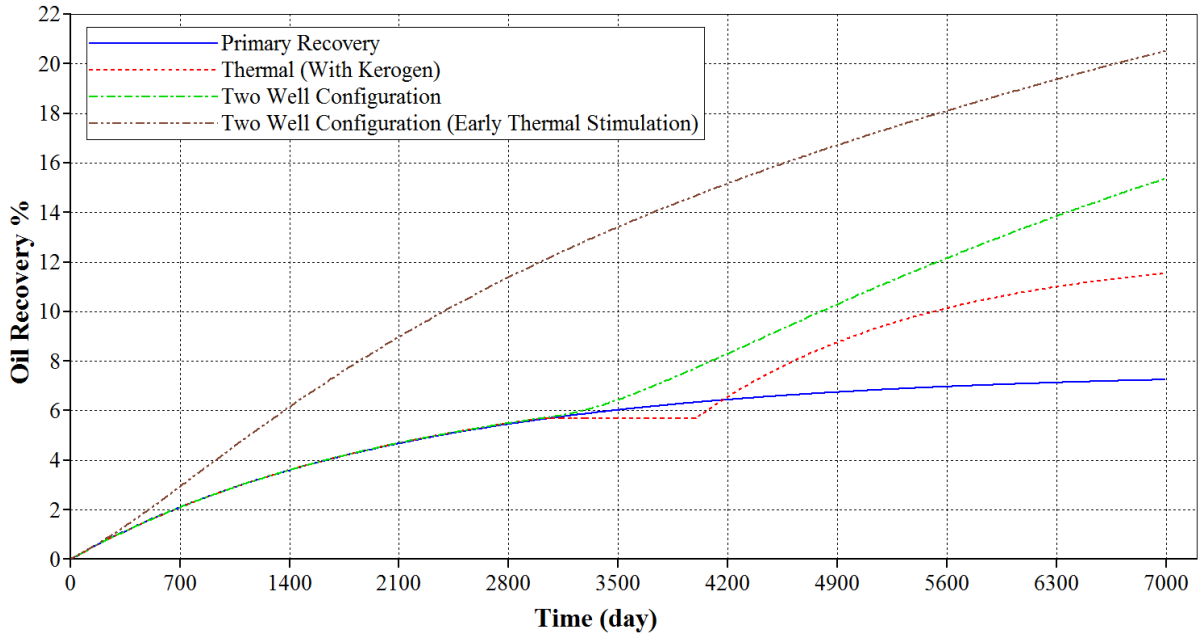

Figure 5-23: Two-well configuration shows favorable oil recovery

Operating a heat injector while producing requires a significant amount of energy; although recovery is greater with simultaneous production and injection, heat requirement is also significantly greater as the following figure shows.

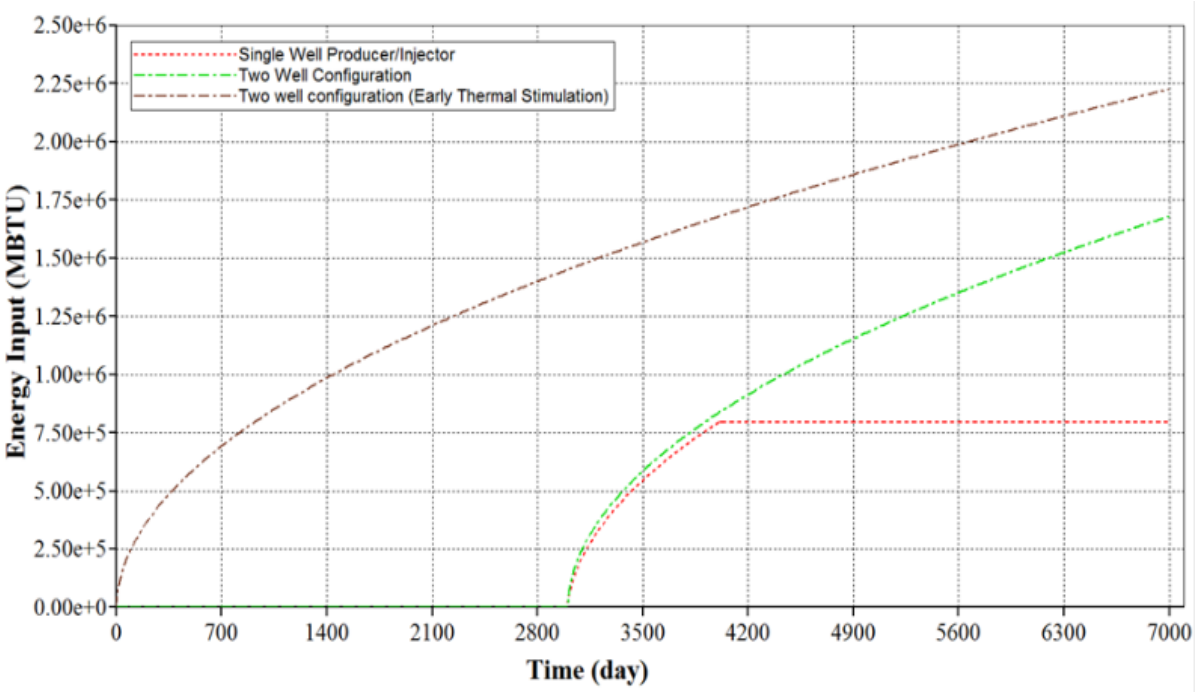

Figure 5-24: Energy requirement for two-well configuration

To determine the advantage of simultaneous heat injection and production over cyclic heat injection, energy cost per incremental barrel of oil produced was calculated from oil produced and heat injected; it is the ratio of heat injected to the incremental amount of oil produced from thermal stimulation. Low energy cost per incremental barrel of oil produced is ideal. Table 5-2 compares energy cost per barrel of oil for three cases: cyclic heat injection from a single well, simultaneous injection and production from two different wells after 3000 days of primary depletion, and simultaneous injection and production from day 1. The scenario with simultaneous heat injection and production beginning on day 1 has the highest recovery and lowest energy cost per incremental barrel of oil produced, making it ideal.

Table 5-2: Energy cost comparison for different thermal schemes

	Energy Cost per Incremental Barrel of oil Produced (MMBtu/bbl of oil)
Single well producer/injector	6.6
Simultaneous injection/production after 3000 days	7.4
Simultaneous injection/production after 1 day	6.0

5.2.7. Heat Loss and Reservoir Thickness

The thickness of the Bakken formation varies from 10 to 70 ft., but we assumed 10 ft. thickness for the previous simulations in this study. However, heat loss to the overburden and underburden, which is a key consideration in thermal processes, depends on reservoir thickness. Fig. 5-25 below shows that as reservoir thickness increases, heat efficiency (given by Eq. 5.8) increases. Consequently, Fig. 5-25 also shows that the energy cost per incremental barrel of oil produced is lower for thicker reservoirs because less of the energy input to the reservoir is lost to the overburden and underburden.

$$efficiency = \frac{heat_{input} - heat_{loss}}{heat_{input}} \times 100\% \tag{5.8}$$

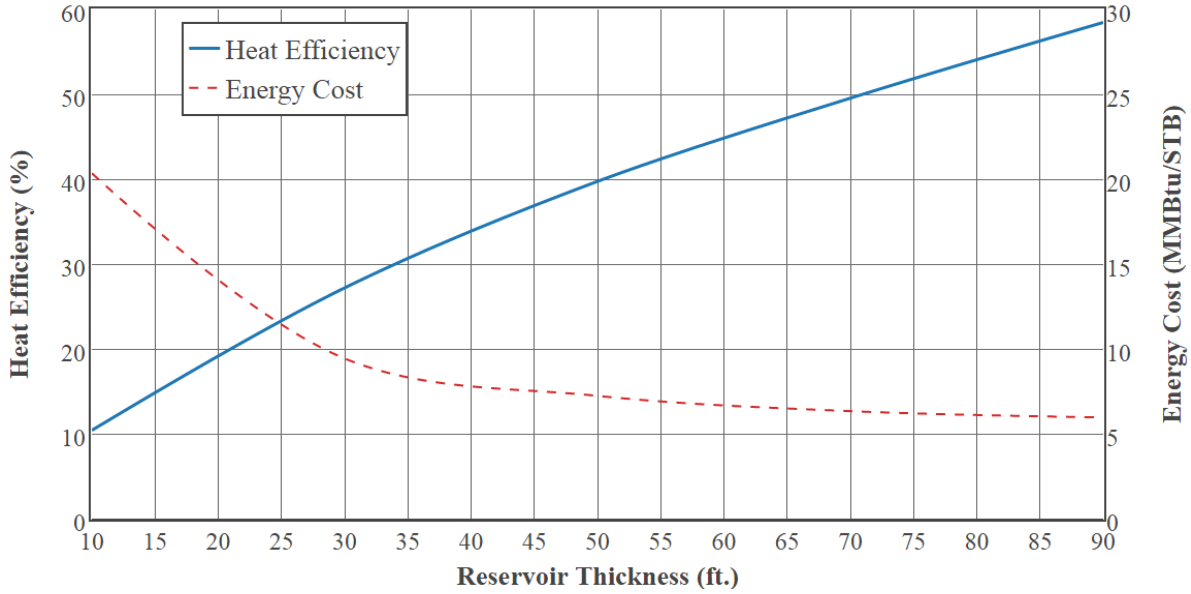

Figure 5-25: Heat efficiency and energy cost variation with reservoir thickness

5.2.8. Economics

An important consideration in thermal recovery processes is the large amount of energy required; the process is not viable if the cost of energy input is greater than the value of additional barrels of oil recovered.

For this study's sample case of 3000 days of primary depletion, followed by 1000 days of heat injection at 700 °F and 3000 days of secondary depletion, cumulative energy input is 793 MMBtu, resulting in 11.5% recovery compared to 7.2% for 7000 days of primary depletion. The original oil in place for this study's computational domain is 2780 bbls; consequently, the difference between 11.5% thermal recovery and 7.2% recovery from primary depletion is 120 bbls in this domain. Eq. 5.9 is used to determine the cost of energy input per incremental barrel of oil produced ($cost_{oil}$) when 793 MMBtu produces

120 extra barrels of oil and the cost of natural gas per MMBtu ($cost_{gas}$) is varied between \$1/MMBtu and \$5/MMBtu. It is important to note that this analysis only considers the additional oil from thermal recovery, i.e. the difference between oil produced with thermal stimulation and oil that would have been produced under primary depletion.

$$cost_{oil} = \frac{793\,MMBtu}{120\,bbls} \times cost_{gas} \times 1/e \tag{5.9}$$

Where e is an efficiency factor for the conversion of energy from natural gas into energy input to the reservoir and was assumed to be 70% in this study. Fig. 5-26 shows the energy cost (\$/additional barrel of oil produced) versus the price of natural gas.

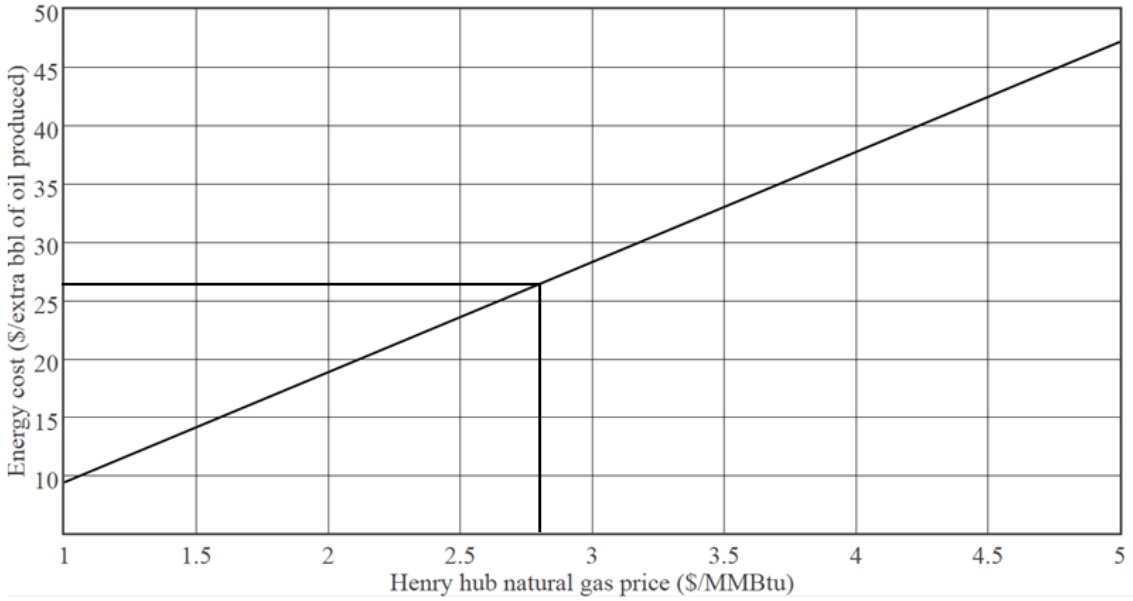

Figure 5-26: Cost of additional barrels of oil recovered

The average cost of natural gas in 2015 was \$2.8/MMBtu (U.S. EIA, 2016c); Fig. 21 shows that at this price, the cost of thermal recovery is about \$26 per additional barrel

of oil produced. Furthermore, this cost can be significantly reduced by using the separator gas from the shale reservoir as the source of energy for heat injection. The capital cost for the heating should also be included in the economic calculations; Rodriguez et al. (2008) estimate the cost of implementation of a 50 MMBtu/day electrical downhole heater to be $350,000 for a 1000 ft. long horizontal well section.

Chapter 6: Conclusions and Recommendations

Results from this study suggest the following conclusions about thermal stimulation in shale oil reservoirs.

1. It is possible to improve oil recovery in shale oil reservoirs by thermal stimulation. The thermal recovery scheme proposed in this paper (primary depletion followed by heat injection and then a secondary depletion period) has the potential to increase oil recovery from approximately 7% to 11-12%, with the possibility of even greater recovery for a more thermally conductive shale reservoir. This study also found that the primary mechanism of improved recovery is the reservoir pressure increase that accompanies fluid temperature increase (thermal pressurization). Viscosity reduction and permeability increase may also improve recovery, but not significantly.

2. Oil recovery during thermal stimulation can be increased further if heating begins at an earlier time (shorter primary depletion), heating temperature is increased or heat is injected for a longer time, and the cost of higher temperatures and longer heating periods is offset by the value of incremental oil produced.

3. An increase in oil in place from kerogen decomposition at elevated temperatures was hypothesized to significantly improve recovery. However, we observed in this study that recovery during thermal stimulation was similar for both a

kerogen-containing reservoir and a reservoir with no kerogen (11.5% versus 10.5%), both significantly greater than the 7.2% observed for primary depletion. Additionally, the increased recovery in the kerogen-containing reservoir can also be attributed to the two-fold increase in permeability as more pores are created during kerogen decomposition.

4. There is potential for improved recovery (up to 21% of OOIP) in a two-well configuration, where heat is injected through a horizontal well, and oil is simultaneously produced from an adjacent well.

5. The high cost of energy required for thermal processes often limits its applicability as an improved recovery method. We found that 793 MMBtu of energy produced 120 extra bbls of oil or about 6.6 MMBtu/bbl of oil, with potential for greater heat efficiency in thicker reservoirs, which translates to about $26 per extra barrel of oil at 2015 average natural gas price. The two-well configuration case with early heat injection had an energy cost of 6.0 MMBtu/bbl of oil. Thermal recovery in shale oil reservoirs can be economical even at low oil prices.

Kerogen decomposition will play a more significant role in recovery if the heated region is better connected to the fracture network, allowing the oil generated from

kerogen decomposition to advance to the wellbore through the fractures, as we saw in the preliminary study where steam was injected.

This study does not take into account thermally driven fracturing and other geothermal effects during thermal stimulation. Recommendations for future work include the following.

1. Additional simulations need to be run to determine the optimum number of cycles. In this study, the effect of a single thermal cycle on recovery was studied. However, there is potential for greater recovery if more cycles are initiated after pressure declines to a level where production is depleted. The effect of additional cycles needs to be investigated as well as the cycle number after which diminishing returns makes extra cycles uneconomical.

2. We found that kerogen decomposition does not significantly affect recovery because the heated region where kerogen conversion takes place is not well connected to the fracture network. Using conductive proppant in the fractures would ensure that heat propagates through the fractures and leads to kerogen decomposition within the fracture network. This can be incorporated in future simulations by assigning higher thermal conductivity to fracture gridblocks.

3. At elevated temperatures, shale loses its elastic properties and behaves increasingly plastically, as well as develops additional fractures. Future simulations should incorporate the effect of temperature on rock mechanical

properties and fractures. CMG STARS allows for geomechanical effects to be included in simulation models.

4. Core-scale heat injection experiments need to be carried out and compared to core-scale simulation runs to validate simulation results and ensure that all relevant physics are included in simulation models.

5. Kerogen decomposition leads to an increase in porosity and a change in permeability. In this study, we assumed the Carmen-Kozeny relationship between rock porosity and permeability is valid for shale rocks. Pore-scale modeling can be used to determine a more accurate relationship between porosity and permeability during kerogen decomposition.

References

Adekunle, O. O., & Hoffman, B. T. (2014, April 12). Minimum Miscibility Pressure Studies in the Bakken. Society of Petroleum Engineers. doi:10.2118/169077-MS

Alvarez, J., & Han, S. (2013). Current overview of cyclic steam injection process. *Journal of Petroleum Science Research*

Breit, V. S., Stright, D. H., & Dozzo, J. A. (1992, January 1). Reservoir Characterization of the Bakken Shale From Modeling of Horizontal Well Production Interference Data. Society of Petroleum Engineers. doi:10.2118/24320-MS

Butler, R. M., & Stephens, D. J. (1981, February 7). The Gravity Drainage of Steam-Heated Heavy Oil to Parallel Horizontal Wells. Journal of Canadian Petroleum Technology. doi:10.2118/81-02-07

Cather, M., Guo, B., Schechter, D. S., & Banik, A. K. (1998, January 1). An Integrated Geology-reservoir Description And Modeling of the Naturally Fractured Spraberry Trend Area Reservoirs. Petroleum Society of Canada. doi:10.2118/98-32

Carrizales, M. A., Lake, L. W., & Johns, R. T. (2010, January 1). Multiphase Fluid Flow Simulation of Heavy Oil Recovery by Electromagnetic Heating. Society of Petroleum Engineers. doi:10.2118/129730-MS

Chen, C., Mohanty, K. K., & Balhoff, M. T. (2013, April 10). Effect of Reservoir Heterogeneity on Improved Shale Oil Recovery by CO Huff-n-Puff. Society of Petroleum Engineers. doi:10.2118/164553-MS

Christie, R. S., & Blackwood, J. C. (1952, January 1). Characteristic and Production Performance of the Spraberry. American Petroleum Institute

Clark, A. J. (2009, January 1). Determination of Recovery Factor in the Bakken Formation, Mountrail County, ND. Society of Petroleum Engineers. doi:10.2118/133719-STU

Coats, K. H. (1980, December 1). In-Situ Combustion Model. Society of Petroleum Engineers. doi:10.2118/8394-PA

Dawson, M., Nguyen, D., Champion, N., & Li, H. (2015, October 20). Designing an Optimized Surfactant Flood in the Bakken. Society of Petroleum Engineers. doi:10.2118/175937-MS

Delamaide, E., Tabary, R., & Rousseau, D. (2014, March 31). Chemical EOR in Low Permeability Reservoirs. Society of Petroleum Engineers. doi:10.2118/169673-MS

Fan, Y., Durlofsky, L., & Tchelepi, H. A. (2010, June 1). Numerical Simulation of the In-Situ Upgrading of Oil Shale. Society of Petroleum Engineers. doi:10.2118/118958-PA

Fowler, T. D., & Vinegar, H. J. (2009, January 1). Oil Shale ICP - Colorado Field Pilots. Society of Petroleum Engineers. doi:10.2118/121164-MS

Gamadi, T. D., Sheng, J. J., & Soliman, M. Y. (2013, September 30). An Experimental Study of Cyclic Gas Injection to Improve Shale Oil Recovery. Society of Petroleum Engineers. doi:10.2118/166334-MS

Gilliam, T. M., & Morgan, I. L. (1987). *Shale: Measurement of thermal properties* (No. ORNL/TM-10499). Oak Ridge National Lab., TN (USA)

Greaves, M., Dong, L. L., & Rigby, S. (2012, January 1). Determination of Limits to Production in THAI. Society of Petroleum Engineers. doi:10.2118/157817-MS

Hascakir, B., Babadagli, T., & Akin, S. (2010, February 1). Field-Scale Analysis of Heavy-Oil Recovery by Electrical Heating. Society of Petroleum Engineers. doi:10.2118/117669-PA

Hoffman, B. T., & Kovscek, A. R. (2003, January 1). Light-Oil Steamdrive in Fractured Low-Permeability Reservoirs. Society of Petroleum Engineers. doi:10.2118/83491-MS

Hoffman, B. T. (2012, January 1). Comparison of Various Gases for Enhanced Recovery from Shale Oil Reservoirs. Society of Petroleum Engineers. doi:10.2118/154329-MS

Kim, J., Zhang, H., Sun, H., Li, B., & Carman, P. (2016, May 5). Choosing Surfactants for the Eagle Ford Shale Formation: Guidelines for Maximizing Flowback and Initial Oil Recovery. Society of Petroleum Engineers. doi:10.2118/180227-MS

Kurtoglu, B., & Kazemi, H. (2012, January 1). Evaluation of Bakken Performance Using Coreflooding, Well Testing, and Reservoir Simulation. Society of Petroleum Engineers. doi:10.2118/155655-MS

Lee, K. J., Moridis, G. J., & Ehlig-Economides, C. A. (2015, Feb 25). A Comprehensive Simulation Model of Kerogen Pyrolysis for the In-situ Upgrading of Oil Shales. Society of Petroleum Engineers. doi:10.2118/173299-MS

Li, H., Hart, B., Dawson, M., & Radjef, E. (2015, August 4). Characterizing the Middle Bakken: Laboratory Measurement and Rock Typing of the Middle Bakken Formation. Society of Petroleum Engineers. doi:10.2118/178676-MS

Martin, R., Baihly, J. D., Malpani, R., Lindsay, G. J., & Atwood, W. K. (2011, January 1). Understanding Production from Eagle Ford-Austin Chalk System. Society of Petroleum Engineers. doi:10.2118/145117-MS

Oba, M., Mita, H., & Shimoyama, A. 2002. Determination of Activation Energy and Pre-Exponential Factor for Individual Compounds on Release from Kerogen by a Laboratory Heating Experiment. *Geochemical Journal* **36** (51 – 60). GJ 36-1-04

Oil and Gas Journal: Eagle Ford Shale Play Map. Retrieved November 29, 2016, from http://www.ogj.com/unconventional-resources/eagle-ford-play-map.html

Pan, Z., Feng, H. Y., & Smith, J. M. 1984. Rates of Pyrolysis of Colorado Oil shale. *AICHE Journal* **31** (5): 721-728. doi: 10.1002/aic.690310504

Pedersen, K. S., Christensen, P. L., & Shaikh, J. A. (2007). *Phase behavior of petroleum reservoir fluids*. Boca Raton: CRC/Taylor & Francis

Permian Basin. Retrieved November 29, 2016, from http://www.shaleexperts.com/plays/permian-basin/Overview

Prats, M. "Thermal Recovery"; Society of Petroleum Engineers, New York, pp. 8-14, 1982

Ramey, H. J. (1971, January 1). In Situ Combustion. World Petroleum Congress

Rodriguez, R. F., Bashbush, J. L., & Rincon, A. C. (2008, January 1). Feasibility of using electrical downhole heaters in Faja heavy oil reservoirs. Society of Petroleum Engineers. doi:10.2118/117682-MS

Sanchez-Rivera, D., Mohanty, K., & Balhoff, M., 2015. Reservoir Simulation and Optimization of Huff-and-Puff Operations in the Bakken Shale. *Fuel,* **147,** 82–94

Singh, S., Nguyen, D., & Wong, S. (1988, May 8). The Commercial Viability and

Comparative Economics of Downhole Steam Generators in Alberta. Journal of Canadian Petroleum Technology. doi:10.2118/88-05-08

Shoaib, S., & Hoffman, B. T. (2009, January 1). CO2 Flooding the Elm Coulee Field. Society of Petroleum Engineers. doi:10.2118/123176-MS

Shuler, P. J., Tang, H., Lu, Z., & Tang, Y. (2011, January 1). Chemical Process for Improved Oil Recovery From Bakken Shale. Society of Petroleum Engineers. doi:10.2118/147531-MS

Song, C., & Yang, D. (2013, November 5). Performance Evaluation of CO2 Huff-n-Puff Processes in Tight Oil Formations. Society of Petroleum Engineers. doi:10.2118/167217-MS

Theloy, C., & Sonnenberg, S. A. (2013, August 12). Integrating Geology and Engineering: Implications for Production in the Bakken Play, Williston Basin. Society of Petroleum Engineers. doi:10.1190/URTEC2013-100

U.S. Energy Information Administration (EIA). (2015, Nov. 23). *U.S. Crude Oil and Natural Gas Proved Reserves – Natural Gas – U.S. Energy Information Administration(EIA)*. Retrieved from http://www.eia.gov/naturalgas/crudeoilreserves/

U.S. Energy Information Administration (EIA). (2016a, Aug. 10). *Shale in the United States – Energy in Brief – U.S. Energy Information Administration (EIA)*. Retrieved from http://www.eia.gov/energy_in_brief/article/shale_in_the_united_states.cfm

U.S. Energy Information Administration (EIA). (2016b, Nov). *Drilling Productivity Report for Key Tight Oil and Shale Gas Regions – U.S. Energy Information Administration (EIA)*. Retrieved from http://www.eia.gov/petroleum/drilling/pdf/dpr-full.pdf

U.S. Energy Information Administration (EIA). (2016c, Aug. 31). *Henry Hub Natural Gas Spot Price – Natural Gas – U.S. Energy Information Administration (EIA)*. Retrieved from https://www.eia.gov/dnav/ng/hist/rngwhhdA.htm

U.S. Geological Survey. (1985). *Future Supply of Oil and Gas from the Gulf of Mexico, 1985*. Washington: U.S. Dept. of the Interior, U.S. Geological Survey

U.S. Geological Survey. (1988). *Thermal properties of Rocks, 1988*. Reston, Va.: U.S. Dept. of the Interior, U.S. Geological Survey

U.S. Geological Survey. (2013). *Assessment of undiscovered oil resources in the Bakken and Three Forks Formations, Williston Basin Province, Montana, North Dakota, and South Dakota, 2013*. Reston, Va.: U.S. Dept. of the Interior, U.S. Geological Survey

Vargas, P. E., He, J., Pei, P., & Ni, X. (2015, November 13). Reducing the Uncertainty in Tight Rock Porosity Estimation by Combining Different Methods-Bakken Formation Case. American Rock Mechanics Association

Vernik, L., & Nur, A. (1990, January 1). Ultrasonic Velocity And Anisotropy of Petroleum Source Rocks: The Bakken Formation. Society of Exploration Geophysicists.

Wang, X., Luo, P., Er, V., & Huang, S.-S. S. (2010, January 1). Assessment of CO2 Flooding Potential for Bakken Formation, Saskatchewan. Society of Petroleum Engineers. doi:10.2118/137728-MS

Yang, Y., Zoback, M., Simon, M., & Dohmen, T. (2013, August 12). An Integrated Geomechanical and Microseismic Study of Multi-Well Hydraulic Fracture Stimulation in the Bakken Formation. Society of Petroleum Engineers. doi:10.1190/URTEC2013-056

Yu, W., Lashgari, H., & Sepehrnoori, K. (2014, April 17). Simulation Study of CO2 Huff-n-Puff Process in Bakken Tight Oil Reservoirs. Society of Petroleum Engineers. doi:10.2118/169575-MS

Zhu, P., Balhoff, M. T., & Mohanty, K. K. (2015, September 28). Simulation of Fracture-to-Fracture Gas Injection in an Oil-Rich Shale. Society of Petroleum Engineers. doi:10.2118/175131-MS

Vita

Nkemakonam Egboga was born and raised in Nigeria. In January 2011, at the age of 16, he moved to Texas, where he enrolled at the University of Texas at Austin. He obtained a Bachelor of Science degree in Petroleum Engineering in December 2014, graduating with High Honors. He attended graduate school at the University of Texas at Austin, where he obtained a Master of Science degree in Petroleum Engineering in December 2016.

Email: nkemegboga@yahoo.ca

This thesis was typed by Nkemakonam Uzodimma Egboga